ADDIS ABABA UNIVERSITY

Addis Ababa Institute of Technology (AAiT)

School of Electrical and Computer Engineering

Study and Design of Multisource and Battery-free Energy Harvesting Architecture for AHM-Aeronautics Applications

By: Mesfin Tsegaye Tadesse

THESIS SUBMITTED TO ADDIS ABABA INSTITUTE OF TECHNOLOGY IN PARTIAL FULFILLMENT OF THE REQUIREMENTS FOR THE DEGREE OF MASTER OF SCIENCE

IN

POWER ENGINEERING

Advisor:

Dr.-Ing. Getachew Biru

Date: June 2018

Addis Ababa, Ethiopia

ADDIS ABABA UNIVERSITY

Addis Ababa Institute of Technology (AAiT)

School of Electrical and Computer Engineering

Study and Design of Multisource and Battery-free Energy Harvesting Architecture for AHM-Aeronautics Applications

APPROVED BY BOARD OF EXAMINERS:

Chairman, Department	Signature	Date
Dr. Ing. Getachew Biru Advisor	Signature	Date
Internal Examiner	Signature	Date
External Examiner	Signature	Date

Abstract

This thesis attempts to study an innovative architecture for an efficient energy generator which powers a wireless sensor network used for Aircraft security Monitoring. This battery-free generator captures energy from its environment due to transient thermal gradients as a main source, and vibrations as a secondary source allowing early biasing of the generator and stores this energy in ultra capacitors. In this way, this multi-source architecture benefits from the synergy between energy scavenging and harvesting: vibration bring low but early and permanent energy. They also contribute to energy harvesting during cruise while thermal gradients have vanished.

This master's thesis deals with the development of a power source based on Micro electrical mechanical system thermoelectric generator. The identification of model parameters is based on a measurement with special test bench. The practical implementation of theoretically outlined principles is illustrated on jet engine control unit with the thermoelectric generator for the electric power backup. The conclusion deals with an application of the presented technology in an aircraft-specific field and the associated issues.
The proposed power source can be used for supplying of an aircraft-specific autonomous sensor unit. System-level point of view on the autonomous sensor includes the sensor with data acquisition and transmission, energy harvester (thermoelectric generator) with system voltage of 3.3V,power rating of 100mW (corresponds to current consumption about 30mA); continuous operation time: 30min; operating temperature range: -50 °C to +85 °C. Proposed thermoelectric generator provides tens of milliwatts of the electric power on the voltage level of 3.3 V. Various serial/parallel/serial-parallel combinations of 1-4 thermoelectric modules will be tested consequently with a boost or buck boost converter.

Keywords*: Thermoelectric generator, energy harvesting, power management, Simulation modeling analysis, Aircraft application, Autonomous sensor node, Structural health monitoring, TEG,MEMS.*

Dedication

I would like to dedicate this work to my wonderful family who are my inspiration, my happiness, and my source of energy, especially to my mother Mulu Biru.

Declaration on Word of Honor:

I statutory declare, that I wrote thesis: Study and design of Multisource and Battery-free Energy Harvesting Architecture for AHM-Aeronautics Applications by myself and under the supervision of my supervisor.

Name: Mesfin Tsegaye Tadesse

Signature: _____

Place: Addis Ababa, Ethiopia

Date of submission: 22th June, 2018

This thesis work has been submitted for examination with my approval as a university advisor.

Dr.-Ing Getachew Biru _____ _____

Advisor's Name Signature

Acknowledgments

First and foremost, I would like to thank my adviser, Dr.Ing Getachew Biru, for his continued support and presence as a source of advice, guidance, and assistance during my academic career. Thank you for all you have done for me, for your encouragement and your unwavering support. Here again, I would like to thank him for the enthusiastic guidance and friendly support during the whole masters study period. Our sessions changed my point of view on the academy research especially to develop my idea to the real world aviation scenario and have been a valuable experience for my future career.

I would also like to extend my appreciation to my research colleague, Bruno Awel for his continued support throughout this research.

I'm grateful for the support given by the committee members, for their time, advice, and guidance. I have had the unique opportunity to reach recent aviation technology in my company environment. My special thanks belong to Ethiopian airlines.

I'm sure that a widespread dedication of scientific papers "To my family…" are not heartwarming. So I just want to thank you for everything my wife Tigist Taye, my daughter Gabriela and my sister Jerry.

Table of Contents

Chapter One 1

1 Introduction 1

1.1 Background 1

1.2 Problem Statement and Motivation 2

1.3 Significance of the Study 3

1.4 Objectives Error! Bookmark not defined.

1.4.1 General Objective 4

1.4.2 Specific Objectives 5

1.5 Methodology 5

Chapter two 8

2. Theoretical Background and Review of Literatures 8

2.1 Theory 8

2.1.1 Thermoelectric Energy Conversion 18

2.1.2 Load Matching 21

2.1.3 Boost Converter 13

2.1.4 Buck Converter 14

2.1.5 Buck-Boost Converter 15

2.1.6 Fly back Converter 16

2.1.7 Maximum Power Point Tracking (MPPT) 17

2.2 Review of Literatures 18

2.2.1 Architecture of multi source battery free energy generator 18

2.2.2 Energy transfer maximization 21

2.2.3 Energy efficiency 22

Chapter Three 28

3. Data collection and experimental analysis 28

3.1 MEMS Thermoelectric Modules 38

3.2 Electronics 40

3.3 Experiment 45

3.3.1 Measurement Setup 45

3.3.2 Open-circuit Voltage Measurement 48
3.3.3 Short-circuit Current Measurement 49
3.4.4 Internal Resistance Measurement 50
3.3.5 Seebeck Coefficient Measurement 51
3.3.6 Calculated Characteristics 52
3.3.7 Comparison of MEMS Thermoelectric Modules 54
3.3.8 Measurement Summary 57
3.4 System-level Design 57
3.4.1 Power Management Concept 61
Chapter Four 65
4. Modeling and Simulation 65
4.1 Model Description 65
4.2 Model Blocks 66
4.3. Simulation in ANSYS 67
4.4 Discussion 68
Chapter five 61
5. Conclusion and Recommendation 61
5.1 Conclusion 73
5.2 Recommendation 74
5.2 Recommendation for future work 75
References 77
Appendix 84

List of Symbols

C_{lp} C_{sp}	[J.kg^{-1}.K^{-1}] [J.kg^{-1}.K^{-1}]	heat capacity of PCM in liquid phase heat capacity of PCM in solid phase
D	[-]	duty cycle
$D_{MPP,boost}$	[-]	duty cycle at maximum power point for a boost
$D_{MPP,buck}$	[-]	duty cycle at maximum power point for a buck
$D_{MPP,buck-boost}$	[-]	duty cycle at maximum power point for a buck-boost converter
$D_{MPP,flyback}$	[-]	duty cycle at maximum power point for a flyback converter
f_s ΔH	[Hz] [J.kg^{-1}]	switching frequency heat of phase change
I_{in}	[A] or [mA]	input current
I_{out}	[A] or [mA]	output current
K	[-]	Constant
M	[kg]	Mass
M_I	[-]	current transfer function
M_U	[-]	voltage transfer function
$M_{U,boost}$	[-]	voltage transfer function of a boost converter
$M_{U,buck}$	[-]	voltage transfer function of a buck converter
$M_{U,buck-boost}$	[-]	voltage transfer function of a buck-boost
$M_{U,flyback}$	[-]	voltage transfer function of a flyback converter
N	[-]	turn ratio
t_{on}	[s]	on-time
t_{off}	[s]	off-time
T	[s]	switching period
T_h	[°C] or [K]	hot-side temperature
T_c	[°C] or [K]	cold-side temperature
T_{jecu}	[°C] or [K]	temperature of JECU
T_{pch}	[°C] or [K]	phase-change temperature
ΔT	[°C] or [K]	temperature difference along the module
ΔT_{peak}	[°C] or [K]	peak temperature difference
P_{el}	[mW]	electric power
$P_{el,\ peak}$	[mW]	peak electric power
$P_{el,\ avg}$	[mW]	average electric power
P_{MPP}	[mW]	output electric power on maximum power point
Q_a	[J]	available heat
Q_c	[W]	heat flow through cold side of thermoelectric

Q_h	[W]	heat flow through hot side of thermoelectric
Q_{Ph}	[W]	Peltier cooling on a hot side of TEM
Q_{Pc}	[W]	Peltier cooling on a cold side of TEM
Q_J	[W]	Joule heating
$R_{heat\ sink}$	[$W.K^{-1}$]	thermal resistance of heat sink
R_{out}	[Ω]	output resistance
R_{load}	[Ω]	load resistance
R_{in}	[Ω]	input resistance
$R_{install}$	[$W.K^{-1}$]	thermal resistance of adapters for eTEG HV56
R_{jecu}	[$W.K^{-1}$]	thermal resistance of path JECU-TEM
R_{tem}	[Ω]	thermoelectric module internal resistance
Rt_{tem}	[$W.K^{1}$]	thermal resistance of TEM
U_{in}	[V] or [mV]	input voltage
U_{load}	[V] or [mV]	voltage on load
U_{oc}	[V] or [mV]	open-circuit voltage
U_{out}	[V] or [mV]	output voltage
ZT	[-]	figure of merit
λ_{tem}	[$W.K^{-1}$]	thermal conductivity of thermoelectric module
H	[-] or [%]	efficiency
$\alpha_{heat\ sink}$	[$W.m^{-2}.K^{-1}$]	convective heat transfer coefficient to ambient air
α_{Σ}	[$V.K^{-1}$]	net Seebeck coefficient

List of Acronyms

AC	alternating current
APU	auxiliary power unit
ASN	autonomous sensor node
CCM	continuous conduction mode
COTS	commercial-of-the-shelf
DC	direct current
DCM	discontinuous conduction mode
ESR	equivalent series resistance
HUMS	health and usage monitoring system
IC	integrated circuit
JECU	jet engine control unit
LDO	low dropout regulator
MEMS	micro electro-mechanical system
MPPT	maximum power point tracking
NDT	nondestructive testing
NEMS	nano electro-mechanical system
P&O	perturb and observe
PCM	phase change material
PFM	pulse-frequency modulation
PWM	pulse-width modulation
RF	radio frequency
RFID	radio frequency identification
SHM	structure health monitoring
SMPS	switching-mode power supply
TEG	thermoelectric generator
TEM	thermoelectric module
TJ	turbo-jet
TP	turbo-prop
TS	turbo-shaft
ULP	ultra low power
WSN	wireless sensor network

Table of Figures

Figure 1-1: Cable length comprehension *3*

Figure 2-1: Opportune spots for placing of TEG on an aircraft [10] ..... ***Error! Bookmark not defined.***

Figure 2-2: Practical realization of a dynamic thermoelectric generator *11*

Figure 2-3: shows a typical voltage response of a TEG under transient thermal gradients. *11*

Figure 2-4: Sample grams of water and the climatic chamber *11*

Figure 2-5: Practical amplitude spectrum of acceleration versus frequency. *13*

Figure 2-6: Practical realization of a static thermoelectric generator[14] *14*

Figure 2-7: CAD drawing of TJ100 turbine with JECU (black box in the rear section) [20] *17*

Figure 2-8: TJ100 turbine with JECU (black box in the rear section) on the test stand [20] *17*

Figure 2-9: Thermography image of JECU during its operation under the maximum operating power [24] *18*

Figure 2-10: Thermoelectric module (right) and its equivalent circuit (left) *19*

Figure 2-11: DC/DC switching converter as a two-port network *11*

Figure 2:12 Concept of load matching (shown on a case of boost-converter) *13*

Figure 2-13: Boost converter *13*

Figure 2-14: Output/input voltage as a function of duty cycle for different relations between source and load resistance when operating the boost converter [39] *14*

Figure 2-15: Buck converter *14*

Figure 2-16: Buck-Boost converter *15*

Figure 2-17: Flyback converter *16*

Figure 2-18: Flowchart of P&O algorithm [43] *16*

Figure 2-19: Electrical schematic of the proposed battery-free multisource energy generator connected to a sensor node *20*

Figure 2-20:

(a).Electrical schematic of the proposed battery-free multisource energy generator connected to a sensor node

(b).Use of two storage devices, UC1 and UC2, to maximize energy transfer

(c).Optimized solution with active diodes and two storage devices *20*

Figure 2-21: Symbols (top) and electrical schematic for the active diodes Dn *21*

Figure 2-22: Proposed nana watt voltage reference. *21*

Figure 2-23: Electrical schematic of the LDO *23*
Figure 2-24: Opportune spot for placing of TEG on the pylon fairing of Airbus A380 [13] *24*
Figure 2-25: CAD drawing and sample Home based realization of the TEG system *24*
Figure 2-26: The sensor is here supposed to be submitted to a temperature of 270°C. The continuous curve represents the output power of a TEG. *27*
Figure 3-1: Micropelt TGP-751 (left: in package, right: with removed package) [44] *26*
Figure 3-2: Micropelt TGP-751 dimensions (in mm) [44] *30*
Figure 3-3: Nextreme eTEG HV56 dimensions (in mm) [45] *40*
Figure 3-4: Decision tree when considering a new aircraft-specific storage element [8] *42*
Figure 3-5: THINERGY thin-film battery [55] *33*
Figure 3-6: AVX BestCap series[55] *34*
Figure 3-7: Increase of internal resistance with low temperatures for a supercapacitor [53] ... *44*
Figure 3-8: 10F supercapacitor by Maxwell [55] *35*
Figure 3-9: Measurement setup *46*
Figure 3-10: 3D drawing of test bench internal structure [56] *47*
Figure 3-11: Test bench for Micropelt TGP-751 ..... *47*
Figure 3-12: Test bench for Nextreme eTEG HV56 ..... *47*
Figure 3-13: Test bench inside the climatic chamber *48*
Figure 3-14: Open-circuit voltage measurement setup *48*
Figure 3-15: Open-circuit voltage measurement results (Micropelt TGP-751, ΔT = 0-100°C) *49*
Figure 3-16: Short-circuit current measurement setup *49*
Figure 3-17: Short-circuit current measurement results (Micropelt TGP-751, ΔT = 0-100°C) *50*
Figure 3-18: Internal resistance RTEM measurement setup *50*
Figure 3-19: Internal resistance measurement results (Nextreme eTEG HV56, Tavg = -50 ÷ +150°C) *51*
Figure 3-20: Internal resistance measurement results (Micropelt TGP-751, Tavg = -50 ÷ +150°C) *51*
Figure 3-21: Seebeck coefficient measurement setup *52*
Figure 3-22: Discrete plot of Seebeck coefficient variations with Tavg (Micropelt TGP-751) ... *52*
Figure 3-23: Power on MPP (Micropelt TGP-751, ΔT = 0-100°C) *53*
Figure 3-24: V-A characteristics comparison (Micropelt TGP-751, ΔT = 10, 30, ... *53*
Figure 3-25: W-A characteristics comparison (Micropelt TGP-751, ΔT = 10, 30, 50°C) *54*

Figure 3-26: Open-circuit voltage comparison (Micropelt TGP-751 vs. Nextreme eTEG HV56, ΔT = 0-100°C).....55
Figure 3-27: Power on MPP comparison (Micropelt TGP-751 vs. Nextreme eTEG HV56, ΔT = 0-100°C).....55
Figure 3-28: V-A characteristics comparison (Micropelt TGP-751 vs. Nextreme eTEG HV56, ΔT = 50°C).....56
Figure 3-29: W-A characteristics comparison (Micropelt TGP-751 vs. Nextreme eTEG HV56, ΔT = 50°C).....56
Figure 3-30: Supplied application under consideration – the (over) speed measurement of TJ/TP/TS100 turbine.....58
Figure 3-31: TJ100 encapsulated in engine bay.....50
Figure 3-32: Placing of TEG on the TJ100 turbine – prospective spots.....50
Figure 3-33: Thermal networks of TEGs based on Nextreme eTEG HV56 (left) and Micropelt TGP-751 (right).....60
Figure 3-34: Concept of power management for proposed TEG.....61
Figure 3-35: Temperature is the big issue when designing the TEG for aerospace applications [8].....62
Figure 3-36: Texas Instruments bq25504 – typical application circuit with thermoelectric generator [48].....63
Figure 3-37: ST Microelectronics SPV1040 – typical application circuit [49].....54
Figure 3-38: System block diagram of TEG power source for aircraft application.....64
Figure 3-39: Power management with buck converter TPS62120.....64
Figure 4-1:Verification of eTEG HV56 model – comparison of measured and simulated open circuit voltage.....68
Figure 4-2: Verification of eTEG HV56 model – comparison of measured and simulated power on MPP.....69
Figure 4-3: Verification of TGP-751 model – comparison of measured and simulated open-circuit voltage.....69
Figure 4-4: Verification of TGP-751 model – comparison of measured and simulated power on MPP.....70

List of Tables

Table 2-1: Opportune spots for placing of TEG on aircraft - temperature differences and output powers *9*
Table 2-2: Energy densities of different energy harvesters [5] *16*
Table 3-1: Comparison of thermoelectric generators suitable for our application *29*
Table 3-2: Prospective ICs for thermoelectric energy harvesting *32*
Table 3-3: Comparison of various energy storage elements *33*
Table 3-4: Measuring instruments *36*
Table 3-5: Seebeck coefficient variations *43*
Table 4-1: Micropelt TGP-751 – Comparison of model, measurement and datasheet values *70*
Table 4-2: Micropelt TGP-751 – Comparison of model, measurement and datasheet values *71*

Chapter One

1 Introduction

1.1 Background

Systems energy independence is one of the biggest issues connected with energy. Engineers have tried over the centuries to design and build various energy autonomous machines and devices. Nowadays, the energy autonomous systems are of a high interest due to their applications in building control, biomedical implants, automotive and aerospace. All of these applications are mainly electrically powered. Supplying of the energy autonomous systems can be implemented using primary cells or rechargeable batteries. Nevertheless, this approach is disadvantageous as the batteries must be replaced or recharged. An intervention into the system causes additional maintenance and maintenance costs. The system-intervention can be life-threatening in the worst case of biomedical implants. The solution might be found in an energy harvesting - a modern way of how to feed the autonomous devices on-site using ambient energy.

The ambient energy sources are represented by vibrations, motion, temperature gradients, light or RF (radio frequency) radiation. Thanks to the modern low-power electronics, the small amounts of locally harvested energy are sufficient for powering the wireless sensors, micro actuators or any other transducers. Energy harvesting is even more promising in a combination with the micro or nano electromechanical systems (MEMS or NEMS). Energy harvesters are particularly advantageous in the places where it is difficult to trace a wiring or where the battery replacement is challenging due to disassemble difficulties [1].

The presented master's thesis is particularly focused to the field of energy harvesting for supplying autonomous systems in aerospace. Thermoelectric generator based on MEMS thermoelectric module was proposed as a suitable power supply. The considered supplied applications include fully-autonomous sensor and electric power backup for a sensor unit connected to the onboard power distribution of an aircraft. System-level point of view on this energy harvester includes the MEMS thermoelectric module itself, power management, power conditioning, energy storage element, control electronics and self-diagnostics.

1.2 Problem Statement and Motivation

The critical parameter of aircraft systems is their weight. Batteries and wiring take a not negligible amount of aircraft unlade weight. In addition to that addressing the challenges related to the expansion of air traffic, to the dramatic increase of jet fuel price, and to environmental concerns, the aeronautics industry is seeking technological and process innovations in aircraft maintenance. In this context, Aircraft Health Monitoring (AHM) is one of the major challenges faced by aircraft manufacturers. Main applications of AHM are the airframe, the main engines and the main systems (such as Auxiliary Power Unit - APU), all major contributors to Aircraft "Delay and Cancellation". One of the major issues is the prediction of failures to prevent structure or system damages by anticipating the maintenance action necessary to avoid "events". Such predictive service is especially relevant for the Structure health monitoring (SHM). SHM therefore consists mainly in the monitoring of corrosion, of cracks and of impact damages taking place during the aircraft life. It is generally considered as a powerful tool to decrease inspection costs, to optimize margins in mechanical design, and consequently, to reduce aircraft weight, fuel consumption and emissions of greenhouse gases.

Only limited implementations of AHM have already been done using wired technology such as Acoustic Airframe Monitoring System by Ultra Electronics Ltd. However, because of the gain associated with a wireless architecture, support of AHM (Aircraft health monitoring) by Wireless sensors networks (WSN) based on Micro electrical mechanical systems (MEMS) technology, is envisioned by major aircraft manufacturers.

In the above context, a network of a relatively large number of self-powered MEMS-based nodes would perform sensing, data processing and wireless transmission of information. However, the main technological barrier to the wide development of WSN is their energy autonomy.

In such a WSN, the most obvious wireless energy supply system consists of primary batteries. However, whatever the batteries performance and size, they only store a limited amount of energy and exhibit a limited lifetime therefore placing an unacceptable upper limit on the network lifetime itself (given the fact that nodes may be placed in remote areas with very limited access). As a result, the replacement of hundreds of dead batteries would induce a prohibitive maintenance cost together with an environmental issue for their disposal. More important, at temperature levels encountered at high altitude in

unpressurized areas far from engines (typically –60°C) their efficiency is drastically reduced whereas unacceptable safety issues (thermal runaway and fire) are raised. Fortunately, primary batteries can be eliminated through the use of environmental energy capture techniques, which use an energy conversion transducer tied to an integrated rechargeable power storage device, then enabling the wireless sensor node an almost infinite lifetime[58].

This study present an ultra-low power converter for a multisource battery-free energy generator dedicated to aeronautics applications that would enable almost infinite energy-autonomy to a WSN node. This new system provides a regulated voltage with a very low quiescent current consumption (≤300nA). The proposed architecture is based on two energy sources and on ultra capacitors for storage.

1.3 Significance of the Study

The critical parameter of aircraft systems is their weight. Batteries and wiring take a not negligible amount of aircraft unladen weight. Moreover, the aircraft load is significantly increased by the test equipment during a test flights. Comprehension of the total cable length in typical aircrafts is given in figure 1.1 below. As the result of these considerations, the most suitable systems for the implementation of thermoelectric energy harvesting include [6]:

- Maintenance support;
- Cabin crew support;
- Flight test instrumentation;
- Power supply backup of critical systems

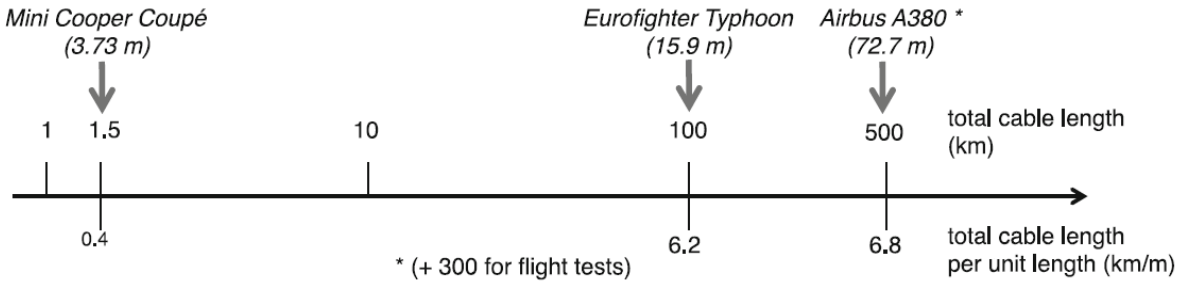

Figure 1-1: Cable length comprehension

From the figure 1.1 above one has to determine whether the network needs to be wireless. The

total electric cable lengths implemented in a car, a jet fighter and an airliner are compared. These lengths are also converted in kilometer per unit length of the car/aircraft as a measurement of complexity. From figure 1.1,it appears that fighter jets and airliners are similarly complex objects considering wiring thus praising for wireless solutions when the development of new electronic sensors is to be considered. As a consequence of such a choice, measurement data need of precise to be transmitted wirelessly; in addition the device has to be autonomous in energy. The utilization of thermoelectric generators in an aerospace industry is usually discussed along with the implementation of wireless sensors networks (WSNs). In the combination with WSNs, energy harvesting using thermoelectric is one of the very promising emerging technologies associated with structural health monitoring (SHM). Future direct incorporation of smart SHM sensors into the aircraft materials structure is possible. Nowadays, the complicated dismounting of casing, inspections through bore scope and damage detection using non- destructive testing techniques (NDT) have to be utilized during the mandatory scheduled checks of an aircraft. The aircraft checks are always associated with enormous manpower needs. The greatest expectation connected with Thermo electric generator-supplied WSNs (wireless sensor networks) is the step forward from scheduled to predictive maintenance. The predictive maintenance is not driven by strict scheduled time intervals but incorporating the real aircraft state instead. The implementation of thermo electric generators along with WSNs might also be helpful for the cabin crew. The state of seatbelts and the presence of passengers in their seats might be monitored using autonomous sensors. Moreover, the reconfiguration of cabin seating would be possible without any further changes in airplane wiring. The last but not least perspective application is the utilization of thermoelectric generator as a power supply backup of critical systems. This approach doesn't eliminate the wires but affects positively the aircraft safety and reliability.

1.4 Objectives

1.4.1 General Objective

To address the challenges related to the expansion of air traffic, to the dramatic increase of jet fuel price, and to environmental concerns,the aeronautics industry is seeking technological and process innovations in aircraft maintenance. In this context, Aircraft Health Monitoring (AHM) is one of the major challenges faced by aircraft manufacturers [1, 2].Only limited implementations of AHM have already been done using wired technology such as Acoustic Airframe Monitoring System by Ultra Electronics Ltd [3].The major objective of this thesis is

to investigate the potential use of thermoelectric generators into the aerospace industry.

1.4.2 Specific Objectives

The specific objective of this thesis is a contribution to utilization of thermoelectric generators into the aerospace industry. An overall understanding of processes inside thermoelectric energy harvester is a valuable side product. More specifically, the specific objectives of presented work are:

- Prepare a set of requirements needed for the design and build of the thermoelectric generator for aerospace applications based on MEMS modules;
- Develop a multipurpose simulation model of thermoelectric generator in ANSYS simulation software;
- Evaluate perfomance of thermoelectric generators based on MEMS modules for aerospace application purposes;
- Draw relevant conclusions and recommendations for further application of thermoelectric generators for aerospace application purposes.

1.5 Methodology

This thesis will be started by collecting different data from live aircraft. Then due to the energy harvested through thermal gradient results in two voltage polarities, even if there is only one polarity switching, a rectifier circuit is mandatory before storage. So, the design of the rectifier circuit with Ultra-low power consumption amplifier to comply with our requirement of a low quiescent current of full converter. The design of the active diodes optimized with the objectives to get a threshold voltage in the range of 10 mV whereas minimizing the quiescent current consumption in the range of few hundreds of nA. This multisource and battery-free energy harvesting architecture will be validated and experimented on two CMOS technologies and experimental setup that allowed validating the thermal-gradient energy-scavenging principle will be simulated on live flying aircraft with the help of thermo electric generator.

For energy capture, two principles may be considered, called energy harvesting (continuous source) and energy scavenging (intermittent source). However, availability of energy is in both cases limited, and for such a self-powered network, energy is therefore a critical issue, and hardware design must consider energy as a main constraint.

It is worth mentioning that coupled energy sources can be considered since it may occur

that a single category would not be enough to power a node during all phases of a flight. More precisely, time shifts in the availability of environmental energy together with intrinsic different time constants of the transducers and the by-nature synergy between scavenging and harvesting may praise for such a multi-source configuration.

Although in terms of energy loss, immediate use of the captured environmental energy by the WSN node would be more efficient, an energy-storage device is required as an energy buffer between the WSN node and the energy source. Additionally, long-term energy storage may be desired to budget for future energy consumption when scavenging or harvesting efficiency is low. In the aeronautics application context, the use of secondary (rechargeable) batteries is prohibited, as they suffer from even worse environmental limitations than primary ones [63]. Electrical double-layer capacitors, also named super-capacitors or ultra- capacitors are the solution for transient storage. They store electrostatic energy between a solid electrode and oppositely charged electrolyte ions. They offer a high capacitance in a small volume together with a virtually infinite lifetime. However, conversely to batteries, they do not provide a fairly constant output voltage, the output of an ultra capacitor dropping from full value to zero during discharge: a voltage regulator is therefore required for biasing the signal processing part of the WSN node. The ultra capacitor from Maxwell we have selected had been extensively tested vs. temperature in a previous work. It had experimentally demonstrated that its performance was unaffected down to -55°C [61] It must be stressed that, at this stage, the parameter of importance is the transfer through the transducer of a maximum of energy from the environment to the ultra capacitor, whatever the conversion efficiency; all energy not captured being ultimately lost. Conversely, energy treatment such as voltage regulation must favor efficiency. In the following, the considered AHM applications preclude external devices mounted on the airfoils outside the aircraft, therefore excluding the use of solar energy, which is known to be one of the most efficient way of capturing energy from a system environment in terms of power density. Similarly, for deployment we consider non-pressurized areas, far from any heat- generating equipment. Above that, an energy harvester is strongly interacting with the supplied load –the low-power system represented by a sensor unit.

Techtronic design principles along with the model-based design have been employed for the development of a proposed complex harvester. Experiences with the model-based design of energy harvesters have been taken over the long-term research of vibration energy harvesters in boeing Company. Simulation modeling has been implemented in ANSYS.

Practical implementation of the proposed system is illustrated on a purpose-developed

technology demonstrator. The presented technology demonstrator was built using the commercial-off-the-shelf (COTS) hardware components whose practical implementation in aerospace should be the task for a further testing procedure. The current results and suggested next steps in the design and development of a reliable thermoelectric harvester for aerospace applications are finally discussed in the conclusion of this thesis.

Energy harvesting is an art of making useful electric power from ambient energy sources. It's a modern way how to feed the autonomous devices on-site using energy in its surroundings. Promising area for the use of these small amounts of locally harvested energy may be found in the supplying of wireless sensors, temporary testing equipment, biomedical devices, etc.[1],[2].The energy harvesting approach is particularly advantageous in the places where is difficult to trace a wiring or where the battery replacement is challenging due to disassemble difficulties.

Chapter two

2. Theoretical Background and Review of Literatures

2.1 Theory

Energy harvesting is an art of making useful electric power from ambient energy sources. It's a modern way how to feed the autonomous devices on-site using energy in its surroundings. Promising area for the use of these small amounts of locally harvested energy may be found in the supplying of wireless sensors, temporary testing equipment, biomedical devices, etc.[1],[2].The energy harvesting approach is particularly advantageous in the places where is difficult to trace a wiring or where the battery replacement is challenging due to disassemble difficulties.

The perspective application areas are shown in the figure 2.25 below. The next logical step is to find the opportune spots for placing thermo electric generator on an aircraft. The spots under consideration include engine with its bay, auxiliary power unit (APU), bleed system, electrical and hydraulic actuators, electronic systems, cabin lining and crown of an aircraft.Figure 2.25 shows some of these opportune spots.

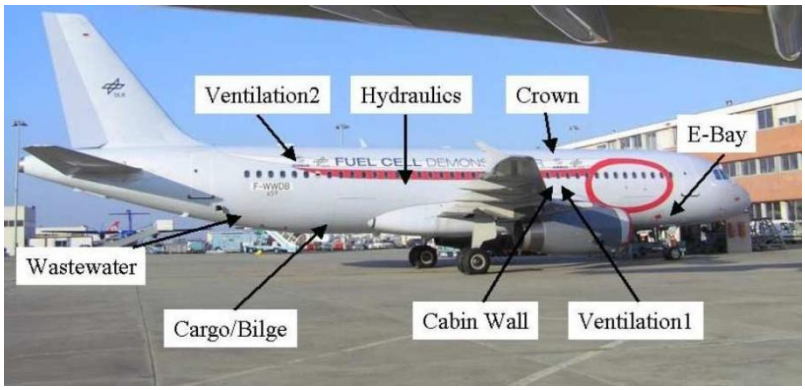

Figure 2-1: Opportune spots for placing of TEG on an aircraft [10]

More generally, the thermoelectric generator can be placed in the areas classified as Pressurized and temperature controlled zone (aircraft cabin);Non-pressurized and non-temperature controlled zone (inside the aircraft structure); extremely harsh environment (around engine or brake) each of the opportune spots on an aircraft can be classified accordingly to the above-mentioned acres. Its placement determines the required specifications. For instance, the thermoelectric generator used for supplying the passenger seat status situated in the aircraft cabin may not necessarily meet that strict regulation as TEG in an engine bay providing the critical sensing tasks for the

engine control or protection. Moreover, the thermoelectric generators inside the aircraft cabin may not be tested for the whole aircraft operation envelope insomuch as their temperature is maintained around room temperature. On the other hand, the critical systems for the control and propulsion of an aircraft are placed outside the pressurized and temperature controlled zone. Utilization of TEG into the critical systems requires a reliable long-lasting solution capable to operate within the whole operating envelope of an aircraft.

In table 2.2 are listed some of the opportune spots from figure 2.25 along with temperature differences and peak/average generated electric power. The stated values are based on a computer simulation. The thermoelectric module under consideration is Micropelt TGP-751. This thermoelectric generator module is based on micro-electro-mechanical-systems (MEMS) technology.

Table 2-1: Possible spots for placing of TEG on aircraft - temperature differences and output powers [10]

Spot (cold and hot side)	ΔT_{peak} [°C]	$P_{el,\,peak}$ [mW]	$P_{el,\,avg}$ [mW]
cargo skin / cargo primary insulation	40	34.15	22.58
hydraulic pipeline 1 / hydraulic pipeline 2	20	7.97	3.07
waste water tank / waste water ambient	15	5.46	2.99
engine bay fuselage skin / engine bay primary insulation	35	18.72	6.42
cabin wall fuselage skin / cabin wall primary insulation	30	13.36	3.97
cabin wall fuselage skin / cabin wall secondary insulation	40	30.06	11.70

Finally, the basic concept for thermoelectric energy harvesting device for the aircraft-specific purposes has to be chosen. The aircraft-specific thermoelectric harvesting can be principally distinguished between these types [6].These are the dynamic thermoelectric energy harvesting (uses temporal temperature variations within the aircraft operation envelope); Static thermoelectric energy harvesting (uses constant spatial temperature differences).

The dynamic thermoelectric energy harvesting device advantageously uses the temperature changes within the aircraft operating envelope after take-off. Dynamic thermoelectric generator concept is shown in figure 2.26. Since from take-off to cruise altitude, atmospheric temperature usually strongly decreases, thermal gradients may therefore appear inside and around the WSN node hardware. Referring to the International Standard Atmosphere (ISA) defined by the International Civil Aviation Organization (ICAO), at an en-route flight altitude of 12000 m, atmospheric temperature is about -60°C [64]. The above

gradients can be converted into voltage via a thermoelectric generator (TEG) based on the See beck effect. However, sooner or later, the node and its surroundings will be back to an isothermal state and no more thermal flux will take place. Therefore, to increase the gradient value and duration, the transient thermal gradient between aircraft mechanical structure and a phase change material is captured [65-67]. Water is identified as a pertinent choice, therefore benefiting from its high specific heat (4.2 J/g.°C – to be compared with that of Si, 0.7 J/g.°C). Water freezing point (0°C) being situated within the aircraft temperature usual operating range, the system also benefits from energy exchanges related to water latent heat of fusion (330 J/g), with the added advantage of water being maintained at a constant temperature during the water freezing or ice melting phases, hence increasing temperature gradient values. Figure 2.26 and Figure 2.22 below shows a cross-section drawing and a photograph of the experimental setup that allowed validating the thermal-gradient energy-scavenging principle respectively.

The temperature difference is formed of a phase-change material (PCM) attached to the thermoelectric generator at the one side and ambient temperature on the other side. The PCM acts as heat storage. It holds a warm ground temperature accordingly to its heat capacity while the outside ambient temperature decreases. When the heat transmission is over and temperature of the PCM reaches the phase-change temperature, additional heat is produced due to the phase-change of the material. The landing scenario works in vice versa. The PCM is cold while the ambient air is hotter. The phase-change has an opposite direction.

All available heat during the dynamic TEG operation can be described as:

$$Q_a = \int_{T_h}^{T_{pch}} mC_{lp}\,(T)dT + M\Delta H + \int_{T_{pch}}^{Tc} mC_{SP}(T)dT \qquad \textbf{(1)}$$

Where is Q_a available heat, m the mass of PCM, T_h is the hot-side temperature, T_{pch} is the phase-change temperature, T_c is the cold-side temperature, C_{lp} is the heat capacity of PCM in liquid phase, ΔH is the latent heat of phase change, *and* C_{sp} is the heat capacity of PCM in solid phase. The available heat can be transferred to useful electric power using thermoelectric energy conversion.

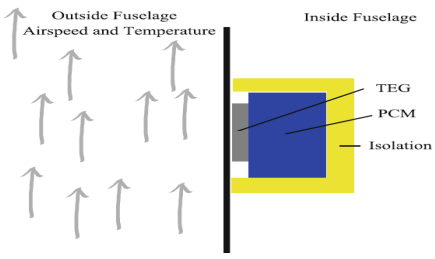

Figure 2-2: Practical realization of a dynamic thermoelectric generator

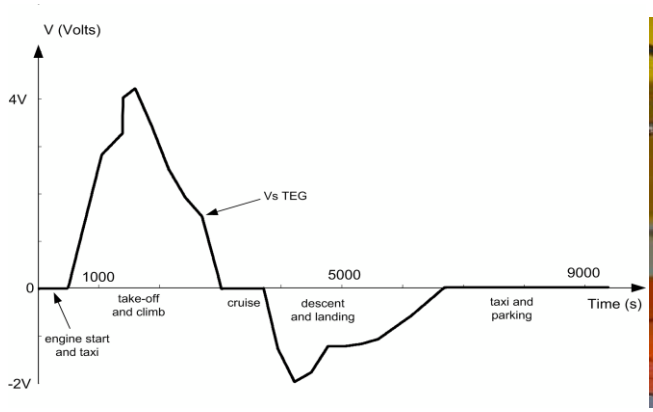

Figure 2-3: shows a typical voltage response of a TEG under transient thermal gradients.

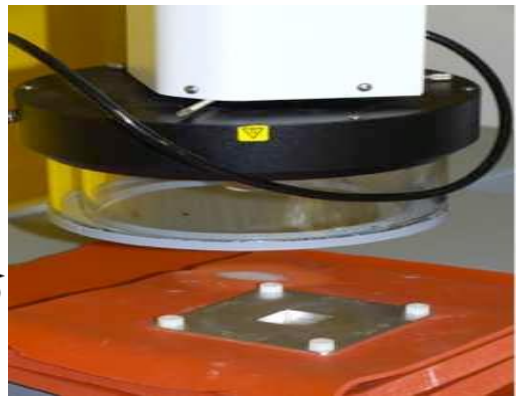

Figure 2-4: Sample grams of water and the climatic chamber

Figure 2.21, also provides the temperature profile applied to the TEG that corresponds to a typical one-hour flight. As can be observed, gradient polarity is reversed during descent, asking for rectifying the TEG output.

To roughly assess the upper limit for the thermal energy that could be captured, let us consider a sealed tank containing 1 g of water. As already mentioned, water exhibits a specific heat C of around 4.2 J/g.° C when liquid, 2.1 J/g.° C when solid, and an enthalpy of fusion H_f of 330 J/g. Stating a water capsule temperature at take-off of 15°C, and a cruise temperature of –60°C, the energy W_T associated with temperature variation ⊗T and phase change is given by:

$$W_T = \Delta T_{solid} * C_{solid} + \Delta \ _{liq} * C_{liq} + H_f = 519 J/\mathrm{g} \quad \textbf{(2)}$$

This value may be doubled as temperature variations take place both during climb and descent that is a total of 1038 J/g. This value may be slightly higher if take-off temperature and therefore initial temperature of the sensor node is higher. Unfortunately, it can conversely be very limited if this temperature is below icing temperature.

As shown in figure 2.26, where thermal energy can be converted into electrical energy by thermoelectric generators using the Seebeck effect. Such generators are current sources converting temperature difference between a cold and a hot surface into electrical energy. Despite the efficiency of such components, the energy available at the TEG output is

around 15J. This efficiency could be even more improved using an appropriate phase change material and an optimized heat storage unit Although the above method is attractive, energy scavenging will only start once the aircraft is climbing; this may raise operational issues if energy-storage devices are initially empty. This latter situation may often occur since ultra capacitors are known to suffer from large self-discharge currents. In particular, monitoring of the structure during take-off is of great interest since it is submitted to high strains. To cope with this drawback, the system devised with a secondary energy source harvesting the mechanical energy associated with the vibrations of the aircraft structure. In an airliner, vibrations are maximum in engine area, and conversely are much less in cabin, with the exception of low (less than 10 Hz) accelerations associated with gust or turbulence. figure 2.23 qualitatively shows the experimental vibration spectrum recorded in close proximity of the jet engine of a large airliner. It is a multi-band spectrum, made of peaks regularly spaced.

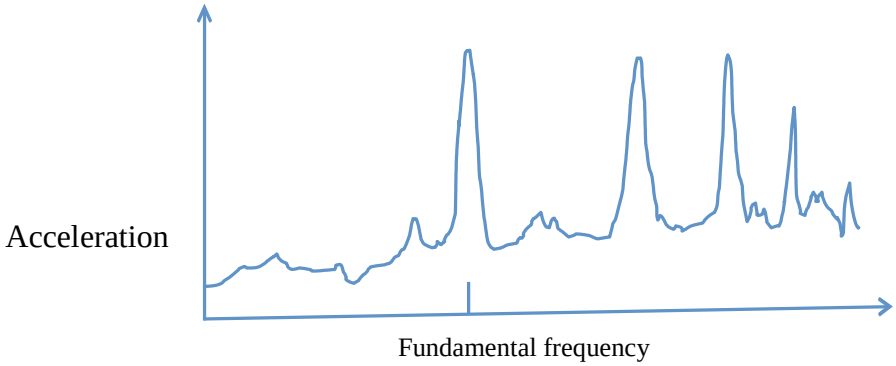

Figure 2-5: Practical amplitude spectrum of acceleration versus frequency.

Acceleration was measured by an accelerometer located in aircraft engine area during descent. Both scales are logarithmic The fundamental frequency component ranges typically between 40 and 60 Hz depending upon flight phase and engine model.To harvest vibrations, we devised a MEMS harvester based on a seismic mass applying the vibrations to piezoelectric beams. It delivers an alternating output which spectrum exhibits a fundamental frequency around 60Hz, i.e. at the rotating speed of the engine inlet fan. These vibrations originating from aircraft engines are not intense enough to power all the functions of the WSN node by themselves. However, as will be shown later, they are sufficient for biasing the electronics associated with the TEG alone as soon as the engines start, therefore saving time with respect to the scavenging of thermal gradients alone.

The static thermoelectric energy harvesting device uses the constant spatial temperature difference without the “additional heat effect” produced by phase-change material. Static

thermoelectric generator concept is shown in figure 2.24. The use of this kind of device is much less popular due to the challenges connected with maintaining the temperature difference along the module. This major challenge is nowadays even more significant along with the MEMS thermoelectric modules. Their hot and cold sides are close to each other (0.1 mm), thus the thermal isolation between the hot and cold side is complicated. The required size for the heat spreader might be much bigger than in the case of dynamic device [5]. On the other hand, the modern thermal insulation materials along with heat exchange systems such as heat pipes or liquid cooling might be utilized to meet these requirements.

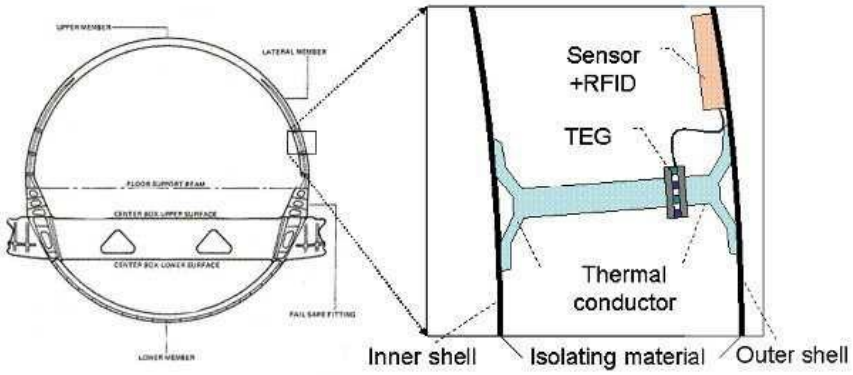

Figure 2-6: Practical realization of a static thermoelectric generator[14]

Thermoelectric energy harvesting is generally very promising for the aeronautic application. However some big issues including the thermal insulation of module sides, withstanding of harsh environments and thermal exchange specificities exist. Aircraft-specific area is very interesting – sonic load in an engine bay, effects of pressure changes, humidity – all of these phenomena affect the heat exchange. Thermoelectric generator thus represents a system strongly interacting with its ambient [8].Recent solutions are reviewed in the next chapter.

Energy harvesting devices form inherently the complex mechatronic system with all its specificities. Its design should be implemented concurrently with the design of surrounding (superior) systems and should be done with consideration of the surrounding environment. This approach leads to the minimal constrains on the harvester mass, size, and implementation [2].
There are a various suitable phenomena of energy conversion which are useful for an energy harvesting:
Thermal energy

- Temperature gradients (thermoelectric effect)
- heat (hydroelectric effect)
- Solar thermoelectric with focused light (thermoelectric effect)

- Radiant energy
- Optical energy (photovoltaic effect)
- Radiofrequency (RF) energy
- Radioactive energy
- Mechanical energy
- Liquid or gas flow
- Vibrations (piezoelectric effect, electromagnetic, electrostatic)
- Pressure variations (acoustic noise, atmospheric pressure variations
- Electromagnetic energy
- Wigand effect
- direct electromagnetic energy conversion
- Biochemical energy
- Biochemical fuel cells

Very promising area for utilization of an energy harvesting can be found in a waste heat. Freely available thermal energy sources from chimneys, hot pipes or engines can be recovered using thermoelectric or hydroelectric effects. The thermoelectric effect is the much more efficient one in the terms of Carnot's efficiency. Radiant energy is a very popular method of obtaining electric energy from autonomous device surroundings. Photovoltaic cell forms a part of every calculator while RFID takes a part in every marathon race. Energy of wind and water is commonly utilized using large-scale devices such as wind farms and water power plants. Utilization of flow energy harvesters at the micro scale is much more challenging due to the issues connected with withstanding to harsh environments. Nevertheless, some progresses in the field of MEMS micro turbines have been achieved. Other kinds of mechanical energy harvesting are using "smart" materials such as piezoelectric and dielectric elastomeric generators. Free electromagnetic energy is available in the form of oscillating magnetic fields surrounding AC power lines. This energy might be useful for power lines monitoring. Biochemical fuel cells are very promising as the "in vivo" supply for biomedical implants.

Energy harvesting systems generally consist of energy harvesting element, energy storage element and interface power electronics. The harvested power must be converted to electricity and transformed to an appropriate form for charging the energy storage element and supplying the final application. The utilization of special power electronics enables the extraction of maximum available electric power.

Each of the energy conversion methods used in an energy harvesting has its own performance

characteristics such as power density described by the power-to-weight, power-to-area or power-to-volume ratio. The illustrative example of energy harvesters' power densities is given in table 2.2 the stated values are describing the overall harvester power density. For instance,in thermoelectric generator power density comprises the heat sink weight and the vibration generator power density comprises the moving mass. The direct comprehension of energy harvesting methods in the terms of power density is misleading. The power density too much depends on the system integration. For instance, the weight of thermoelectric module in table 2.2 represents only 0.1 % of the whole system mass. The majority of TEG weight is represented by the heat sink. There is a lot of space for the "smart integration" in this field. More comprehensive overview of energy harvesting energy densities could be found in.

Table 2-2: Energy densities of different energy harvesters [5]

Harvester type and operating conditions	*Power density* [mW/kg]
Flexible silicon solar cell inside room or cabin (luminance: 1000 lx)	9
Flexible silicon solar cell on daylight (luminance: 10 000 lx)	338
Vibration generator VEH 360 (a = 0.24 m/s^2, 60 Hz)	3
Vibration generator VEH 360 (a = 0.98 m/s^2, 60 Hz)	42
Thermoelectric generator Eureka TEG1-9.1-9.9-0.8/200 (ΔT = 10K)	10
Thermoelectric generator Eureka TEG1-9.1-9.9-0.8/200 (ΔT = 40K)	34

The two most useful phenomena connected with the aircraft specific energy harvesting include thermoelectric and electromechanical energy conversion.Thermoelectric devices are advantageous for the applications on fixed-wing aircrafts while electromagnetic transducers are preferable on helicopters with significant low natural frequencies of rotor vibrations.

The further work will be focused only into the field of thermoelectric energy harvesting due to their valuable specificities for fixed-wing aircraft applications.

Aircraft-specific regulations are obsessed with a backup and redundancy of onboard systems. Sensor units placed on an aircraft propulsion system are no exception. Power supplies for these units are a subject of backup and redundancy; hence an unconventional approach to their supplying by electric power is opportune. The main task given to this thesis is a design and development of autonomous sensor unit supplied by the means of thermoelectric energy harvesting. Thermoelectric generator should be based on MEMS technology which was reviewed in the previous work [15]. The autonomous sensor unit should prospectively form a part of the Jet Engine Control Unit (JECU) produced by UNIS [19]. JECU is currently used

with the TJ100 engine from Hamilton Engine Company [20].

The main tasks given on JECU are engine start-up and stop, acceleration and deceleration and maintenance of turbine angular velocity. JECU is also taking a role of Health and Usage Monitoring System (HUMS) [23]. Reliability of these functions is critical. It's evident, that utilization of TEG into the JECU might be advantageous as a backup for the low-power electronics. An angular velocity sensor was selected as appropriate pilot application. TEG should ensure a continuous electric power delivery in the case of failure in turbine integral generator or onboard power distribution.

The key requirements for the design and development of TEG for aerospace applications based on MEMS thermoelectric module were set as follows: supplied system voltage: 3.3 V; supplied application power consumption: 100 mW (corresponds to current consumption about 30 mA); continuous operation time: 30 min; operating temperature range: -50 °C to +85 °C.

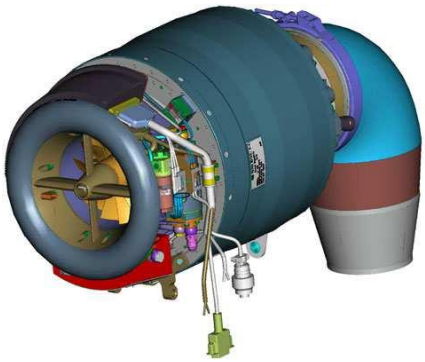

Figure 2-7: CAD drawing of TJ100 turbine with JECU (black box in the rear section) [20]

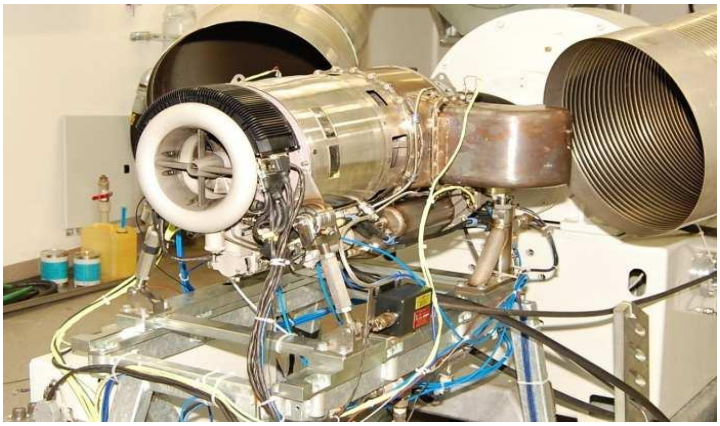

Figure 2-8: TJ100 turbine with JECU (black box in the rear section) on the test stand [20]

Above-mentioned requirements might be a subject of further changes. As an instance it can be

taken the values of supply voltage and current. These values can be decreased assuming the low- or ultra-low-power electronics design.

The hot side of TEG will be placed directly on the surface of JECU. Power electronics inside the package of JECU provide some waste heat which results in the surface temperatures of up to 80 °C. The thermography image of JECU in operation is shown in figure 2.21. The cold side of TEG will be cooled by the ambient air flow. Thus the cold side temperature might be close to the temperature of surrounding environment. The considered location of TEG represents a typical case of static thermoelectric harvesting approach. Sufficient temperature gradient is guaranteed over the dominant part of operating envelope of an aircraft.

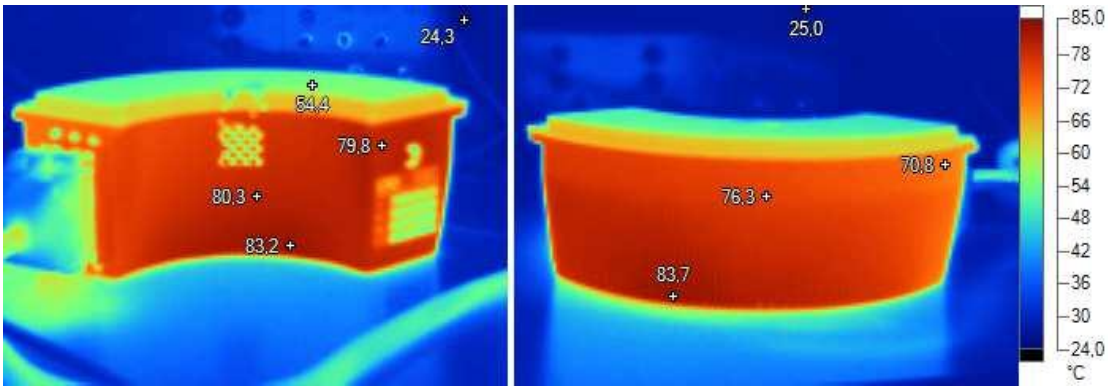

Figure 2-9: Thermography image of JECU during its operation under the maximum operating power [24]

Design of a final prototype should be done with the respect to minimal influence of JECU and turbine normal operation. Certification of TEG according to RTCA DO-160/178/254 might be a subject of future demand. Utilization of model-based design principles is a must due to the high complexness of this mechatronic system. Simulation modeling outcomes will be useful for the analogical systems such as waste heat recovery systems and systems for human body energy harvesting. A final product in the scope of this thesis is a technology demonstrator.

2.1.1 Thermoelectric Energy Conversion

Physical nature of thermal energy harvesting is the Seebeck effect. Its principal is based on the diffusion of electrons through the interface between two different materials. This diffusion is achieved by applying a heating at the junction of two materials which make a thermocouple. Heating causes the net changes in the materials and allows electrons to move from material where they have lower energy into material where the energy of electrons is higher. Because

the electrical current is exactly a flow of electrons, this effect of passing electrons from one material to another makes an electromotive force (voltage) across the terminals of thermoelectric module. Generated open circuit voltage is linearly dependent on the temperature difference between hot and cold sides of a thermoelectric module [3], [26].

$$Uoc = \alpha_{\Sigma} \Delta T \quad \textbf{(3)}$$

Where

U_{oc} is the open circuit voltage on the output terminals of the thermoelectric module,

α_{Σ} is the net Seebeck coefficient of TEM and ΔT is the temperature difference along the module ($Th - Tc$).

The net Seebeck coefficient is a characteristic parameter of each TEM.

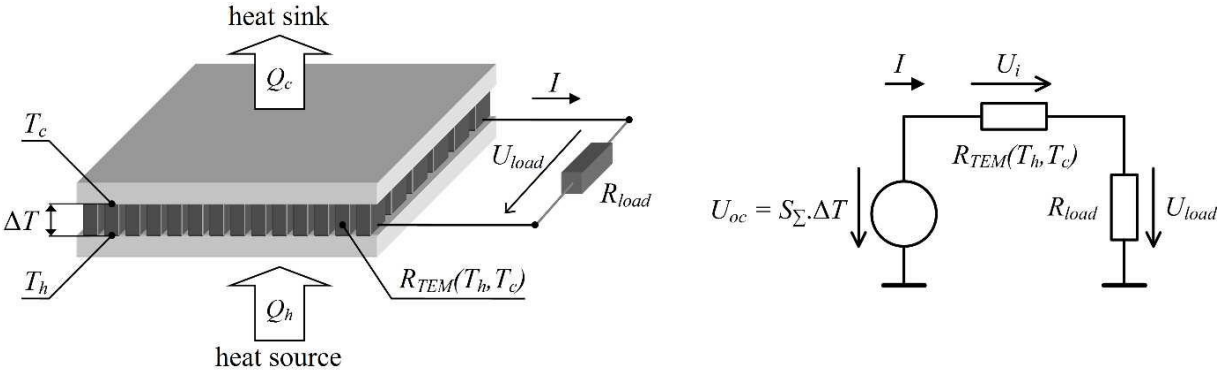

Figure 2-10: Thermoelectric module (right) and its equivalent circuit (left)

Much more interesting part of analyses comes up with the connection of TEM into a closed circuit. Situation is depicted in figure 2.22. On the right is depicted the equivalent circuit of TEM in the terms of Thevenin's theorem. Circuit is comprised of an ideal voltage source according to (Eq. 2), TEM internal resistance *RTEM* and load *Rload*. The output voltage along the load can be actually considered as the output voltage of voltage divider *RTEM* / *Rload*:

$$Uload = \frac{Rload}{Rload + RTEM} Uoc \quad \textbf{4)}$$

Thus the power which can be delivered to the load is strictly dependent on the internal resistance of module and resistance of the load connected on its terminals. The maximum power P_{MPP} which can be delivered to the load is [3]:

$$P_{MPP} = \frac{(a_{\varepsilon} \Delta T)2}{4 R_{TEN}} \quad \textbf{(5)}$$

This maximum power transfer can be achieved only under the condition:

$$R_{load} = R_{TEM} \quad \textbf{(6)}$$

This state is called the impedance match. Unfortunately, there are practically just a very few supplied applications having their internal resistance matched with energy harvester. Moreover,

the internal resistance R_{TEM} is a function of module temperature (T_h, T_C)[27],[28]. Differences between R_{TEM} and R_{load} are usually significant. Dynamic impedance matching is of high interest during the design of power management electronics for an energy harvesting device [3],[4],[6]. The dynamic impedance matching is usually implemented using a switching converter controlled by the Maximum Power Point Tracking (MPPT) driver. Further analyses of the impedance matching for TEG will be provided the cases of boost, buck, buck-boost and fly back DC/DC converters.

As a next challenge, the mechanical installation constraints have to be taken into an account when designing the thermoelectric generator. The application that is considered on JECU as stationary temperature difference source. This reasoning leads to the major simplifications. It claims that the temperature difference along the thermoelectric module is the same regardless on the heat flow through the thermal network of TEG. The applications with "soft" temperature difference sources are much more complicated. The temperature difference can rapidly drop down with inappropriate thermal network (heat spreader, heat sink, etc.).Examples of such an application are the wearable thermoelectric devices [29]. Moreover, as the thermoelectric generator is a highly complex system, its electric behavior can be significantly influenced by the thermal constraints. Then the further optimization procedures have to be involved in the solution of an appropriate TEG [30].

An interesting area is the connection of more TEMs into electric circuits. The electric schematic has to be taken into an account when considering the electrically connected non-uniform heated TEMs.Recent investigations shown that a serial connection of TEMs is more advantageous. Parallel or serial-parallel connections lead to parasitic heating of certain TEMs in the circuit. Heating is caused by the Peltier effect and yields in the temperature drop on certain modules. Thus a lower voltage and power is produced [31]. Another solution might be found in the individual module power point tracking. Each individual TEM (or string of TEMs) in such a systems has its own converter. A similar approach is used in photovoltaic. This approach is commonly used on the large arrays of bulk technology TEMs [32], [33].

For the sake of completeness should be mentioned a Carnot's character of the thermoelectric conversion. The maximum theoretic achievable efficiency of the thermoelectric energy conversion is:

$$\eta = \frac{P_{el}}{Q_h} \quad \textbf{(7)}$$

(Eq. 7)

Where P_{el} is the electric power delivered to load and Q_h is the heat flux through the hot side of module. The overall performance parameter which couples together the thermal and electric behavior of thermoelectric module is a device figure-of-merit ZT [27]:

$$ZT = \frac{a_{\Sigma}^{2}}{\lambda_{TEM}\, R_{TEM}}\mathrm{T} \qquad (8)$$

ZT is a function of the net Seebeck coefficient $\alpha\Sigma$, thermal conductivity of module λTEM and electric resistance of a module $RTEM$. The interpretation of this equation results in the need for thermal insulating modules with high Seebeck coefficient and low electric resistance. The higher the ZT is, the better the performances of TEM are. Normal value for commercial MEMS TEMs is around ZT = 0.75.

2.1.2 Load Matching

As was mentioned above, the load (or impedance) matching is of high interest in the power management electronics for energy harvesters. Load matching is usually implemented using the switching mode power supplies (SMPS). Most frequently used topologies of the following DC/DC switching converters are [34]:

Boost converter – output voltage is always greater than input voltage;

Buck converter – output voltage is lower than input;

Buck-boost converter – output voltage can be either higher or lower;

Fly back converter – isolated buck-boost converter with transformer at the input;

Charge pump-special inductorless case of SMPS, various input/output relations.

The DC/DC converter can be simplified as a two-port network.

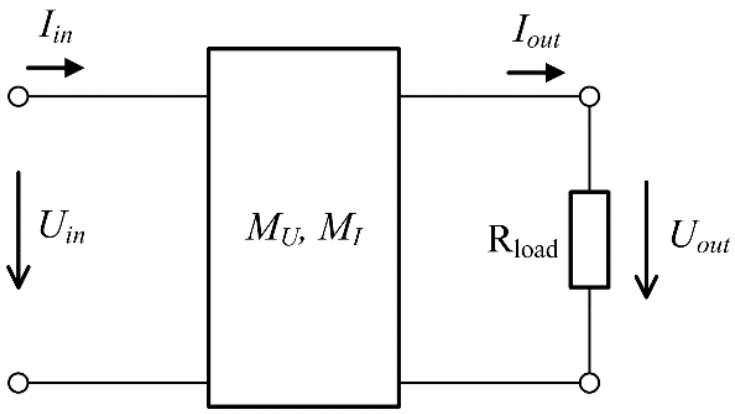

Figure 2-11: DC/DC switching converter as a two-port network

This approach is depicted according to figure 2.23 can be derived the voltage (M_U) and current (M_I) transfer functions for the two-port network of a converter:

$$M_{U=}\frac{U_{out}}{U_{in}} \quad \textbf{(9)}$$

$$M_1 = \frac{I_{out}}{I_{in}} \quad \textbf{(10)}$$

$$M_1 = \frac{1}{M_u} \quad \textbf{(11)}$$

An initial idea of the load matching is adjustment of the converter input resistance according to R_{TEM}. Output and input resistance of such a converter can be expressed as:

$$R_{in=}\frac{U_{in}}{I_{in}} \quad \textbf{(12)}$$

$$M_{U=}\frac{U_{out}}{I_{out}} \quad \textbf{(13)}$$

Which yields in the equation for the input resistance in the terms of output resistance (load):

$$R_{in=}\frac{1}{M_U{}^2}R_{out} \quad \textbf{(14)}$$

Load matching is simply the impedance (resistance) accommodation of output resistance to suitable input resistance. A DC/DC converter works as an impedance adapter. Ratio between the output and input resistance is adjusted using the duty cycle controlled switch. Load matching can be achieved using PWM driver with MPPT control. The pulsed-frequency modulation (PFM) might be considered to minimize the switching loses on low load currents [35]. PFM is usually implemented as a constant on-time or constant of-time controller. Its implementation is of rising interest among the power management circuits for energy harvesting [36]. Several designs combining the PFM and PWM with current threshold have been also introduced [37]. Figure 2.24 shows the concept of load matching on specific case of a boost converter. The switching duty cycle *D* applied on switch S can be expressed as

$$D = \frac{t_{on}}{T} = \frac{t_{on}}{t_{on}+t_{off}} = f_s\, t_{on} \quad \textbf{(15)}$$

Which demonstrates the possibility to control the duty cycle by either PWM or PFM? PWM is ensured by changing the *ton* while the PFM is implemented by the changes in switching frequency f_s with constant on-time t_{on}.

Transfer functions of M_U, M_I and R_{in}/R_{out} for the most frequently used DC/DC converters in continuous conduction mode (CCM) will be stated in the following chapters. The

comprehensive overview of SMPSs can be found in [38].

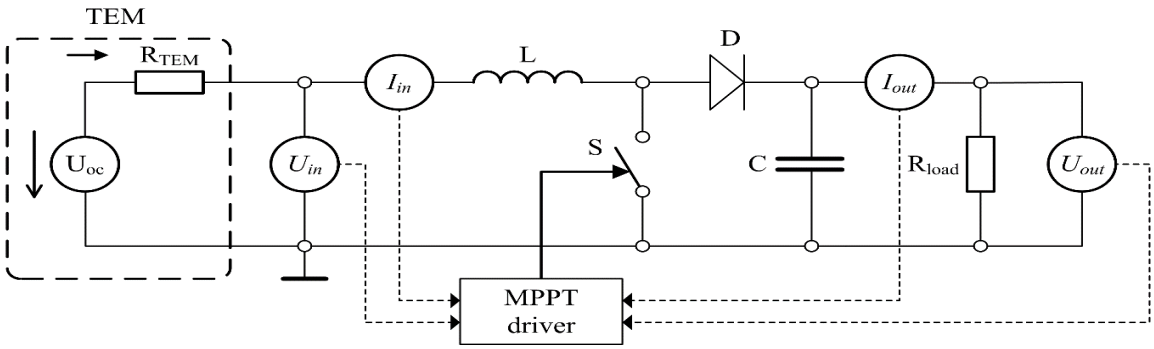

Figure 2-12: Concept of load matching (shown on a case of boost-converter)

2.1.3 Boost Converter

The boost converter under consideration is shown in figure 2.25. It is the most important converter topology in energy harvesting as the harvested voltage levels are usually quite low.

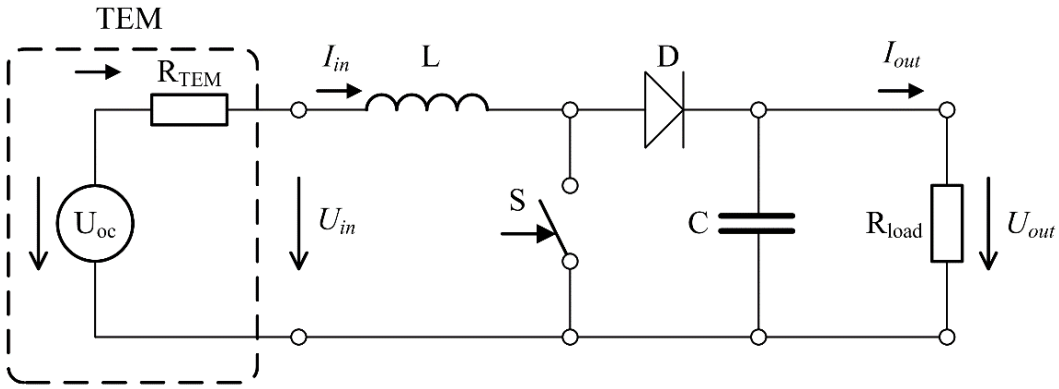

Figure 2-13: Boost converter

Voltage and current relations are:

$$M_{U,boost} = \frac{1}{1-D} \quad \textbf{(16)}$$

$$U_{out} = \frac{1}{1-D} U_{in} \quad \textbf{(17)}$$

$$I_{out} = (1-D) I_{in} \quad \textbf{(18)}$$

Combination of Eq. 13-15 yields in the function describing the input/output resistance:

$$R_{in} = (1-D)^2 R_{out} \quad \textbf{(19)}$$

Duty cycle for the maximum power point condition (Eq. 5) can be expressed as:

$$D_{MPP,boost} = 1 - \sqrt{\frac{R_{TEG}(T_h T_c)\, I_{out}}{U_{out}}} \quad \textbf{(20)}$$

Note, that the internal resistance of module $RTEM$ is a function of module temperature. Figure 2.26 shows the maximum achievable ratios between the output and input voltages with appropriate load and source resistances. A converter is not capable of providing the "unlimited" conversion ratio.

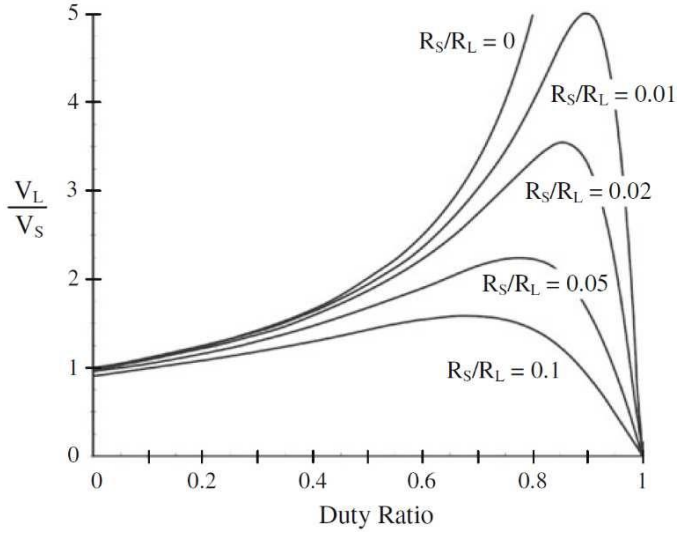

Figure 2-14: Output/input voltage as a function of duty cycle for different relations between source and load resistance when operating the boost converter [39]

2.1.4 Buck Converter

Typical example of a buck converter is shown in figure 2.21. Output voltage of a buck converter is always lower than input. This type of converter is advantageously used in photovoltaic or piezoelectric energy harvesting applications.

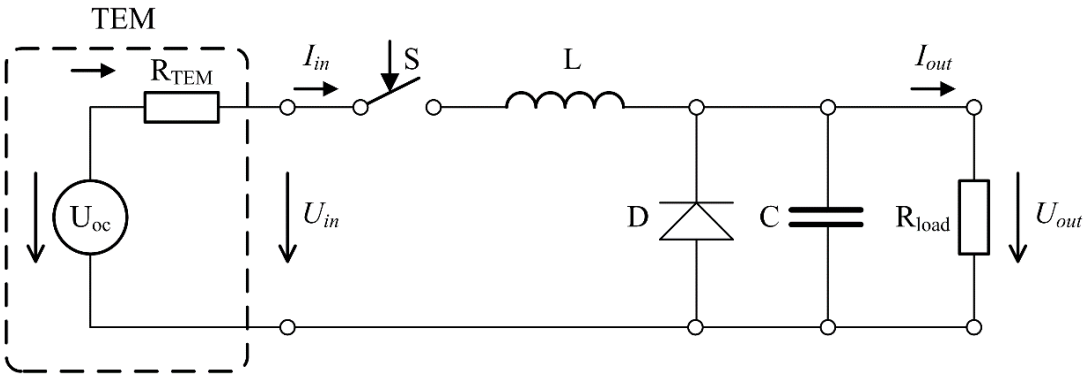

Figure 2-15: Buck converter

Equations describing the operation are:

$$D_{MPP,buck} = D \tag{21}$$

$$U_{out} = DU_{in} \tag{22}$$

Desired relation between the input and output resistance can be expressed as:

$$I_{out} = \frac{1}{D^2} R_{out} \tag{23}$$

and a combination with MPP condition yields in:

$$D_{MPP,buck} = \sqrt{\frac{U_{out}}{R_{TEG}(T_h T_c) I_{out}}} \tag{24}$$

2.1.5 Buck-Boost Converter

Buck-boost converter is widely used and implemented in many commercial integrated circuits for energy harvesting. Its application area covers all the kinds of energy harvesting. Typical example is given in figure 2.250.

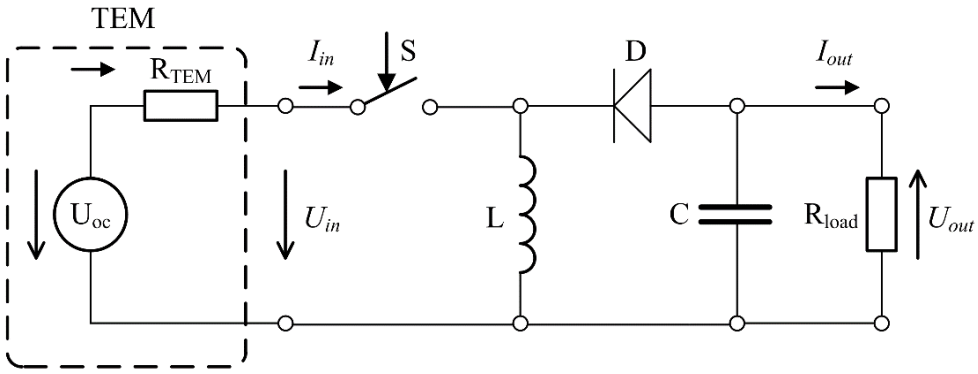

Figure 2-16: Buck-Boost converter

Basic voltage and current equations for a buck-boost converter in CCM are:

$$M_{U,buck-boost} = \frac{D}{1-D} \tag{25}$$

$$U_{out} = \frac{D}{1-D} U_{in} \tag{26}$$

$$I_{out} = \frac{1-D}{D} I_{in} \tag{27}$$

Input resistance is:

$$R_{in} = \left(\frac{1-D}{D}\right)^2 R_{out} \tag{28}$$

and the maximum power point is achieved under the duty cycle set according to:

$$D_{MPP,buck-boost} = \frac{1}{1+\sqrt{\frac{R_{TEG}(T_h,T_c)I_{out}}{U_{out}}}} \quad (29)$$

2.1.6 Fly back Converter

Flyback converter is capable of providing the output voltages much higher than input. Its typical application lays in power management for thermoelectric generators operating with very low temperature differences. Input voltages are starting at tens of mV [40], [41]. The control electronics of commercially achievable flyback converters is usually separately supplied using charge pumps which allow these very low start-up voltages. Typical operating scheme is shown in figure 2.251.

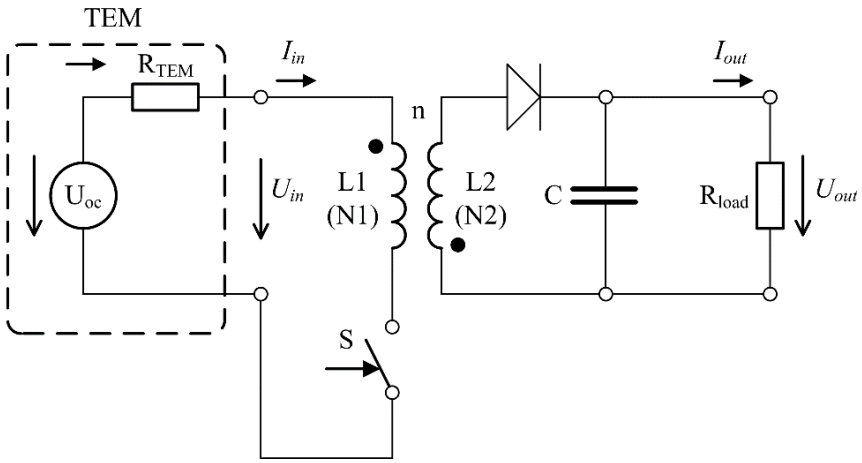

Figure 2-17: Flyback converter

Flyback converter has an isolated input ensured by the input transformer with turn ratio *n*. Operation voltages and currents are described as:

$$M_{U,flyback} = \frac{D}{n(1-D)} \quad (30)$$

$$U_{out} = \frac{D}{n(1-D)} \quad (31)$$

$$I_{out} = \frac{n(1-D)}{D} \boldsymbol{I_{in}} \quad (32)$$

This yields in required function for input resistance:

$$R_{in} = \left(\frac{n(1-D)}{D}\right)^2 R_{out} \quad (33)$$

and a maximum power transfer is achieved under the condition:

$$D_{MPP,buck-boost} = \frac{n}{1+\sqrt{\frac{R_{TEG}(T_h,T_c)I_{out}}{U_{out}}}} \quad \textbf{(34)}$$

2.1.7 Maximum Power Point Tracking (MPPT)

The key problem of load matching is the lack of direct measurement of internal resistance R_{TEM} during the operation. For the maintenance of $DMPP$ belonging to maximum power point can be employed various maximum power point tracking methods. MPPT for applications in thermoelectric is taken over the established photovoltaic solutions [42]. The most common methods used in recent TEGs are Perturb and Observe (P&O) and Fractional Open-Circuit Voltage (FOCV). FOCV method is periodically disconnecting the TEM from converter. Consequently, an open-circuit voltage on the terminals of TEM is measured. FOCV is based on the observation that MPP voltage can be obtained as a fraction of open circuit voltage:

$$U_{MPP(U_{oc})} = kU_{oc} \quad \textbf{(35)}$$

Duty cycle is then set to maintain the $UMPP$ input voltage which ensures the maximum power transfer. Typically, k = 0.5 is used in the most of TEG applications.

At first are measured values of the input current and voltage which are entering the algorithm. As the next step is computed the exact power on the input terminals of DC/DC converter.

P&O method is perturbing the duty cycle and adjusting its new value based on the measurement of voltage and current on the input terminals of a switching converter. Factually, it's a search for a power maximum in the terms of D. Flowchart of the algorithm is provided in figure 2.252. The biggest disadvantages of this method are the oscillations around the MPP. System is not absolutely stable [39],[42]. It's the most frequently used MPPT algorithm for harvesting higher currents.

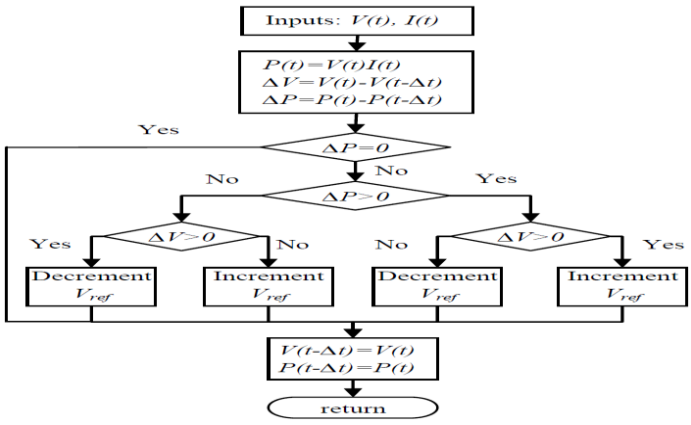

Figure 2-18: Flowchart of P&O algorithm [43]

2.2 Review of Literatures

2.2.1 Architecture of multi source battery free energy generator

As already mentioned, the large deployment of wireless sensors, in particular for SHM is still limited by the issue of energy autonomy of the sensor node. Energy harvesting is an attractive solution to provide battery lifetime extension or even almost infinite autonomy to a battery-free sensor node. In this context, many authors have contemplated multisource harvesting to achieve a generic power generator for wireless sensors. In four sources (solar, vibrations, RF, thermal gradients) are combined and in thermal energy harvesting is coupled to RF power to charge a micro battery. Both papers mainly focus on the validation of multi harvesting concept and its related power management. In both cases, the storage unit is placed after the voltage regulation block. Even more complex multi-source energy platforms have been theoretically envisioned in the literature The main originality of the architecture consists of complementary energy sources for a rapid start-up of the self-powered battery-free system. It was initially motivated by aeronautics applications but is also applicable to other SHM scenarios and is compatible with other energy sources. The basic principle is to use a TEG as the primary source of energy whereas a piezoelectric generator is used as a secondary source. The latter one provides the necessary bias for the rectifier circuit required for the TEG and partially compensates the WSN node energy consumption during cruise over a long flight. The energy provided by the secondary source, through a voltage doublers with external Cin capacitor, is stored after rectification in a small capacitor Cobias that biases the voltage reference circuit (PTAT/BGR block). This circuit provides the bias current for the amplifiers in the active diodes. Once activated, these diodes low harvesting energy from the TEG and storing it in ultra capacitors (UC1 and UC2) to be chosen with optimized leakage currents to minimize losses. Consequently, depending upon ultra capacitors charge level, power captured is not permanently maximized. Finally, voltage regulation is implemented using a low-dropout (LDO) regulator based on a PMOS power transistor. The energy generator should be able to supply a wireless sensor node. To allow an adequate use of the available energy, a careful power management of the WSN node (appropriate periodic measurement and communication, sleeping mode management) has to be implemented to save energy.

The main design challenges for the energy generator are:

- Firstly, maximizing the transfer of energy from the transducer to the storage devices.
- Secondly, as the voltage on the ultracapacitor storage devices will vary according to their discharge, a voltage regulation needed. In this case, priority should be given to conversion efficiency.
- For both of these design challenges, another important requirement is micro compatibility thus prohibiting the use of bulky passive devices as the ones needed for some impedance matching strategies for example.
- Finally, harvested energy being limited, the quiescent power consumption of the energy generator should be as low as Possible. This is required for two reasons: the first one is that many SHM scenarios are using duty cycles with much longer periods in quiescent mode than in the active one and the second is related to the self-discharge current of ultra capacitors Which is in the order of µA? The quiescent current of the power converter should not be higher than this value or even be made negligible compared to it. A trade-off will then have to be made between efficiency and power consumption.

For this latter challenge, it's decided t o minimize the number of transistors for the design of each analog block of the circuit to have efficient system.

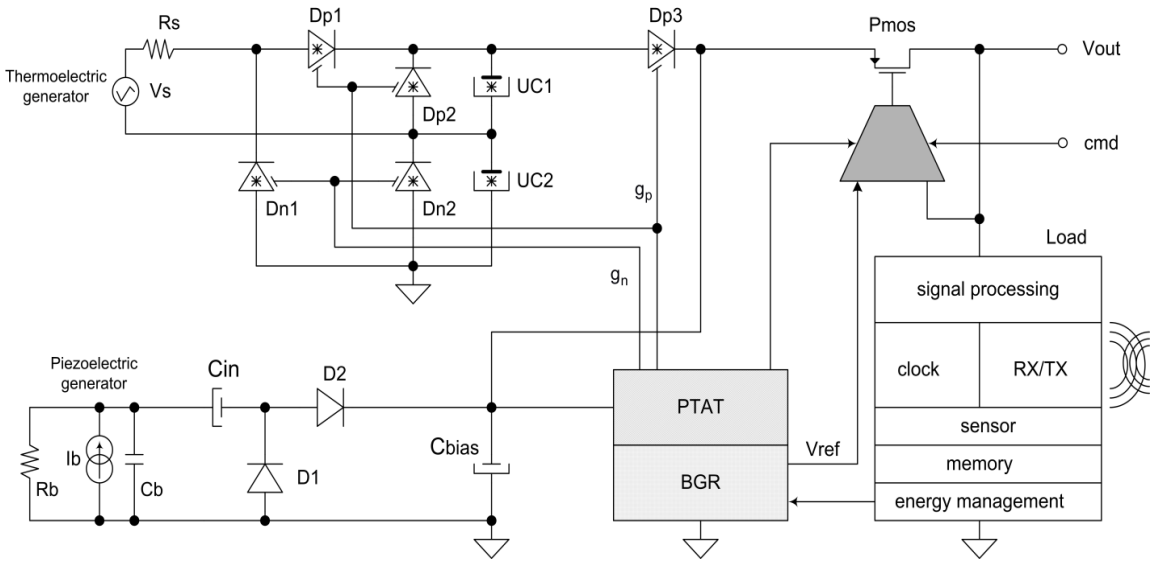

Figure 2-19: Electrical schematic of the proposed battery-free multisource energy generator connected to a sensor node

Diode symbols (Dp1, Dp2, Dn1, Dn2, Dp3) labeled with * are active diodes (see electrical schematic in figure 2.254) and capacitor symbols (UC1 & UC2) labeled with * are ultra capacitors. PTAT/BGR block provides the bias current for the active diodes and the voltage reference for the LDO. The energy

transducers are represented by their respective electrical model.

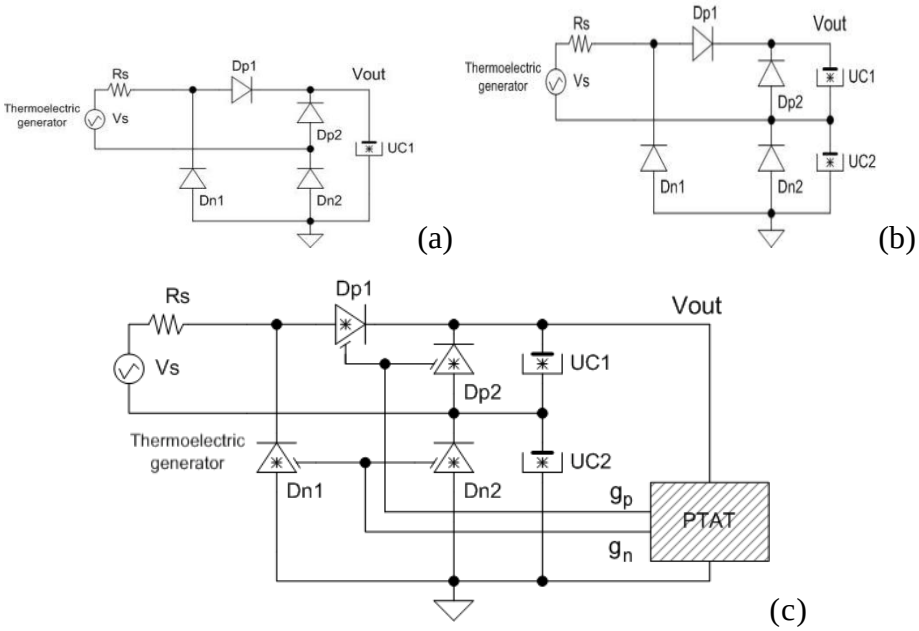

Figure 2-20:

(a).Electrical schematic of the proposed battery-free multisource energy generator connected to a sensor node

(b).Use of two storage devices, UC1 and UC2, to maximize energy transfer

(c).Optimized solution with active diodes and two storage devices

2.2.2 Energy transfer maximization

As the energy harvested through thermal gradient results in two voltage polarities, even if there is only one polarity switching, a rectifier circuit is mandatory before storage. The classical solution consists in using a diode bridge such as the Grates circuit, figure 2.254(a). The first drawback of this solution is that it does not allow maximizing the transfer of energy. For example, if the first voltage alternation is higher than the second one (it is the case in figure 4), it will not be possible to harvest the energy from this second alternation. To cope with this problem, the solution consists in implementing two ultra capacitors for the storage as shown in figure 2.254(b): UC1 for the positive alternation and UC2 for the negative one. The second drawback of the Grates circuit is that two diode thresholds are lost for the rectification of each voltage alternation.

To avoid this power loss, It is then implemented the Grates circuit using active diodes [74-76] as shown in figure 2.254(c). However, as shown in figure 2.255, the active diode requires a voltage reference circuit to bias the amplifier (g_n an g_p bias signals provided by

PTAT block in figure 2.254 (c). The design of this amplifier is critical and three important properties are required:

- Ultra-low power consumption to comply with our requirement of a low quiescent current of the full converter.
- Threshold voltage of MOS transistors as low as possible and independent of process variations as well as layout mismatching. The main issue could be the oscillation of the driving signal provided by the operational amplifier to the gate of the MOS switch. For example, in the 0.35µm HV CMOS technology, we used isolated high-voltage (20V) MOS transistors with a typical threshold voltage of 0.5V
- High DC gain.

  This latter condition, although requiring large size transistors, guarantees the second condition.

  For the start-up of the active diodes, a minimum voltage around 0.9V (V_{th} + V_{Dsat}) is required to bias the current mirrors and the differential pairs shown in the electrical schematics of figure 2.255. Once this voltage is reached, the threshold voltage of the active diode is given by the source to drain voltage of the MOSFET switch. Thanks to the regulation loop introduced by the operational amplifier that is designed with a high DC gain, this voltage is equal to the offset of the operational amplifier and can then be very small (few tenths of mV are targeted) compared to a classical diode threshold voltage. Nevertheless, before reaching this start-up voltage, the parasitic body diode of the MOSFET switch allows starting the rectifier with a standard diode threshold (~ 0.7V). In the case of totally discharged ultra capacitors and a single energy source (namely TEG), several minutes are needed to reach 0.9V.

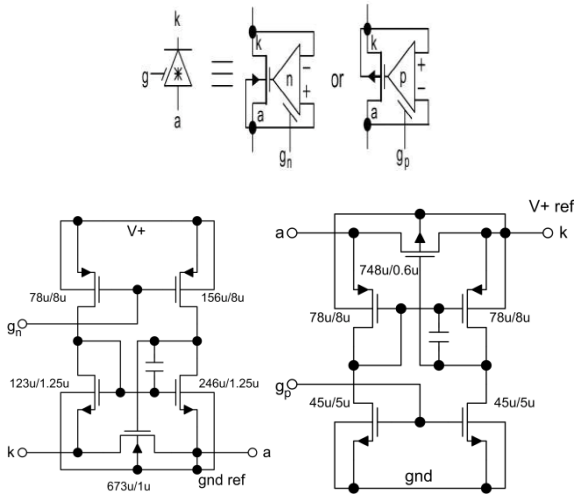

Figure 2-21: Symbols (top) and electrical schematic for the active diodes Dn

2.2.3 Energy efficiency

The design is optimized with the objectives to get a threshold voltage in the range of 10 mV whereas minimizing the quiescent current consumption in the range of few hundreds of nA. To generate such a low bias current (10nA/branch), It is designed a nanowatt voltage and current reference [77-79]. To this purpose, the combined subthreshold MOS devices with transistors working in the linear region and did not use any resistor as shown in figure 2.256.

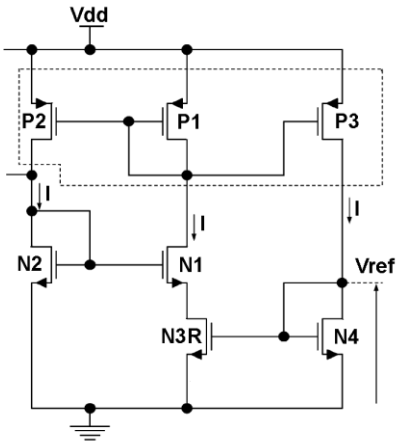

Figure 2-22: Proposed nana watt voltage reference.

In this circuit, all transistors are working in saturation except N1 and N2 NMOS transistors that are in weak inversion (subthreshold region) and N3R, a very long channel transistor operating in the linear region, which acts as a high-value resistor[22].Since N1 and N2 are working in the subthreshold region, the source voltage of N1 and then the drain voltage of N3R are given by:

$$V_{SN1} = V_{DN3R} = U_T \ln\left(\frac{S_{N2}S_{P1}}{S_{N1}S_{P2}}\right) \quad \textbf{(36)}$$

Where UT=KT/q thermal voltage, proportional to absolute to absolute temperature(PTAT),and SN1,SN2,SP1,SP2 are W/L ratios of the respective MOSFETs.

As a result, the current flowing in N3R transistor is:

$$I = \frac{U_T}{R_{onN\ 3R}} \ln\left(\frac{S_{N2}S_{P1}}{S_{N1}S_{P2}}\right) \quad \textbf{(37)}$$

with R_{onN3R}, the on-resistance of N3R transistor. This current is then proportional to the

absolute temperature. To define a very low reference current (~10nA), a high value resistor 5Mohm is needed. To reach such a value, the channel length of N3R transistor was designed as long as 330µm. It has to be noticed that, for matching reasons, N4 transistor has also the same very long channel.

The expression of the reference voltage V_{ref}, that is equal to the gate voltage of N_4, is the following:

$$V_{ref} = \sqrt{\frac{2I}{\beta_{N4}}} + V_{th} \quad \textbf{(38)}$$

Where β_{N4} is the transconductance of transistor N4 and V_{th} its threshold voltage. Since V_{th} has a negative temperature coefficient, V_{ref} can be made independent of temperature. The value of V_{ref} can then be adjusted though the size of transistors. It is chosen to define it at 0.8V. In the 0.8µm SOI CMOS technology, respective aspect ratios W/L in µm of the transistors are: 60/30 for P1, P2 and P3, 20/20 for N_1 and 160/20 for N2, 6.4/330 for N3R and 3.2/330 for N_4.

A very similar current source sub circuit was proposed by Ueno et al [80] to generate a nano watt voltage reference. The main differences are the choice of using all the transistors in the sub threshold region except for the long-channel transistor, a more complex bias voltage subcircuit and the need for a start-up circuit. Compared to our proposed voltage reference, it has better performance regarding temperature sensitivity (15 ppm/°C vs 290 ppm/°C) and line sensitivity (20 ppm/V vs 800 ppm/V).

Nevertheless, the reduced number of transistors of our proposed voltage reference allows a very low quiescent power consumption of 600 nW with a 3V power supply for the whole multisource converter to be compared to the 300 nW at 1.5V for the single voltage reference circuit.

In addition, to limit the effects of process mismatches, particular care was taken for the layout and routing of the amplifier and voltage reference circuit (use of dummy devices, common centroid patterns...). Moreover, the very long channel transistors, N3R and N4, are designed in an isolated well including guard rings and good well contacts to insure a constant biasing of the substrate along the long channel.

As mentioned earlier, the originality of the proposed energy generator circuit is the

combination of the TEG with a piezoelectric transducer to provide a rapid start-up of the energy scavenging from the TEG and a complementary source of energy during cruise.

Another important parameter that allows maximizing the energy transfer is the value of the storage ultracapacitor (UC). The time required to charge an UC depends on the time constant R_S.UC of the circuit. This is particularly relevant since the energy generation is only transient during take-off and descent. If the value of the UC is too small, it will be rapidly charged but its maximum operating voltage, together with its small value, will limit the stored energy. On the contrary, if its value is too large, the time constant will prevent collecting the maximum of energy since the UC will not have the time to reach the voltage saturation. To optimize this trade-off, it is better to analyze the charge of an UC via an ideal diode during the aircraft take-off and compared the open-circuit voltage to the one of a matched load. In our case, given the fact that two UCs in series, the optimized value of each one is 1F It has to be noticed here that the piezoelectric transducer can also directly provide energy to the output, the active diode Dp3 providing isolation from the UCs since the piezoelectric transducer would not be able to directly charge them given the very small current (~µA) generated by mechanical vibrations in the aeronautics environment. However, this direct connection to the output V_{OUT} could be very useful to provide energy to the WSN node either on ground, as soon as aircraft engines start, or during long flights (several hours) since in these cases, the TEG might be inactive.

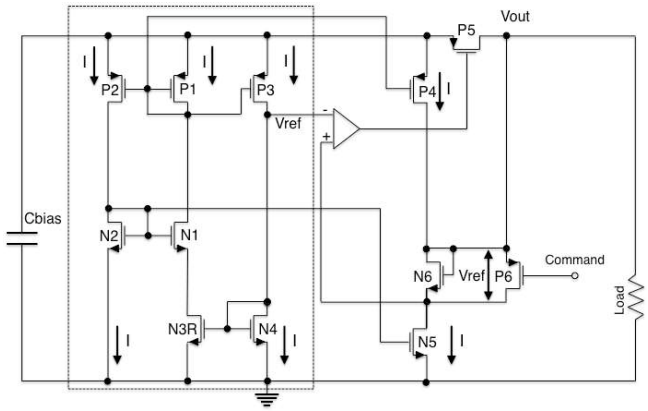

Figure 2-23: Electrical schematic of the LDO

Electrical schematic of the LDO with the proposed voltage reference circuit and the capability of generating two regulated output voltages, V_{ref} or $2V_{ref}$, according to the command on transistor P6.

Finally, a voltage regulation stage is required after the UC. Ideally, it should exhibit high conversion efficiency. The best candidate would be a switching regulator. However, given

its complexity, in terms of quiescent power consumption, it will be less efficient than a simple linear regulator. A low-dropout regulator (LDO) using a PMOS power transistor is implemented because of its simpler driving (no charge pump needed). The proposed nanowatt band gap reference (BGR) circuit based on MOS devices allows providing the voltage reference for the LDO that is designed to supply a maximum peak current of 20mA.

The proposed energy generator provides two regulated voltage values: V_{ref} or $2V_{ref}$ that can be switched using an external command (figure 21). It has to be mentioned that in this circuit, N3R, N_4 and N_6 transistors have both a very long-channel and can be designed in the same isolated well.

Regulated voltages are required for supplying signal processing and memory circuits. For less sensitive circuits, a direct power supply from the UCs could be implemented. This would have the advantage to greatly increase the global efficiency.

Opportune spot for its placing is shown in below, Temperature gradient is provided by the engine waste heat and ambient environment [8].

Figure 2-24: Opportune spot for placing of TEG on the pylon fairing of Airbus A380 [13]

Power density of this particular aircraft-specific TEG is around 4 W/kg[7], [16], [17].

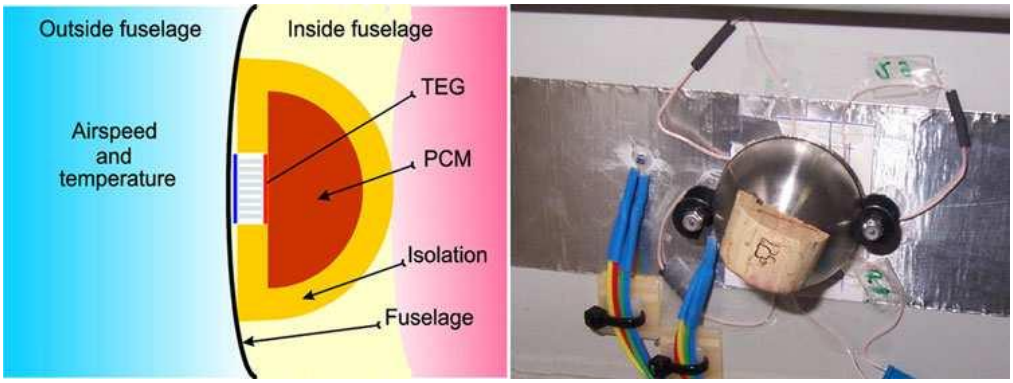

Figure 2-25: CAD drawing and sample Home based realization of the TEG system

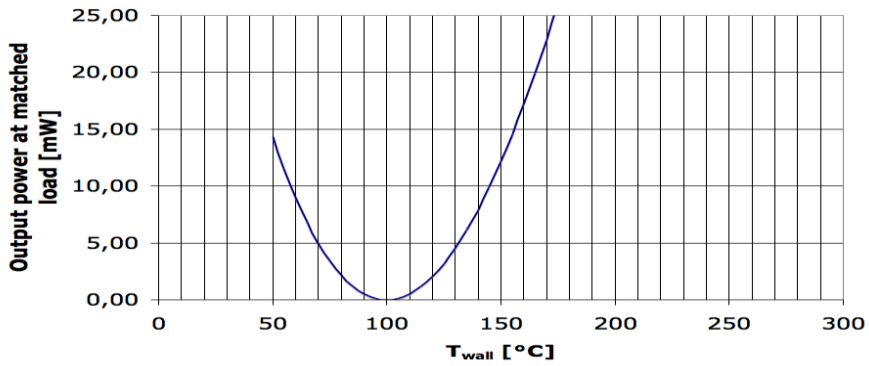

Figure 2-26: The sensor is here supposed to be submitted to a temperature of 270°C. The continuous curve represents the output power of a TEG.

All of the reviewed TEG applications in aerospace are mainly focused to the powering of autonomous sensor nodes for the structural health monitoring by the means of energy harvesting. My proposed application is focused to the new field of power backup for already supplied systems. Such a system is in normal operating states fed from an on-board power distribution bus of an airplane.

Chapter Three

3. Data collection and experimental analysis

The practical design and development of MEMS thermoelectric generator for aerospace applications have started with a necessary technology review and components review. The available commercial-of-the-shelf (COTS) components were selected. The most critical parameters of these components were consequently investigated. Components covered in the overview include thermoelectric modules from the two established MEMS TEM manufacturers – Micropelt GmbH and Laird Technologies (formerly Nextreme Thermal Solutions, Inc.). Various energy storage elements including modern thin-film batteries and supercapacitors are compared. As a base for the development of power management were selected some special purpose integrated circuits.

3.1 MEMS Thermoelectric Modules

There are only a few existing commercially achievable MEMS thermoelectric modules. Micropelt GmbH and Laird Technologies (formerly Nextreme, Inc.) are two rare examples. Two very different thermoelectric modules were chosen for the further experiments. Micropelt TGP-751 is a thin-film generator encapsulated in standard package [44]. See figure 3.1 for disambiguation. This approach ensures an easy manipulation with such a MEMS generator. Dimensions of this thermo generator-in-package are depicted in figure 3.2. The footprint is around 10x15 mm which guarantee the easy soldering and mounting operations. On the other hand, eTEG HV56 from Nextreme, Inc. is genuine MEMS [45]. Its footprint is around 3 x 3 mm which makes a manipulation with this device very difficult.

The electric-end mounting- related parameters are listed in table 3.1, Comparison of thermoelectric generators suitable to select appropriate TEG. Generally, the eTEG HV56 is a harder voltage source with internal resistance around 10 Ω. On the other hand, Micropelt TGP-751 provides the higher output voltages while its internal resistance is much greater (300 Ω).

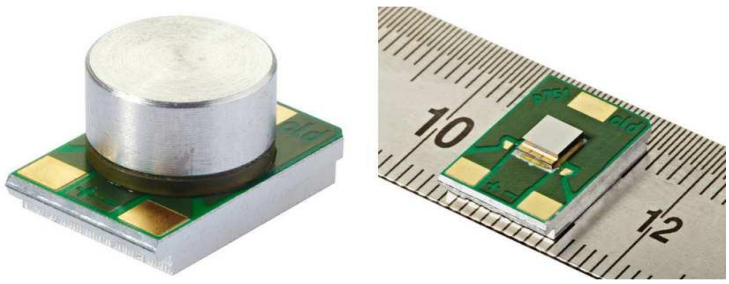

Figure 3-1: Micropelt TGP-751 (left: in package, right: with removed package) [44]

Table 3-1: Comparison of thermoelectric generators suitable for our application

	Nextreme eTEG HV56	Micropelt TGP-751
Uoc (ΔT = 10 °C) [V]	0.26	1.25
PMPP (ΔT = 10 °C) [mW]	1.5	1
UMPP (ΔT = 10 °C) [V]	0.13	-
IMPP (ΔT = 10 °C) [mA]	12	-
Isc (ΔT = 10 °C) [mA]	24	-
Footprint [mm]	3.31 x 3.12	15 x 10
Square area [mm^2]	10.34	150
Thickness [mm]	0.57	9.3
m [g]	-	2.2
Th [°C]	25 ÷ 200 °C	-
Tc [°C]	0 ÷ 50 °C	-
ΔT [°C]	10 ÷ 200 °C	-
max *Tavg* [°C]	150	100
Operating *T* [°C]	-	0 ÷ 85 °C
Storage *T* [°C]	-	-20 ÷ 85 °C
Number of tcs [-]	72	540
Rthermal [K/W]	13.1	18
RTEM [Ω]	10.7	250 ÷ 350, ref: 300 (*Tavg*=25 °C)
$\alpha\Sigma$ [V/K]	25	110

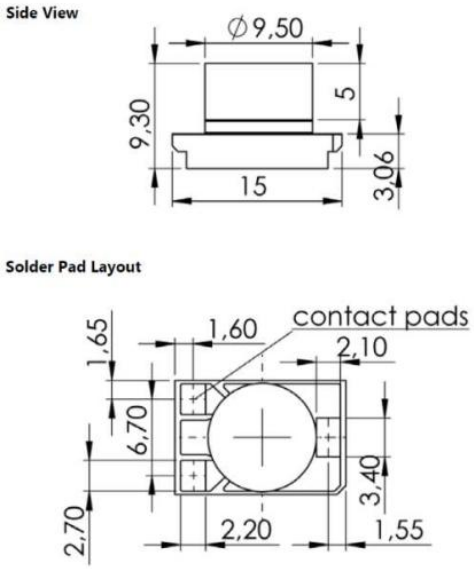

Figure 3-2: Micropelt TGP-751 dimensions (in mm) [44]

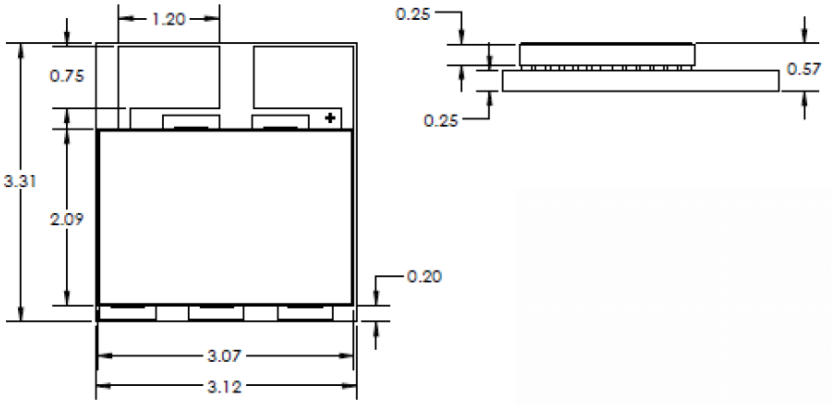

Figure 3-3: Nextreme eTEG HV56 dimensions (in mm) [45]

The main reason for the limited commercial market with MEMS TEMs is the length of its research and development process [46].The way from the new thermoelectric material to the fully-functional module takes at least 5 years.

3.2 Electronics

Power management electronics for energy harvesting is usually based on a special switching mode power supplies (SMPS) embedded in purpose-built integrated circuits. These circuits are necessarily equipped with the MPPT control algorithm. Some mature solutions are based on shunt regulators or SMPSs without an MPPT option. As an example may be taken MAX1770[47] or step-up converter directly embedded into the RF modules from Micropelt GmbH[44].

Hardware implementation of power management electronics for the energy harvesting is of rising interest amongst integrated circuits manufacturers. Various specialized ICs are commercially available. The main customer requirements for energy harvesting power management electronics include the Ultra Low Power (ULP) operation, minimum of external components and efficient MPPT algorithm. New trends in ULP electronics replace PWM by the Pulse Frequency Modulation (PFM) for a more efficient operation on low load currents. Key parameters entering the design process are the input/output voltages and currents delivered by TEM and consumed by supplied application.

Table 3.2 sums up the most prospective ICs for our thermoelectric generator. Different ICs are compared in terms of implemented converter type, MPPT algorithm, input voltage range (U_{in}), output voltage range (U_{out}) and maximum output current ($I_{out,MAX}$). Selected ICs are tailored for the use without an external electromagnetic transformer. An innovative PFM is implemented in

Texas Instruments bq25504 [48]. SPV1040T from ST Microelectronics combines P&O algorithm adopted from photovoltaic's and requires minimum of external components [49]. SPV1040 is implemented in practical TSOOP8 package. SPV1050 is a brand new buck-boost ULP IC in the stage of prototype [50]. LTC3105 is a long-proven energy harvesting solution from Linear Technology. This integrated circuit enables the connection of external U_{ref} voltage for adjusting the MPP [51]. The above-mentioned integrated circuits are quite simple since their application circuit contains only one inductor. Another opportunity is the use of commercial flyback converters [40], [41] whose applicability is usually advantageous with the very low start-up voltages. For instance, the LT LTC3108 chip provides a start-up option form as low as 20 mV of input voltage. ICs from Linear Technology are usually more complex and provide a various output voltage options including LDOs.

Integrated circuits ST SPV1040T and TI bq25504 were selected for the design and build of a functional technology demonstrator. The selected ICs are implementing a different MPPT algorithm which allows a proper evaluation and final selection of the TEG electronic hardware.

Table 3-2: Prospective ICs for thermoelectric energy harvesting

	Conv. Type	MPPT	*Uin* [V]	*Uout* [V]	*Iout,MAX* [mA]
TI bq25504	Boost	FOCV	0.13-3.0	2.5-5.25	300
ST SPV1040T	Boost	P&O	0.3-5.5	2.0-5.2	1800
ST SPV1050	buck-boost	FOCV	0.18-5.3	2.1-5.3	70
LT LTC3105	Boost	FOCV	0.25-5.0	1.4-5.0	500
LT LTC3129	buck-boost	FOCV	1.92-15	1.4-15.75	200

Energy storage element for aerospace industry has to meet a lot of specific requirements. The main issues are connected with temperature range according to aircraft operation envelope. These requirements are met very difficult by the mature battery technology. Overview is presented in table 3.3. The decision tree when considering a new energy storage element for an aircraft application can be seen in figure 3.4.

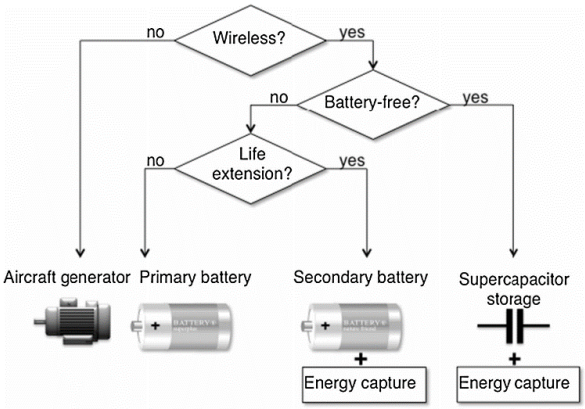

Figure 3-4: Decision tree when considering a new aircraft-specific storage element [8]

The new promising technologies are supercapacitors or ultracapacitors [17],[52]-[54]. It's still a new technology suffering for the low energy densities. On the other hand the extensions in lifetime and applicable operation temperatures are significant. The tiny thin-film batteries which can be directly embedded into chips on a wafer create a special instance of energy storage elements. Their classification is somewhere between supercapacitors and classic chemical batteries. Their use is especially advantageous in the combination with ULP electronics. Relatively high internal resistance (tens of Ω) is a special feature of thin-film batteries.

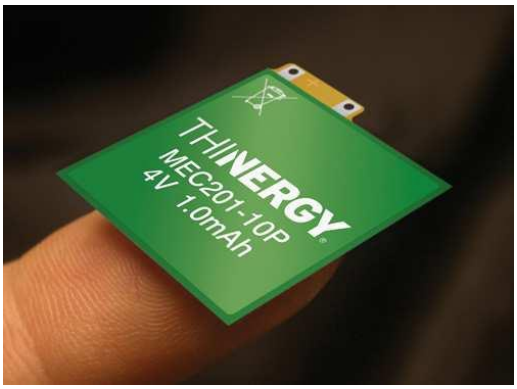

Figure 3-5: THINERGY thin-film battery [55]

The mature electric energy storage technologies have not been considered for the application. Their main disadvantages include the blocking effects at low temperatures as well as troubles under the high temperature conditions.

Table 3-3: Comparison of various energy storage elements

Energy storage principle	Rated (cell) voltage [V]	Energy density [Wh/kg]	Capacity [Ah] or [F]	Number of charging cycles	Operation temperature [°C]
NiMH	1,2	80	0,01 – 10 Ah	max. 1000	5 °C – 45 °C
Li-Ion	3,7	200 – 500	0,1 – 10 Ah	max. 1200	-10 °C – 45 °C
Li-Pol	3,7	300 – 400	0,1 – 5 Ah	min. 1200	-10 °C – 45 °C
Supercapacitor	2,5/3,5	5 – 6	0,1 – 100 F	1 000 000	-40 °C – 85 °C
Thin-film bat.	4	550	0,1 – 5 mAh	10 000	-40 °C – 85 °C

Supercapacitors are recently produced by a lot of established component manufacturers. Companies such as AVX, Maxwell Technologies, Celery, Cooper Bussman, Panasonic, WIMA or Kemet produce a broad variety of supercapactiors. Some of them are classified as "extended temperature range"

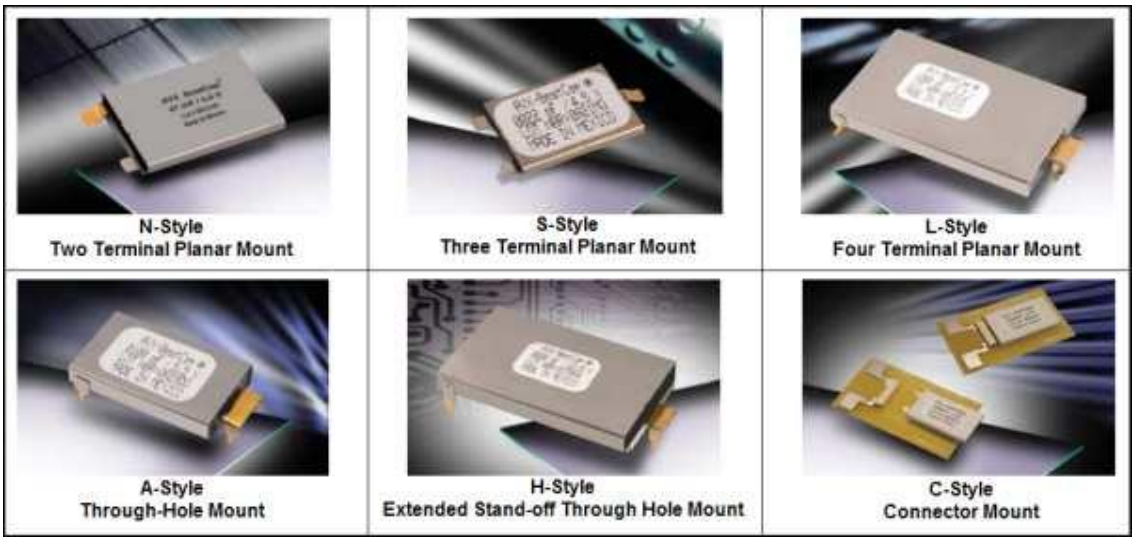

Figure 3-6: AVX BestCap series[55]

The main problem with the temperature changes over the operation range lies in the corresponding changes of internal resistance of the supercapacitor. Typical characteristics of Maxwell supercapacitors over the temperature range are depicted in figure 3.7. Nevertheless, the characteristics vary with temperature; the biggest advantage of supercapacitor is the low freezing point of the organic electrolyte. This feature prevents the damage on low operating temperatures.

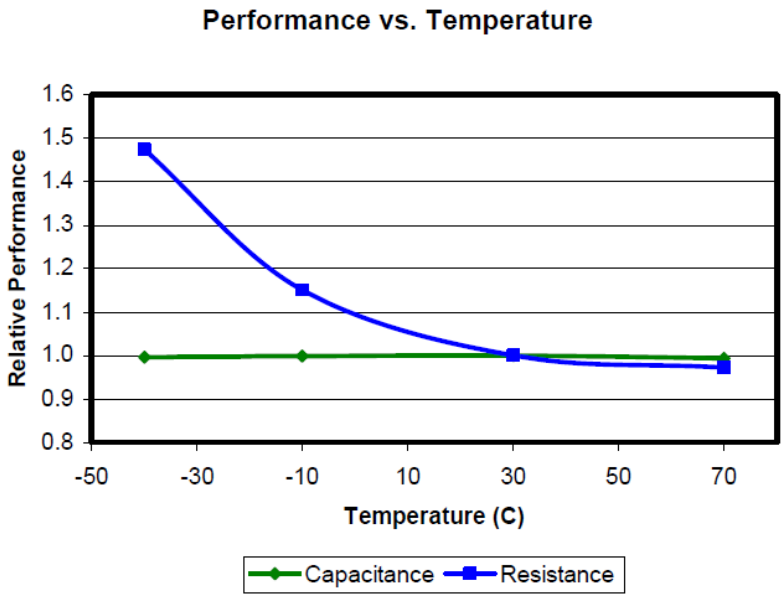

Figure 3-7: Increase of internal resistance with low temperatures for a supercapacitor [53]

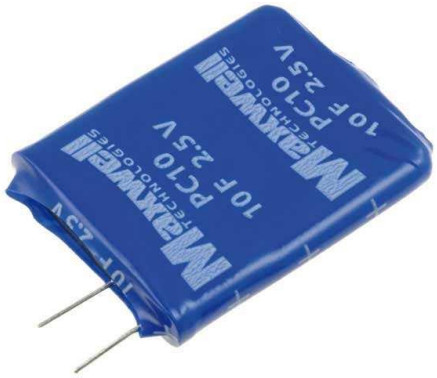

Figure 3-8: 10F supercapacitor by Maxwell [55]

As an appropriate solution for our application were selected the AVX BestCap ultra-low ESR supercapacitors. Their capacitance is up to 1 F. AVX provides these ultracapacitors in attractive packages as mentioned in figure 3.8. Interesting for further testing would be also the 10F PC-series ultracapacitors from Maxwell. Manufacturer provides also the extended temperature range versions applicable in aerospace industry. The extended temperature lies in the span -40 ÷ +85 °C [54].

3.3 Experiment

In as much as the data about MEMS TEMs provided by manufacturers are very poor, the development of custom testing procedures for evaluation purposes is essential. Applications of COTS components in aircraft industry require a much broader spectrum of testing procedures than industrial applications. Characteristics of electrical components strongly vary with

temperature, pressure or humidity. MEMS thermoelectric modules are no exception.

The main purpose of this first stage is the verification of derived models and verification of datasheet information provided by manufacturers. Necessary step is also the evaluation of MEMS TEM devices for their further aircraft-specific application. The whole testing and measurement process was extremely valuable for further considerations about MEMS TEMs manipulation, mounting and durability.

3.3.1 Measurement Setup

Thus the real testing conditions are very often poorly described in manufacturers' datasheets; the special test bench was prepared for the testing procedures under the controlled conditions. Schematic view of measurement setup is given in figure 3.9. The special test bench with MEMS TEM is placed inside the climatic chamber. The cold-side temperature T_C was controlled by the climatic chamber cooling circuit. The entire test bench is chilled out down to desired T_C until its stabilization. The AC power supply is subsequently turned on which began warming the hot-side of module T_h through the 50 W resistive heating element. Once the hot-side temperature reaches the desired value, the data set is acquired. The temperature feedback is provided by the Pt100 sensors connected to PC via datalogger. Electrical characteristics were measured using precise laboratory multimeters. All the used instruments are listed in table 3.4.

Table 3-4: Measuring instruments

Designation	Type
Climatic chamber	WEISS WKL100
Pt100 datalogger	OMEGA OM-CP-OCTRTD (8 Channel RTD temperature recorder)
V/A/Ω/Ω_1	Agilent 34401A (6 1/2 digit multimeter)
Ω_2	FLUKE 175 (True RMS multimeter)
AC power supply	Diametral AC250K1D (isolation transformer, 0-255V/1A)

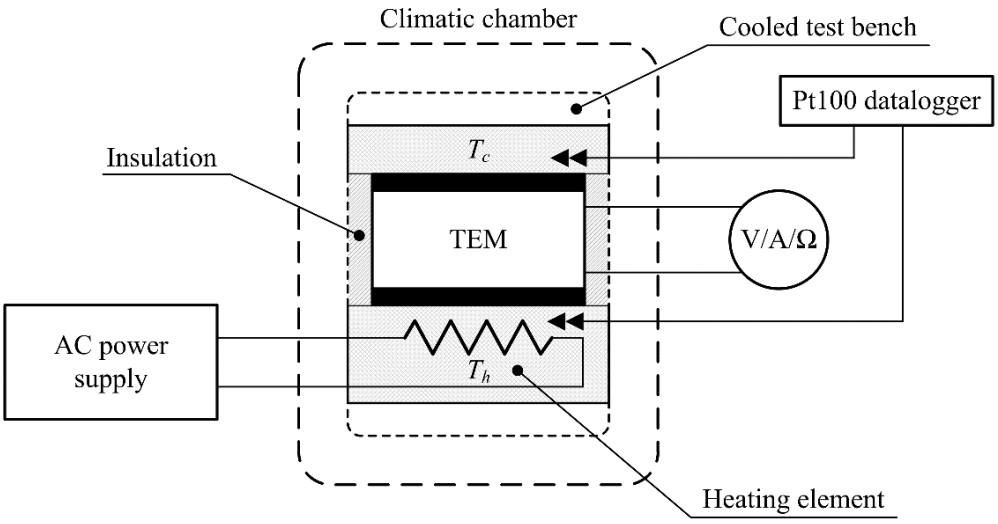

Figure 3-9: Measurement setup

A 3D drawing of the test bench internal structure is depicted in figure 3.10. The whole structure is encapsulated in a milled plastic box. Hot side of the module is heated up using a 50 W resistive heater. Thermal insulation between hot and cold sides is ensured by a mineral wool. Aluminium plates are used as heat spreaders. Pt100 sensors are placed in the milled slots as close as possible to the measured TEM. Figure 3.11 and Figure 3.12 show a various customizations of TEM installation inside the test bench. Each of measured TEMs (Micropelt TGP-751, Nextreme eTEG HV56) needed a specific adjustments in an inside structure of the test bench. The test bench inside the climatic chamber is depicted in figure 3.13. The contact pressure on TEM is ensured by the central screw. Contact pressure can be easily adjusted using a torque screwdriver.

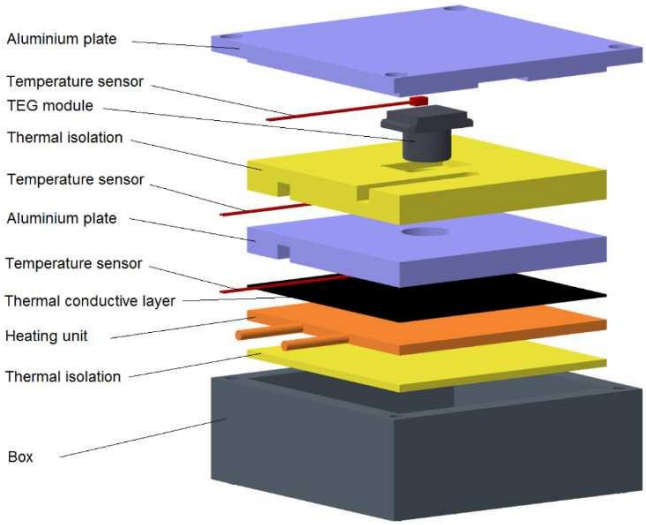

Figure 3-10: 3D drawing of test bench internal structure [56]

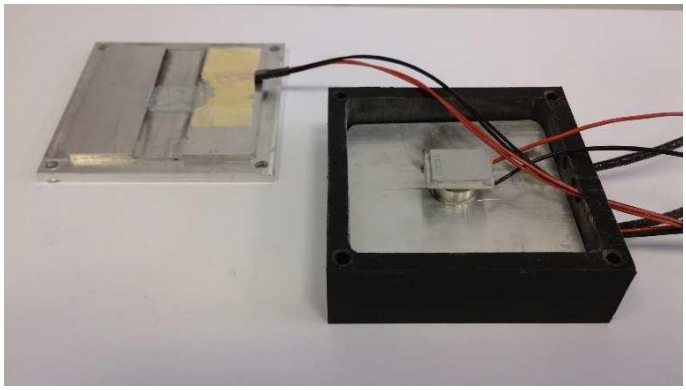

Figure 3-11: Test bench for Micropelt TGP-751

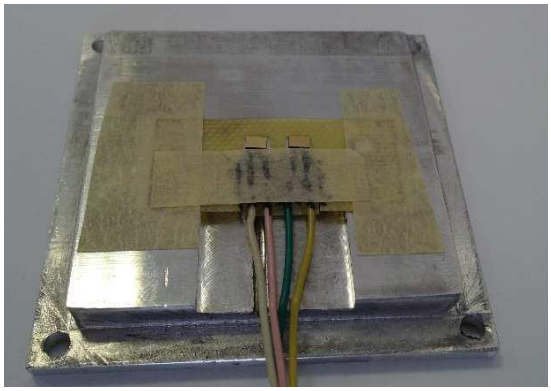

Figure 3-12: Test bench for Nextreme eTEG HV56

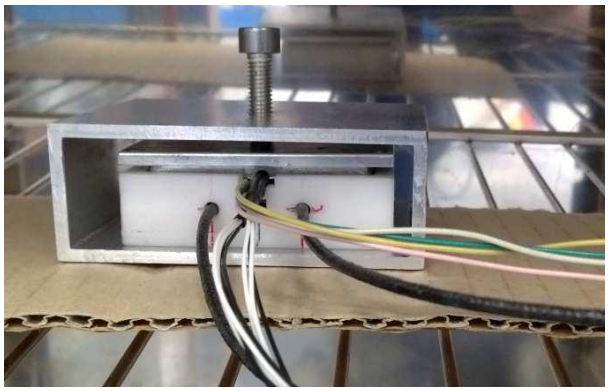

Figure 3-13: Test bench inside the climatic chamber

The first verification tests of installation concept were performed after the test bench assembly. Unfortunately, the Micropelt eTEG HV56 tests failed in their beginning. The test bench wasn't capable of providing the sufficient temperature difference along eTEG HV56 module. Thermal insulation of both sides of TEM is quite complicated due to the tiny thickness of module. Tests described in 5.2, 5.3 and 5.6 were carried out with Micropelt TGP-751 only. Moreover, some of the eTEG HV56 modules were damaged during the soldering, installation or dismantling. Their dimensions (ca. 3x3x0.6 mm) are too tiny for a conventional manipulation.

3.3.2 Open-circuit Voltage Measurement

The open circuit measurement was carried out using a simple method shown in figure 3.14. The linear characteristics of open-circuit voltage U_{OC} in terms of temperature difference ΔT was obtained. This trend perfectly matches the theory of thermoelectric Seebeck effect described in Eq.2. On the other hand, when comparing the results with datasheet values, the slope of the U_{OC} characteristics is not as such linear. This can be caused by the incorrect data from manufacturer or more probably by the inappropriate placing of Pt100 sensor. See appendix for the exact measured values and measurement conditions.

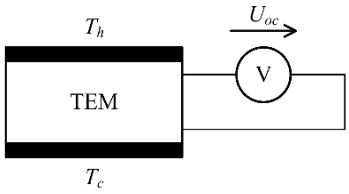

Figure 3-14: Open-circuit voltage measurement setup

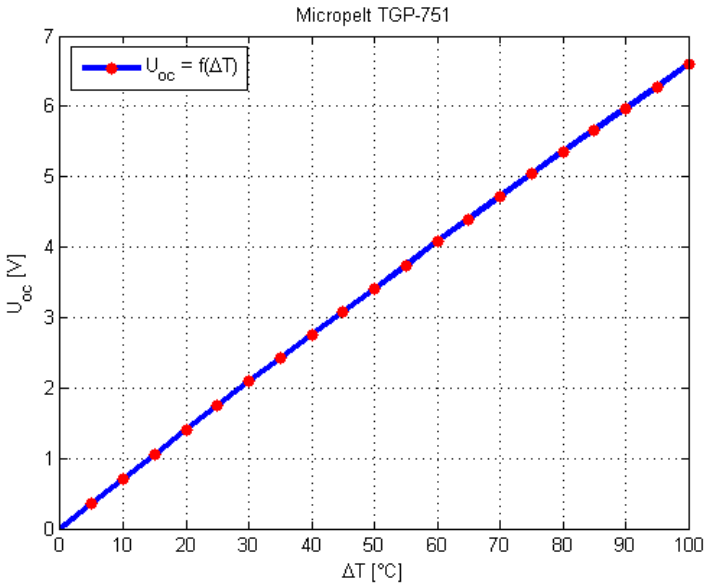

Figure 3-15: Open-circuit voltage measurement results (Micropelt TGP-751, ΔT = 0-100°C)

3.3.3 Short-circuit Current Measurement

The short circuit measurement was carried out using a simple method shown in figure 3.16. The linear characteristics of short-circuit current I_{SC} in terms of temperature difference ΔT was obtained. The measured data are plotted in figure 3.1. Small disturbances between the linear fit and measuring points are caused by the specific behavior of Micropelt TGP-751 TEM. While

short-circuited, TGP-751 varies in its internal resistance. Some settling time is needed to measure the exact value. The results of short-circuit current measurement satisfactorily match the expected linear behavior. See appendix for the exact measured values and measurement conditions.

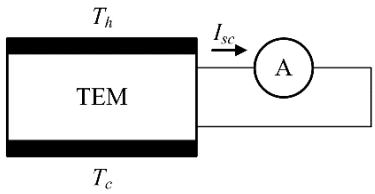

Figure 3-16: Short-circuit current measurement setup

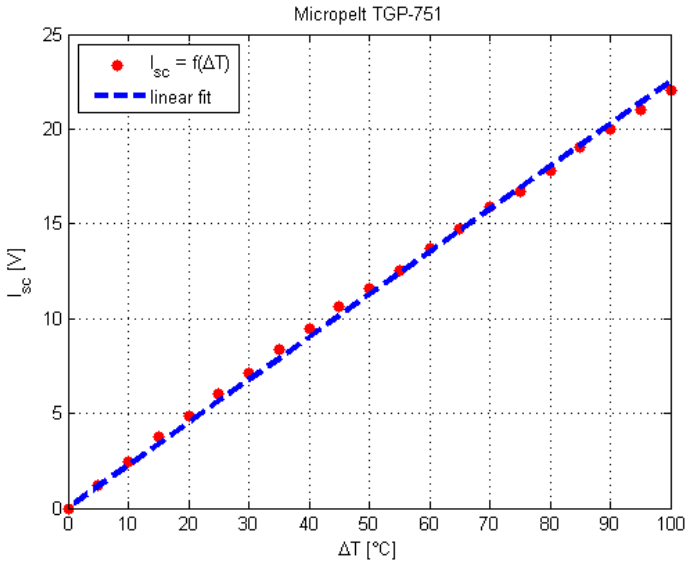

Figure 3-17: Short-circuit current measurement results (Micropelt TGP-751, ΔT = 0-100°C)

3.4.4 Internal Resistance Measurement

The internal resistance measurement was performed concurrently on both different thermoelectric modules (eTEG HV56, TGP-751). The temperature measurement was acquired by the Pt100 sensor placed close to both of the modules. *RTEM* temperature characteristics were examined in the temperature span of 200 °C (From -50 to +150 °C).This temperature span is much broader than the one guaranteed by TEM manufacturers. Manufacturers declare in their datasheets quite narrow operating temperature ranges Measurement setup is depicted in figure 3 .18. Measurement results for Nextreme eTEG HV56 are depicted in figure 3.19. Results for Micropelt TGP-751 are following in figure 3.20. See appendix for the exact measured values and measurement conditions. This measurement will be used as an essential input parameter to

the model. Its value could be never determined without this measurement (manufacturers guard such a data). Validity of *RTEM* measurement can't be verified due to the unknown material properties of the modules.

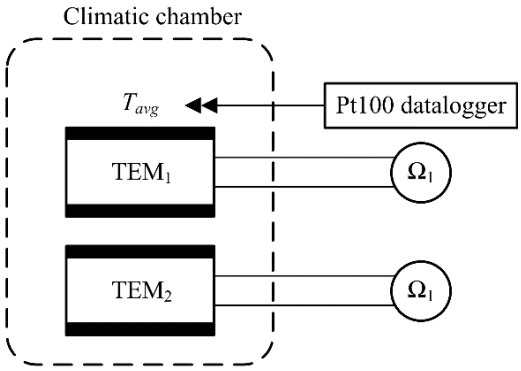

Figure 3-19: Internal resistance RTEM measurement setup

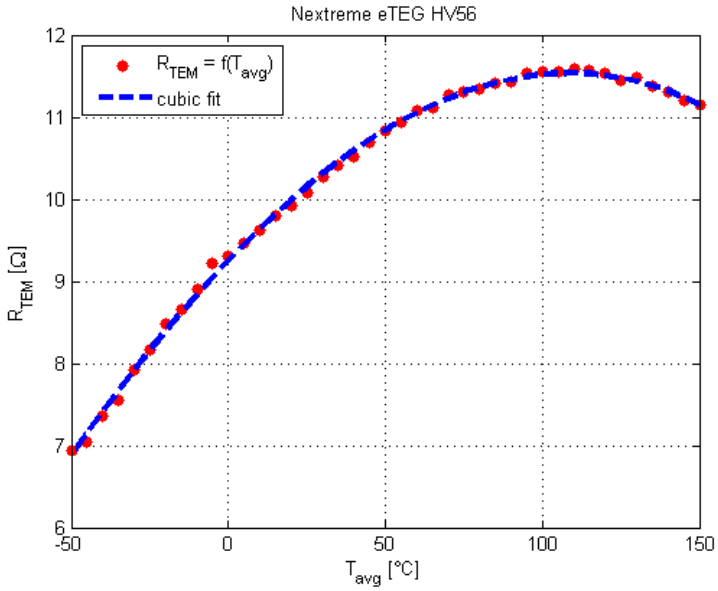

Figure 3-20: Internal resistance measurement results (Nextreme eTEG HV56, Tavg = -50 ÷ +150°C)

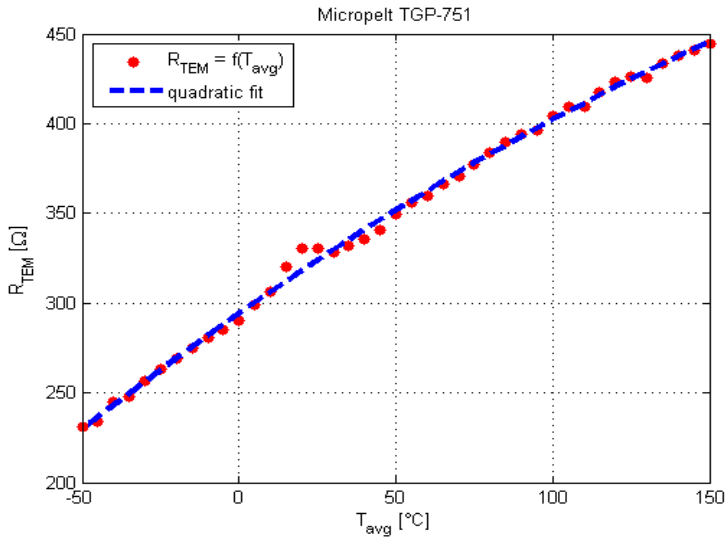

Figure 3-21: Internal resistance measurement results (Micropelt TGP-751, Tavg = -50 ÷ +150°C)

3.3.5 Seebeck Coefficient Measurement

The measurement of Seebeck coefficient has only an indicative character. Exact measurements of Seebeck coefficient require a well stabilised temperature source with minimal changes in ΔT. Therefore, this measurement is impractical with our test bench. The acquired data are listed in table 3.5 and plotted in figure 3.22. The three measured values have an unequal distribution of the test average temperature *Tavg*. Some variations of Seebeck coefficient can be observed. This knowledge will lead to the design of a new testing procedure for the exploration of MEMS TEM characteristics.

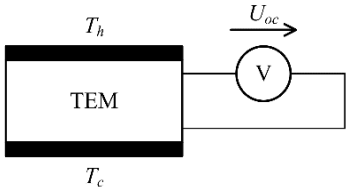

Figure 3-22: Seebeck coefficient measurement setup

Table 3-5: Seebeck coefficient variations

Tavg [°C]	$\alpha\Sigma$ [V/°C]	*Uoc* [V]	ΔT [°C]	*Th* [°C]	*Tc* [°C]
-27.5	0.059	0.588	10.0	-22.5	-32.5
18.5	0.070	0.35	5.0	21	16
97.0	0.074	1.031	14.0	104.0	90.0

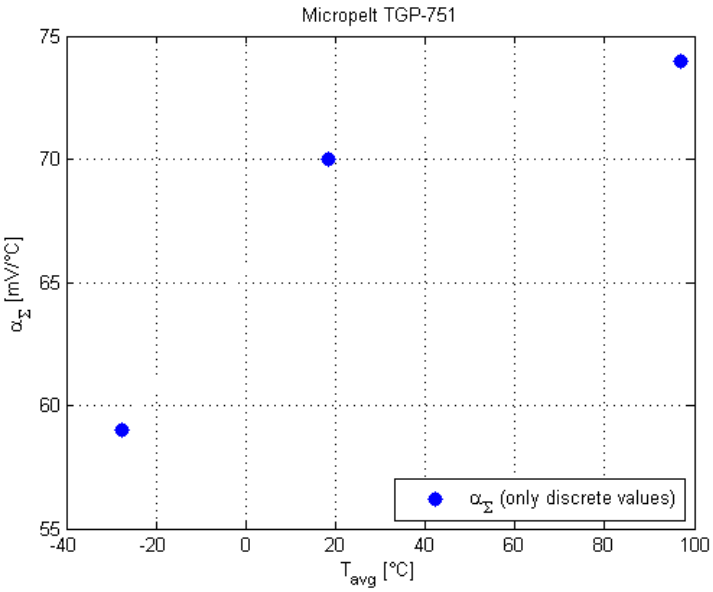

Figure 3-23: Discrete plot of Seebeck coefficient variations with Tavg (Micropelt TGP-751)

3.3.6 Calculated Characteristics

The MPP power provided by TEM can be derived as a function of open-circuit voltage and short-circuit current.

$$P_{MPP} = \frac{1}{4} U_{oc} I_{sc} \quad \textbf{(39)}$$

This equation is valid for an electric power source with linear V-A curve. Results of this computation method for $PMPP$ are shown in figure 3.23. The $PMPP$ computed using Eq. 4 is plotted subsequently. As a reference can be taken the blue curve ($RTEM$-based), since the red one (Isc- based) is influenced by the error described in figure 3.23 below.

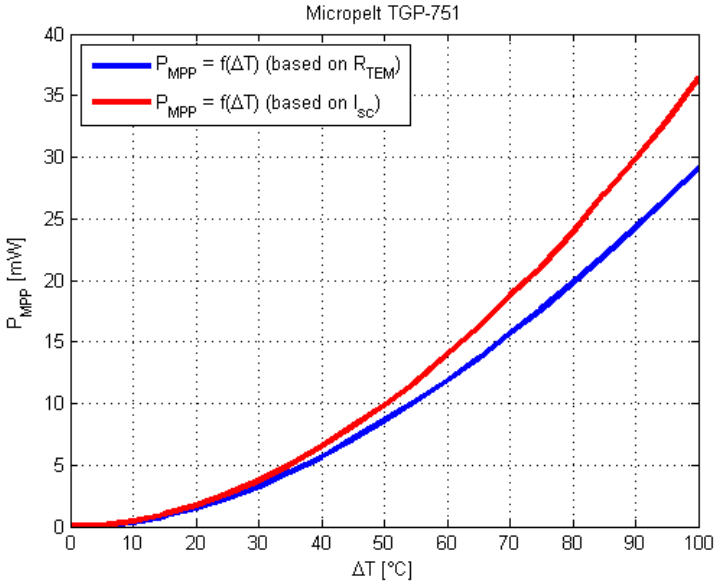

Figure 3-24: Power on MPP (Micropelt TGP-751, ΔT = 0-100°C)

Assuming that TEM is a temperature-difference-controlled voltage source with internal resistance *RTEM*, the V-A characteristics describing its load capability is expressed as:

$$U = U_{oc} I - R_{TEM} I^2 \quad \textbf{(40)}$$

Plot of this characteristic for three particular temperature differences is provided in figure 3.24.

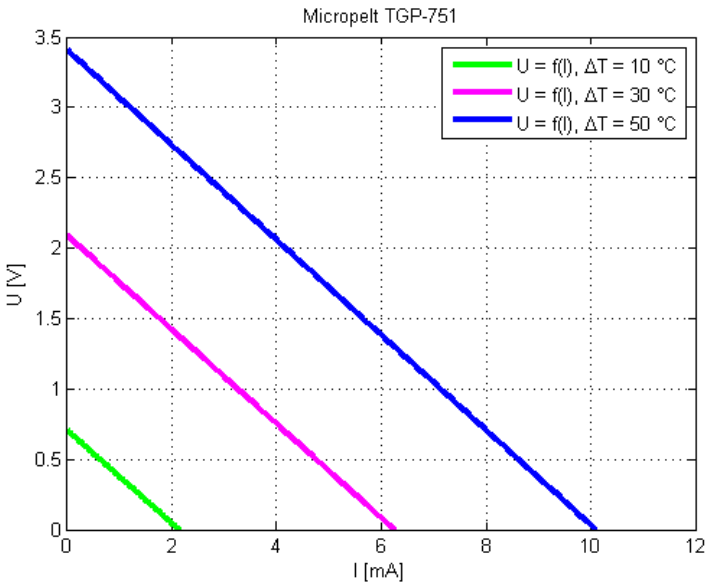

Figure 3-25: V-A characteristics comparison (Micropelt TGP-751, ΔT = 10, 30, 50°C)

The power to current characteristics (denoted as W-A) yields in integral of V-I characteristics according to current:

$$P = U_{OC}\, I - R_{TEM} I^2 \quad \textbf{(41)}$$

The obtained parabolic dependency is plotted in figure 3.25. Shape of the W-A characteristics has an appropriate form for the voltage source with linear internal resistance R_{TEM}.

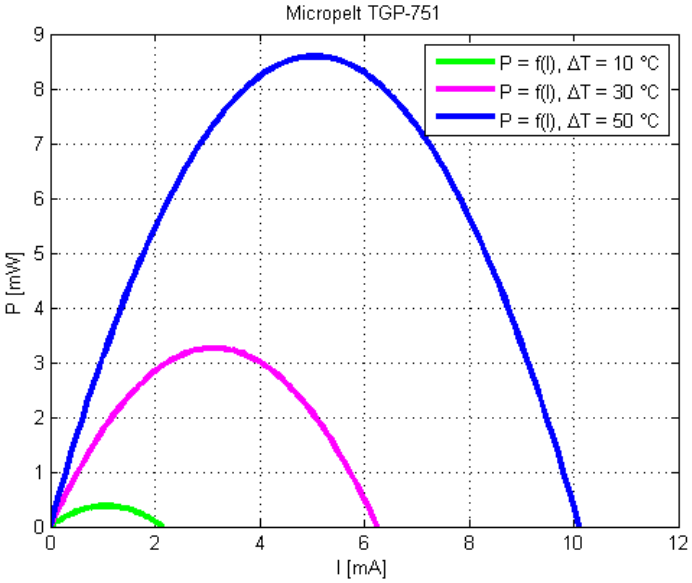

Figure 3-26: W-A characteristics comparison (Micropelt TGP-751, ΔT = 10, 30, 50°C)

3.3.7 Comparison of MEMS Thermoelectric Modules

The older data achieved in [15] were used as a reference values for the Nextreme eTEG HV56 module. The empirical functions describing the open circuit voltage and power output on MPP for eTEG HV56 are given as:

$$U_{oc} = 0.0194\Delta T \quad \textbf{(42)}$$

$$P_{MPP} = 0.0097(\Delta T)^2 + 0.0632\Delta T \quad \textbf{(43)}$$

These empirical functions will be further used for comparison of TEMs. Figure 3.27 shows the open-circuit voltage for both compared modules. As could be easily seen, Micropelt TGP-751 provides much steeper slope of open-circuit voltage with temperature. This result was expected due to the higher number of thermocouples integrated in TGP-751. Open-circuit voltage is a product of Seebeck coefficient, number of thermocouples and temperature difference along the module.

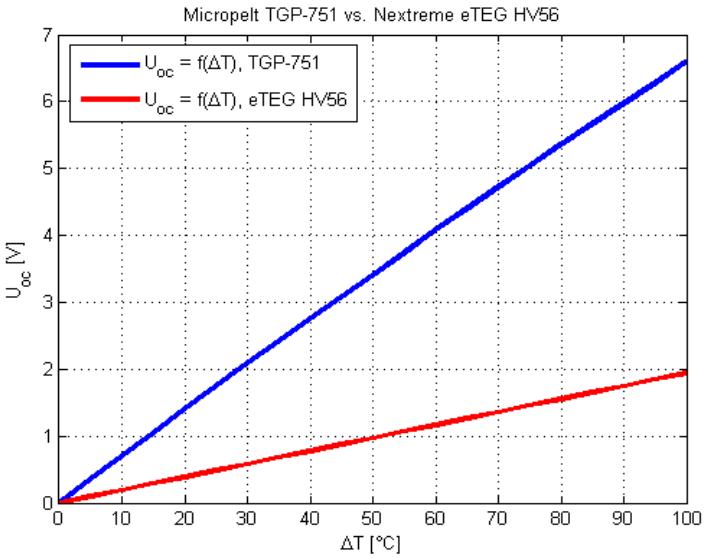

Figure 3.28: Open-circuit voltage comparison (Micropelt TGP-751 vs. Nextreme eTEG HV56, ΔT = 0-100°C)

The following characteristics are the domain of Nextreme eTEG HV56. As depicted in figure 3.27, the module is capable of providing four time higher power when operating on its maximum power point. This significant difference is caused by the internal structure of both modules. HV56 is tailored for a high power on MPP (low internal resistance) while TGP-751 aims to the maximum possible voltage (high resistance and net seebeck coefficient).

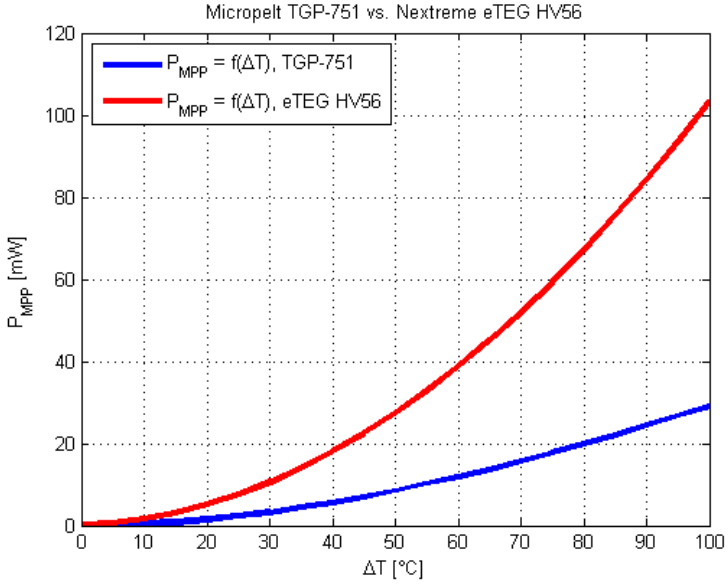

Figure 3-29: Power on MPP comparison (Micropelt TGP-751 vs. Nextreme eTEG HV56, ΔT = 0-100°C)

The above-mentioned specificity of both modules is additionally depicted in V-A characteristics in figure 3-28. TGP-751 has steep characteristics while eTEG HV56 drops down

much more gradually.

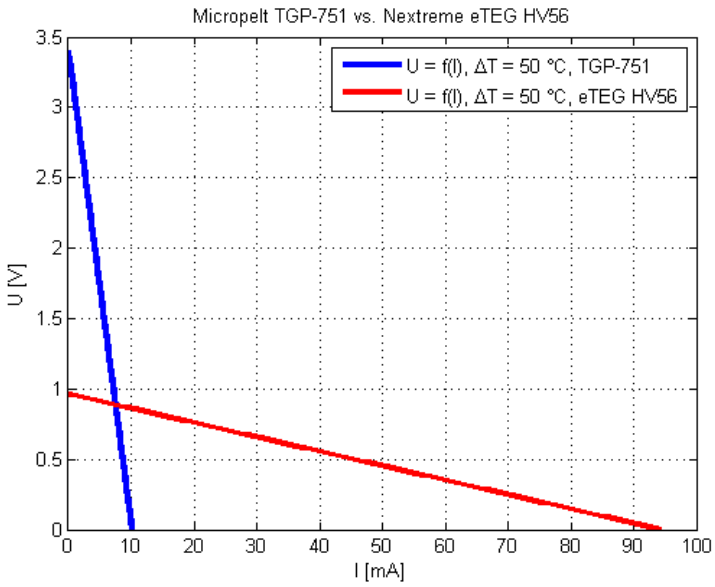

Figure 3-30: V-A characteristics comparison (Micropelt TGP-751 vs. Nextreme eTEG HV56, ΔT = 50°C)

W-A characteristics in figure 3.29 shows the capability of supplying the required power to connected load. eTEG HV56 has a much better capability to do that. Its MPP lays on 50 mA. On the other hand the voltage potential along the module is quite low (tenths of volts). Fortunately, it can conveniently use some MPPT algorithm to ensure the maximal power extraction. All the "power" characteristics were evaluated using ΔT = 50°C

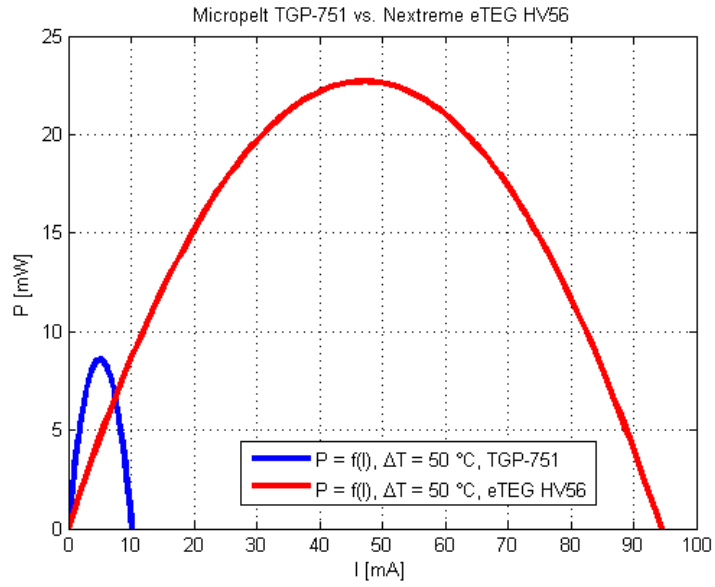

Figure 3-31: W-A characteristics comparison (Micropelt TGP-751 vs. Nextreme eTEG HV56, ΔT = 50°C)

3.3.8 Measurement Summary

For the full identification of thermoelectric module all components of Eq. 7 are needed: its thermal resistance, net Seebeck coefficient and electric resistance. The above-described measurement fully identified only the value of *RTEM* along the whole operating temperature range. This measurement introduces a new level of quality into the models since the electrical resistance was estimated as constant given by manufacturer until this point. As it's shown in figure 3.19 and figure 3.20, *RTEM* almost doubles when passing through the whole operating temperature range. Identification of *RTEM* as a function of temperature is a must in the practically useful models.

The Seebeck Effect is another very important parameter for the identification of TEM. Its value can be approximately obtained from the-open circuit voltage. However the Seebeck effect obtained as a slope of figure 3.15 reaches just 65 % of datasheet value. Only two options are possible: imperfection in measurement or excessive expectations of manufacturer.
Finally, the measurement errors should be mentioned. Various errors can occur when performing these "indicative" measurements with MEMS devices and disproportionally larger measurement methods. For the precise determination of thermoelectric properties should be employed methods such as Harman probe measurement, infrared microscopy, et[27],[28]c. The largest expected error and challenge lies in the placing of Pt100 sensors to measure the exact temperature difference on such a device.

3.4 System-level Design

The key requirements for the design and development of TEG were in chapter 2 set as follows: supplied system voltage: 3.3 V; supplied application power consumption:100 mW(corresponds to current consumption about 30 mA);continuous operation time: 30 min; operating temperature range: -50 °C to +85 °C.
In figure 3.30 is depicted the simplified system diagram of supplied application along with TEG. The supplied application is data acquisition and processing from a reluctance wheel speed sensor. This sensor is in its physical principle active and thus doesn't require any power supply instead of data acquisition and processing. The supplied circuitry consists of filter and comparator which transfers the input signal from sensor to square wave. The following block is some evaluation logic which evaluates the actual state of the turbine and sends data to the output.

The overall system is critical for the control of turbine or an aircraft. Therefore the utilization of thermal energy harvesting for uninterruptible power supply is considered.

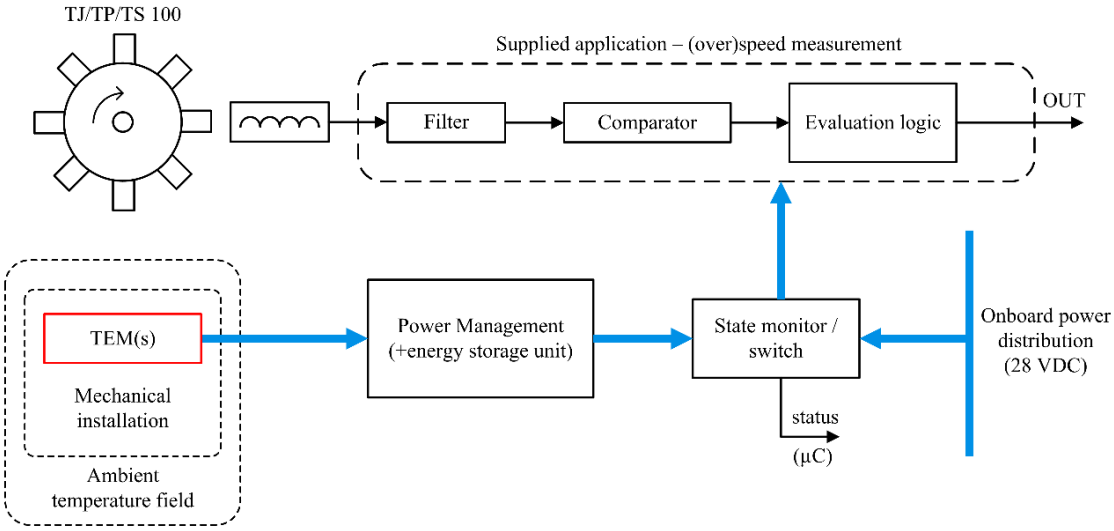

Figure 3-32: Supplied application under consideration – the (over) speed measurement of TJ/TP/TS100 turbine

TEG-part of figure 3.32 consists of thermoelectric module (or modules) interacting through the mechanical installation with ambient environment – temperature field outside and inside the engine bay. Electric energy from TEM is delivered to power management with energy storage unit. This block is of high importance. It has an interface role between TEM and supplied application. Energy from the TEM is accumulated in energy storage element. Energy from thermoelectric generator is used only if the state monitor finds some failure in the on-board power distribution. Then the switch ensures flow of energy from thermoelectric generator to supplied application.

The TJ00 jet turbine with JECU encapsulated in engine bay as shown in figure 3.31. As the JECU device is placed close to the intake air flow, the first considerations led to cooling of cold side through the forced convection from air intake.

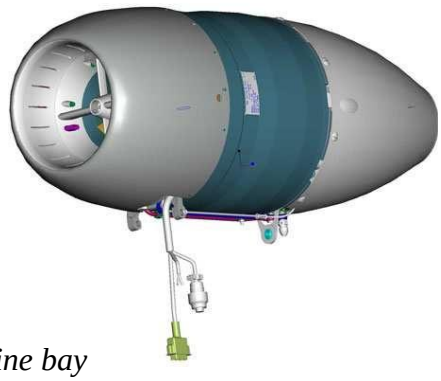

Figure 3-33: TJ100 encapsulated in engine bay

Preliminary analyses showed the two prospective spots for placing the TEG. These spots are market as “spot A”, “spot B” in Figure 3.32. Spot B needs the additional heat sink for the heat dissipation from the JECU box to the ambient environment. In spot B, the hot side of generator is placed on the JECU box and the cold-side temperature is ensured by the natural convection to the ambient environment outside the engine bay. Spot A was rejected at the beginning of design process. Thermal camera analyses shown, that the intensive intake flow to the turbine is extensively heating up the turbine inlet. Temperature of the inlet wall is higher than the temperature of JECU. The only possible solution close to JECU is therefore on the spot B.

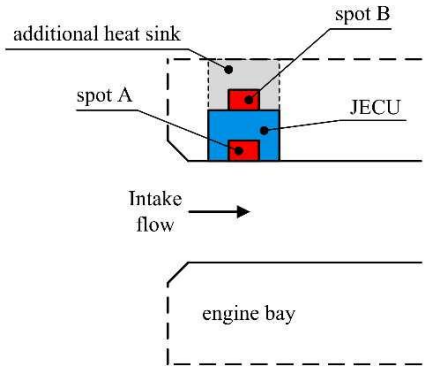

Figure 3-34: Placing of TEG on the TJ100 turbine – prospective spots

Two different thermal networks were proposed for the application of TEG on the spot B. In the first one are utilized eTEG HV56 modules. The second one uses TGP-751 which is slightly less challenging in terms of mounting ant mechanical integration. On the other hand each TGP-751 provides significantly less power then eTEG HV56. Proposed thermal networks are depicted in figure 3.33.

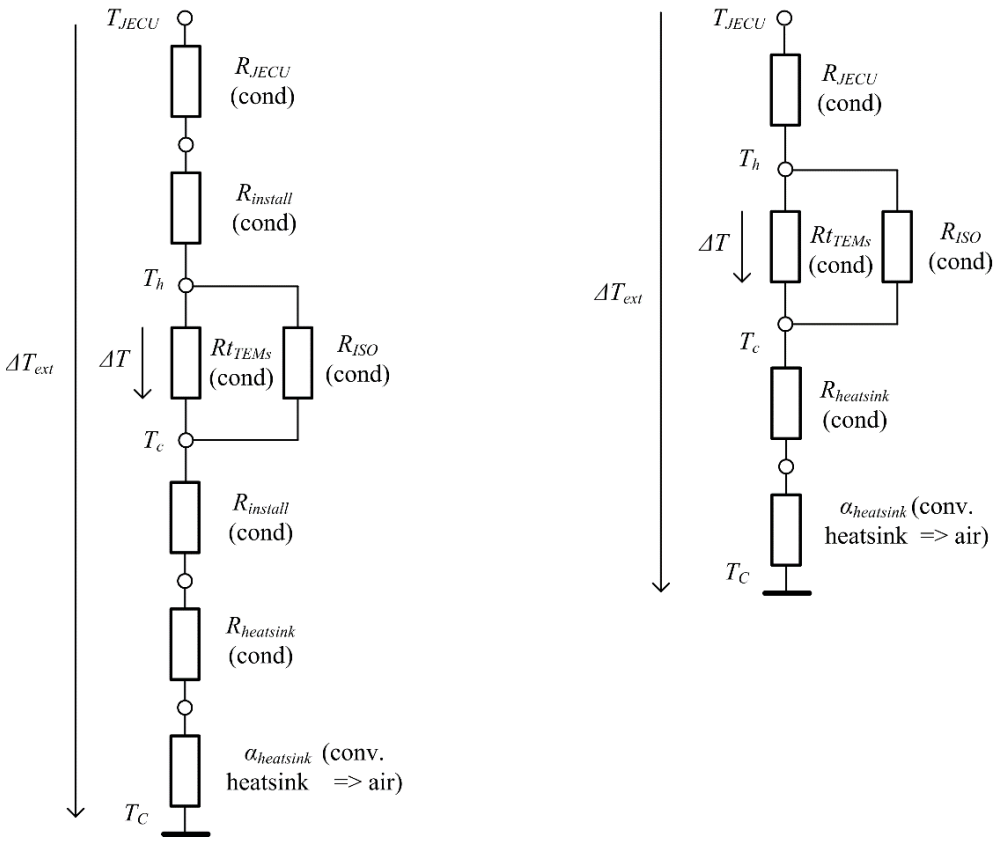

Figure 3.35: Thermal networks of TEGs based on Nextreme eTEG HV56 (left) and Micropelt TGP-751 (right)

Thermal network on the left belongs to Nextrem eTEG HV56. These modules are tiny and difficult to manipulate. Thus some special aluminum adapters are necessary to accommodate these TEMs into the TEG internal structure. These aluminum adapters are denoted as $R_{install}$. Other components of thermal network are common in the both cases:

T_{JECU} – temperature of JECU (temperature source);

R_{JECU} – thermal resistance of path JECU-TEM;

R_{TEM} _ thermal resistance of TEM;

$R_{heatsink}$ – thermal resistance of heat sink;

$\alpha_{heatsink}$ – convective heat transfer coefficient to ambient air;

$R_{install}$ – thermal resistance of adapters for eTEG HV56;

T_c – cold-side temperature (ambient air according to a proper flight level).

An initial idea for thermoelectric part of TEG is a connection of 1-4 TEMs to serial combination to obtain the sufficient power level for the supplied application. The higher number of MEMS TEMs would be economically disadvantageous. For the first estimation of parameters for the thermoelectric generator for JECU was used the worst-case scenario [6].This approach is used

very often when there is no further knowledge about the exact temperature fields, heat flux, etc. Input parameters were set “as bad as usually are”.

3.4.1 Power Management Concept

The main tasks set in design of the power management electronics include the impedance matching known as Maximum Power Point Tracking (MPPT), power conditioning, interconnection with energy storage element and self-diagnostics. Proposed TEG should provide tens of milliwatts of the electric power on the voltage level of 3.3 V. Various serial/parallel/serial-parallel combinations of 1-4 TEMs will be tested consequently with a boost or buck boost converter.

The basic concept of power management for the proposed TEG is shown in figure 3.34. Blue lines are denoted as electric energy flows. Blocks are representing the detachable subsystems of the technology demonstrator.

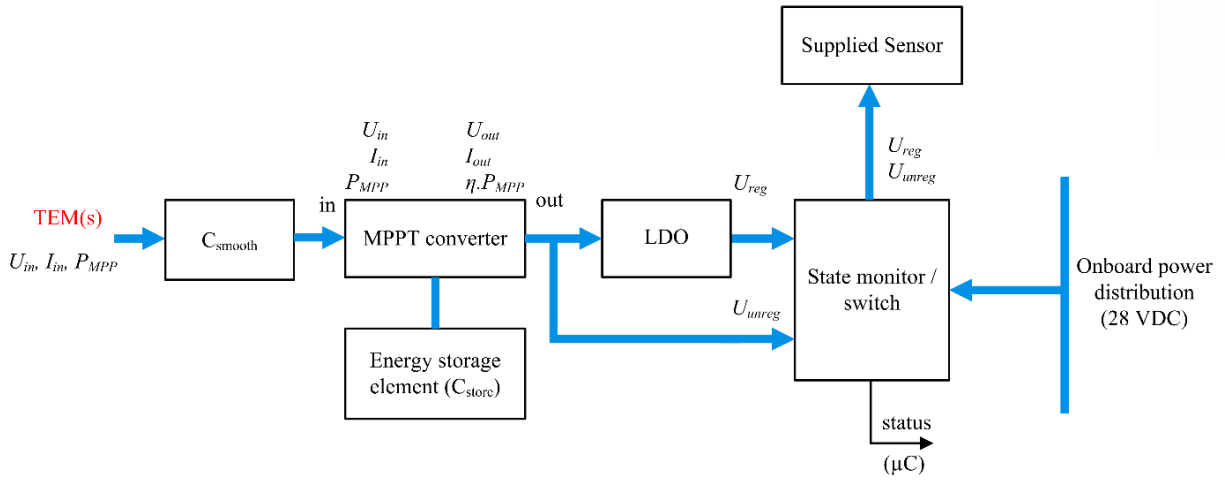

Figure 3-36: Concept of power management for proposed TEG

The power output from thermoelectric module (or modules) enters the power management through the C_{smooth} capacitor. This capacitor reduces the input voltage ripple. *Csmooth* also has a positive effect on power converter stability. Maximum power point tracking is implemented as a boost or buck-boost converter. Topology will depend on the exact input voltage on the final application. The particular ICs under consideration for Nextreme eTEG HV56 modules include TI bq25504 and ST SPV1040. These ICs are depicted in their typical operation scheme in figure 3.36 and figure 3.37 respectively.

Another part of thermoelectric generator circuitries are LDOs. Low dropout regulators are not required in all the applications. LDOs are designed for providing the voltage references and supply voltage for critical devices. Many such a devices have integrated LDOs in their own structure. LDOs are very frequently provided at some pins of energy harvesting electronics ICs (e.g. form Linear Technology).

State monitor / switch acts as an observer of airplane onboard power distribution. While it goes to failure state, the energy harvesting circuit is asked for operation.

The energy storage unit will be based on Super capacitors, as discussed in chapter 4. As can be seen in figure 3.35, super capacitors are the holdup of the proposed energy harvesting system. They are limited by the narrow temperature operating range. On the other hand, if considering the classic chemistry batteries, this holdup is even narrower.

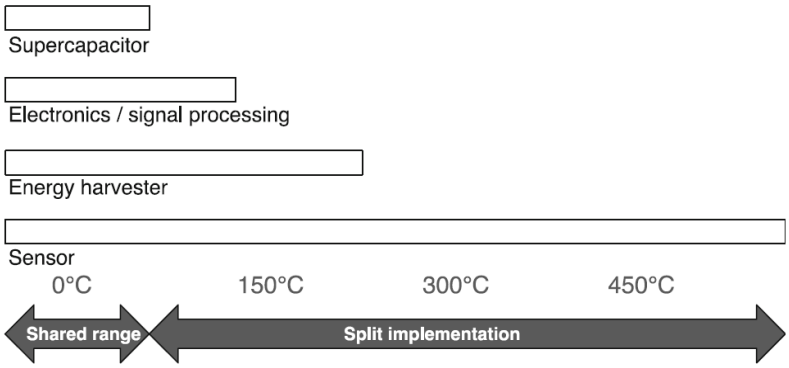

Figure 3-37: Temperature is the big issue when designing the TEG for aerospace applications [8]

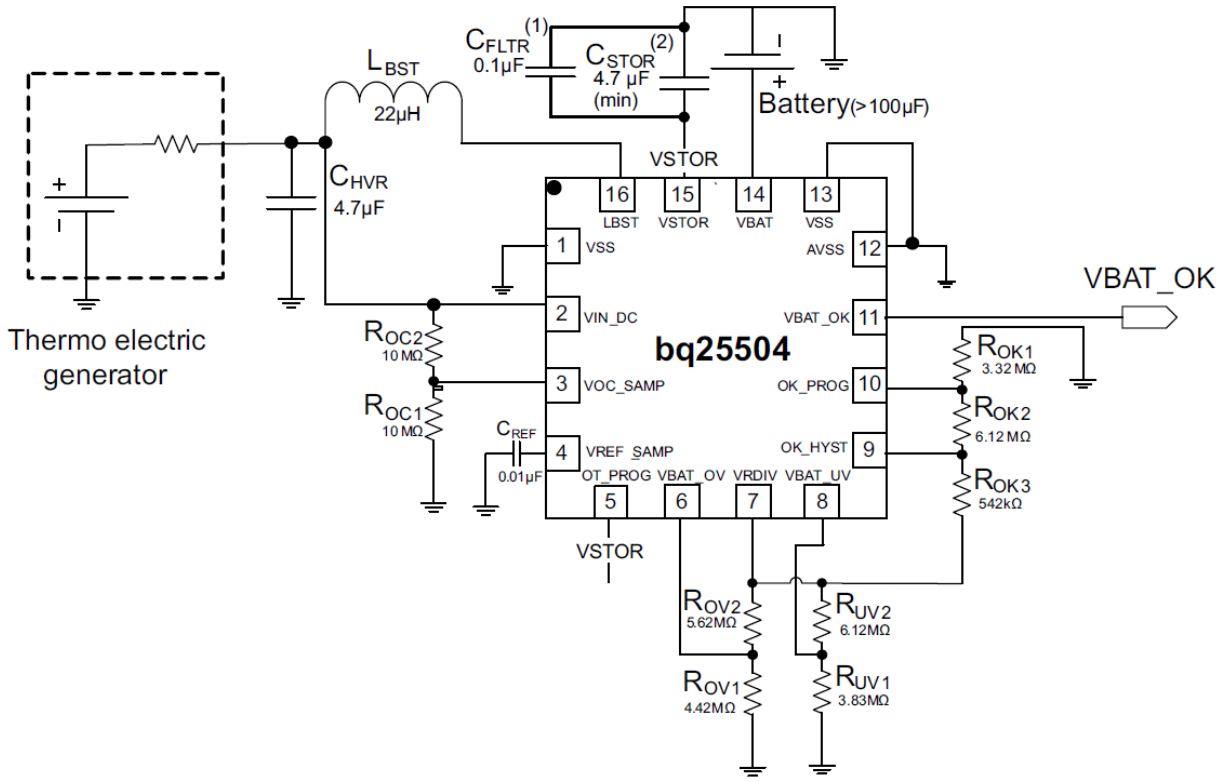

Figure 3-38: Texas Instruments bq25504 – typical application circuit with thermoelectric generator [48]

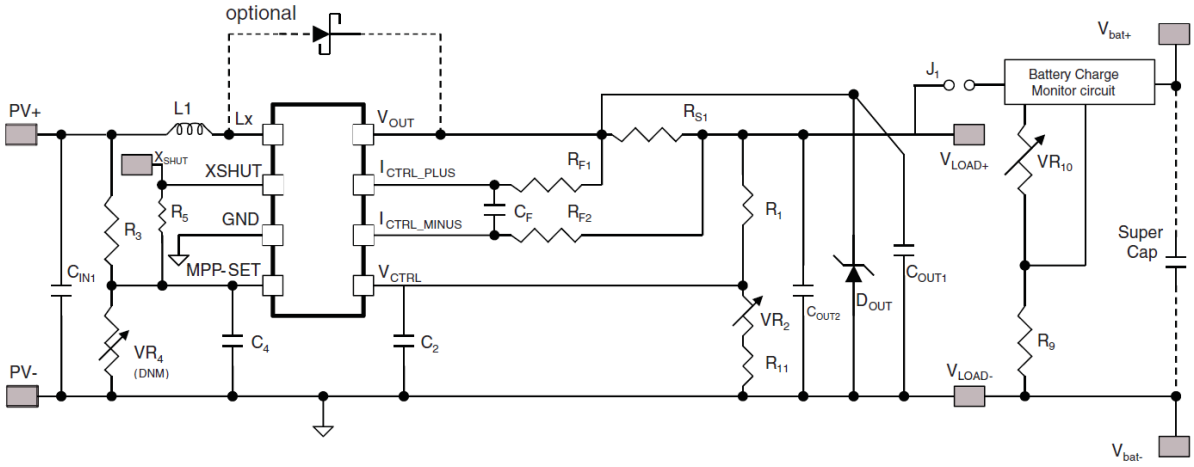

Figure 3-39: ST Microelectronics SPV1040 – typical application circuit [49]

The power management converts the raw generated energy at the output terminals of the harvester to the useful electric power. The 15 V, 75 mA high efficient buck converter TPS62120 from Texas Instruments is utilized in the design. The TPS62120 is a high efficient synchronous step down DC-DC converter optimized for low power applications. The wide operating input voltage range of 2 V to 15 V supports energy harvesting, battery powered and as well 9 V or 12

V line powered applications.

The block scheme of power management is shown in the following figure Figure 3.38 below.

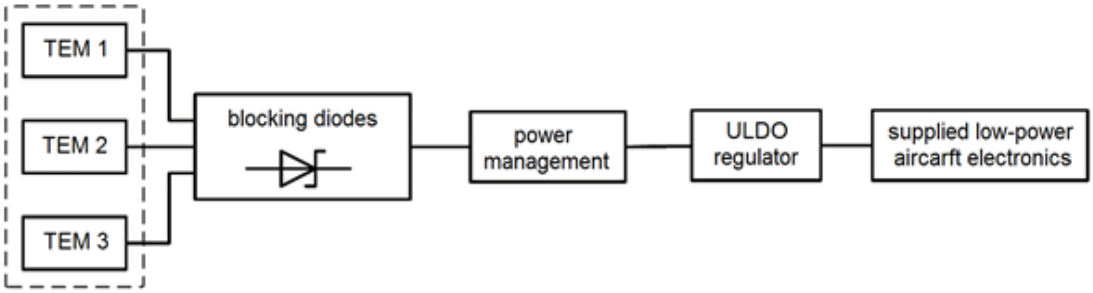

Figure 3-38: System block diagram of TEG power source for aircraft application

The power management was realized and successfully tested, see Figure 3.38 below.

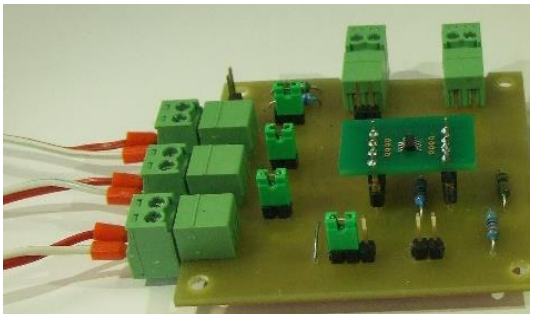

Figure 3-39: Power management with buck converter TPS62120

Chapter Four

4. Modeling and Simulation

The model of complex thermoelectric generator is implemented in ANSYS. The model consists of interchangeable parts which can be used in any analogical issue. Thermoelectric modules implemented in ANSYS can be connected thermally into any thermal network implemented in the software. The same goes to electric circuits. First sketch of the ANSYS TEM model was given in Universality predisposes the presented model for the further use in energy

4.1 Model Description

As any model working with some level of abstraction, the TEG model contains several assumptions:

- 1D heat flow;
- lumped parameters model of TEM;
- thermal and electric contact resistances are negligible;
- temperature drop on the wafer of TEM is negligible - temperature on the thermocouples is equal with temperature on wafer border;
- TEM is capable of MPP operation;
- temperature differences on all the parallel TEMs in the thermal network are equal;
- thermal resistance and Seebeck coefficient are constant over the whole operating range;

Operation of TEM model is based on the following phenomena and equations:
Peltier cooling at the both sides of module:

$$Q_{ph} = \alpha_{\sum} I T_h \quad \textbf{(44)}$$

$$Q_{pc} = \alpha_{\sum} I T_c \quad \textbf{(45)}$$

Joule heating from the current passing through TEM:

$$\frac{Q_J}{2} = \frac{1}{2} R_{TEM}\, I^2 \quad \textbf{(46)}$$

Seebeck effect -the rule of thermoelectric energy conversion:

$$U_{OC} = \alpha_{\sum}(T_h - T_C) \quad \textbf{(47)}$$

Internal resistance of such a module is computed using a lookup table which replaces the function:

(Eq.45)

$$R_{TEM} = f(T_{avg}) \quad \textbf{(48)}$$

$$T_{avg} = \frac{T_h + T_c}{2} \quad \textbf{(49)}$$

Where $Q_{Ph:}$ Peltier cooling on a hot side of TEM in W

$Q_{Pc:}$ Peltier cooling on a cold side of TEM in W

$\alpha_{\sum:}$ net Seebeck coefficient in $V.K^{-1}$

$T_{h:}$ hot-side temperature in [°C] or [K]

$T_{c:}$ cold-side temperature in [°C] or [K]

Q_J: Joule heating in W

$R_{tem:}$ thermoelectric module internal resistance in [Ω]

$I_{in:}$ input current in [A] or [mA]

$U_{oc:}$ open-circuit voltage in [V] or [mV]

$T_{ave:}$ average temprature in [°C] or [K]

4.2 Model Blocks

Thermal Reference - the thermal reference point to which is related all the temperatures defined in the system.

I. Temperature Source - ideal source of thermal energy that is powerful enough to maintain the desired temperature difference.

II. Heat Flow Source - ideal source of thermal energy which is powerful enough to maintain the desired heat flow regardless on temperature difference along itself.

Conductive Heat Transfer:

$$Q = K\frac{A}{D}(T_A - T_B) \quad \textbf{(50)}$$

Where K is the material thermal conductivity, A is the area normal to the heat flow direction, D distance between layers, and T_A and T_B temperatures of layers.

Convective Heat Transfer (Newton law of cooling):

$$Q = KA(T_A - T_B) \quad \textbf{(51)}$$

Where K is the convection heat transfer coefficient, A is the surface area and T_A and T_B

are temperatures of layers.

Temperature Sensor - measures the temperature difference between two defined points without any effect on a measured system. Thermal resistance of the Ideal Temperature Sensor is infinite.

Electrical Reference - sets the point of electric ground (point with zero potential). Controlled Voltage Source - provides the constant voltage regardless on the current drawn by the load connected on its terminals.

Resistor - linear resistor with V-I characteristics according to the Ohm's law

Current Sensor - measures the current passing through the circuit. Its internal resistance is equal to zero hence has no effect on measured circuit.

Voltage Sensor - measures the voltage drop between its terminals. Its internal resistance is infinite hence has no effect on measured circuit.

ANSYS A converter - allows to convert numeric values to the ANSYS physical signals.

ANSYS B converter -allows to convert physical signals values to the numeric values.

Solver Configuration - defines the solver settings used for simulation.

4.3 Simulation in ANSYS

Input parameters to the model include:

R_{TEM} [Ω] - thermoelectric module internal resistance

Rt_{TEM} [W.K^{-1}] - thermal resistance of TEM

η [-] or [%] - efficiency of converter

$\alpha_{\sum}$ [V.K^{-1}] - net Seebeck coefficient thermal resistance of the whole heat path from

T_H – temperature of the hot side of TEG ($TJECU$)

T_C – temperature of the cold side of TEG

All the input parameters were taken from the measurement presented in chapter 5.

4.4 Discussion

Verification of built TEM modules was performed based on comparison of measured and simulated data for the same outputs (temperature difference). TEMs were connected to a simple thermal end electric circuit.Thermal input of TEM model was exposed to the same temperatures as real module under the test conditions. Results are satisfying for our required accuracy. Open-circuit voltage results perfectly match each another. Small differences between

model and measured values at higher temperatures might be caused by the change of Seebeck coefficient with temperature. This characteristic is not yet implemented in our simulation model. In figures from 4.1-4.4 below diverge the measured and simulated values for a higher temperature differences. This problem may be connected with the use of older data for the identification of HV56. The older data weren't measured that precisely like the new ones used in the TGP-751 model.

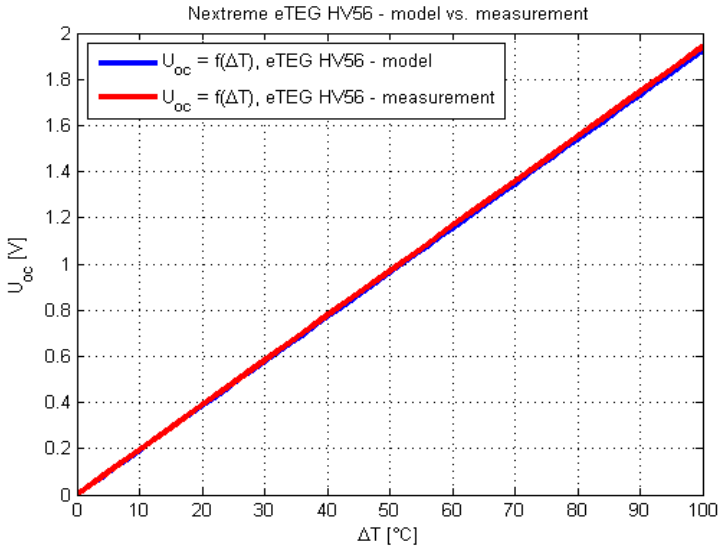

Figure 4-1: Verification of eTEG HV56 model – comparison of measured and simulated open circuit voltage

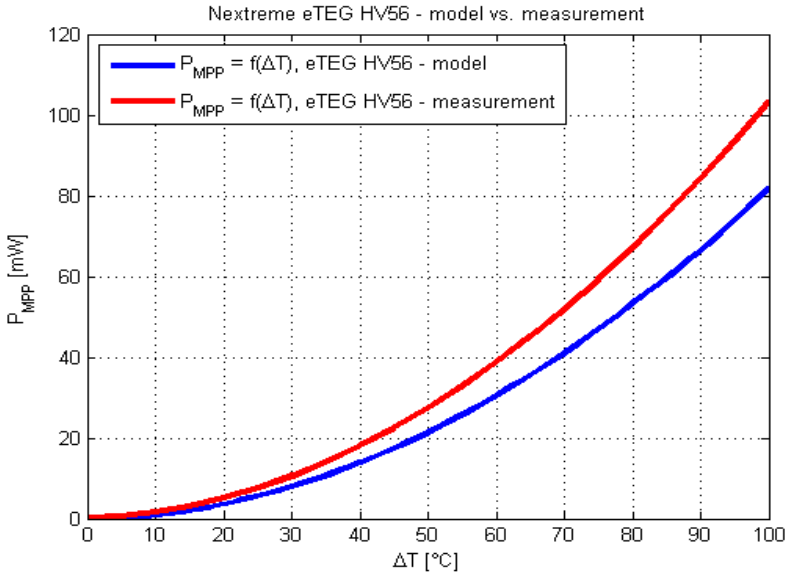

Figure 4-2: Verification of eTEG HV56 model – comparison of measured and simulated power on MPP

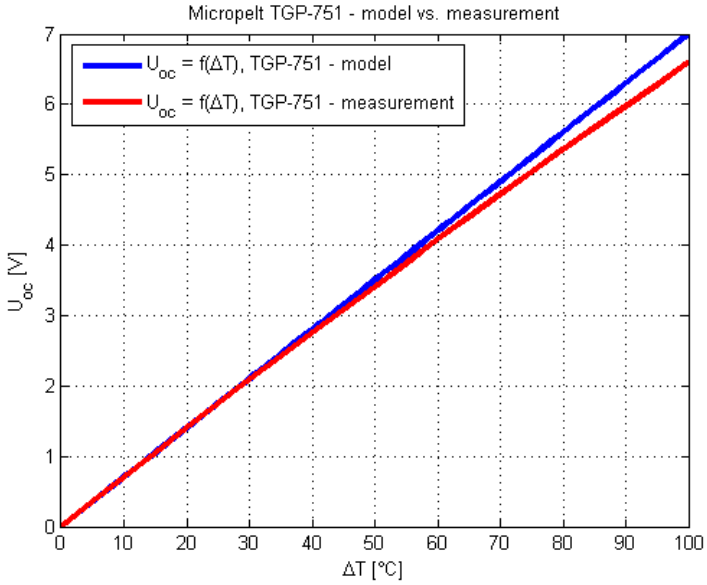

Figure 4-3: Verification of TGP-751 model – comparison of measured and simulated open-circuit voltage

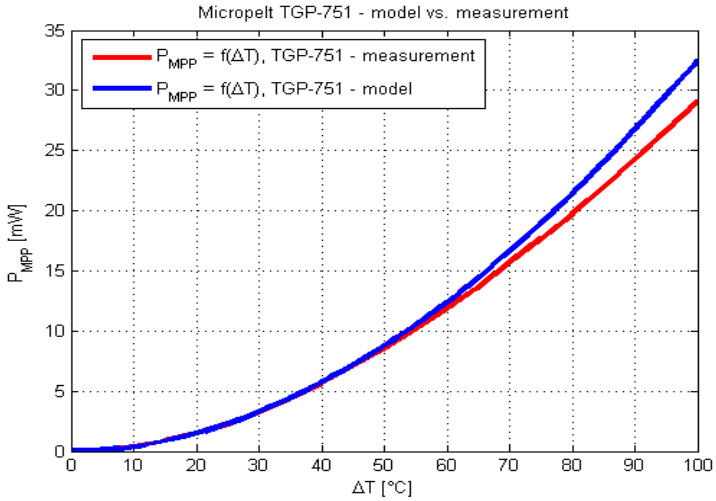

Figure 4-4: Verification of TGP-751 model – comparison of measured and simulated power on MPP

Table 4.1 and Table 4.2 deal with a comprehension of experiment, model and datasheet values provided by manufacturer at several temperature difference levels. The main variations in comparable values come out with a high temperature differences. The better match between the measured and datasheet values will be the major task for the next generation of test bench.

Table 4-1: Micropelt TGP-751 – Comparison of model, measurement and datasheet values

	ΔT = 10 °C	ΔT = 30 °C	ΔT = 50 °C	ΔT = 100 °C
U_{OC} [V] (experiment)	0.705	2.088	3.405	6.6
U_{OC} [V] (model)	0.6998	2.099	3.499	6.997
U_{OC} [V] (datasheet)	1.25	3.75	5.5	11.1
I_{SC} [mA] (experiment)	2.449	7.154	11.575	22.05
I_{SC} [mA] (model)	2.134	6.254	10.01	18.54
I_{SC} [mA] (datasheet)	-	-	-	-
P_{MPP} [mW] (experiment)	0.432	3.734	9.853	36.383
P_{MPP} [mW] (model)	0.3735	3.283	8.763	32.45
P_{MPP} [mW] (datasheet)	1	8.5	-	-

Table 4-2: Micropelt TGP-751 – Comparison of model, measurement and datasheet values

	ΔT = 10 °C	ΔT = 30 °C	ΔT = 50 °C	ΔT = 100 °C
U_{OC} [V] (experiment)	0.194	0.582	0.97	1.94
U_{OC} [V] (model)	0.1924	0.5772	0.962	1.924
U_{OC} [V] (datasheet)	0.26	0.75	1.2	2.5
I_{SC} [mA] (experiment)	-	-	-	-
I_{SC} [mA] (model)	18.74	54.85	88.82	170.1
I_{SC} [mA] (datasheet)	24	73	115	210
P_{MPP} [mW] (experiment)	1.602	10.626	27.41	103.32
P_{MPP} [mW] (model)	0.9016	7.1915	21.36	81.84
P_{MPP} [mW] (datasheet)	1.5	17	36	130

N.B: The difference between the datasheet and the tested values are shown in the above tables Table 4.1 and Table 4.2.The value obtained by testing is a bit lower because of lower temperature gradient on TEM, which is caused by location of temperature sensors.

AHM of aircrafts consists in permanently monitoring key parameters to assess aging effects. This is a major challenge with the objective to replace scheduled maintenance by predictive

maintenance, therefore reducing costs. This may also reduce exploitation costs by reducing mechanical safety margins and consequently aircraft weight and fuel consumption. SHM is a key player for airlines facing the "continual challenges of maximizing asset utilization at low operating cost and maximum revenue."

Commercial wired sensor networks are already being proposed for this purpose, at least for early detection of cracks within the metal structure of military aircrafts being operated for many more years than originally planned [6].

In that context, the system implementation has had the opportunity to be implemented on the Aft Pylon Fairing (APF) of Ethiopian airlines, for the implementation of a WSN for AHM. APF is an important device whose task is to reduce drag and to protect the pylon primary and secondary rear structures from extreme temperature (see Figure 2.24). It is itself submitted to strong sonic load, high mechanical vibration levels and extreme temperatures (hundreds of °C for some areas). It is therefore a piece of choice for AHM

Considering energy harvesting, the permanent thermal gradients developing during cruise between APF walls and inner air, look like an ideal source of energy. However, apart from the fact that the devices used for energy capture will have to qualify vs. very stringent aeronautical requirements, sonic load is here a very specific and robustness-demanding parameter. As a consequence, appropriate acoustic tests up to levels above 150 dBa, and a special certification process are mandatory in addition to classical certification.

However, above all, the final result of the holistic design of a comprehensive WSN node may also be quite surprising where the main functions of a node are considered: sensing, energy harvesting and storage, energy management and signal processing.

On figure 2.26, the parabolic curve represents the output power of a TEG with the temperature of the wall to which it is bonded. For the purpose of illustration, the inner air temperature is supposed to be 100°C and the targeted power output is supposed to be at least 17 mW. Consequently the TEG must be affixed in areas where the wall temperature is at least 160°C.

On the other hand, the sensor monitoring the parameter used for SHM answers to other requirements, such as a location near the mechanical part to be monitored. For obvious reasons, this location is likely to be close to the hottest zones of the APF, and for the purpose of demonstration this temperature will be there supposed to be above TEG maximum operating temperature. Therefore, TEG sensor cannot be affixed together and will need to

be wired to each other.

Similar considerations for the electronics and energy storage devices lead to the conclusion that, even if the Sensor Network is macroscopically wireless, it is locally necessarily wired, as a result of the harsh environment.

This illustrates the unorthodox fact that for such harsh environments, the usual scheme in which all functions are integrated together (all-in-one topology) is no longer true and that a split topology is mandatory. One may even consider a single TEG implemented in an optimized location delivering power to close by devices.

Chapter five

5. Conclusion and Recommendation

5.1 Conclusion

"Aviation is he branch of engineering that is least forgiving of mistakes." (Freeman Dyson)

Thermoelectric generators for aerospace applications are still in their infancy. Airbus Innovation Works is the only one company striding in leaps and bounds to the practical application in wireless sensor nodes.

In the previous chapters were presented the recent findings in this very perspective area of energy harvesting applications. The major attention was paid to the theoretical aspect of the design and development of thermoelectric autonomous power sources. Some basic background about the thermoelectric measurements was outlined.

The dissertation thesis deals with the verification of autonomic thermoelectric sources of electric energy for aircraft applications. The research was based on a study of state-of-the-art in this field. The previously presented solutions in available sources utilized the common thermoelectric modules, while there were applied the MEMS thermoelectric modules in this research. The presented work has shown new significant results.

Two commercially available MEMS thermoelectric modules Nextreme HV56 and Micropelt TPG-751 were selected for the design. The precise simulation models of both modules were created and verified with datasheets. The selected modules were experimentally tested in a wide range of operation conditions. The module Micropelt TPG-751 was selected for further development on the base of results of previous experimental testing and simulation modelling

The over-speed transducer for turbo-shaft aircraft engine TS100 was chosen as a prospective application, which supposed to prove the functionality of this technology under the real conditions. The thermal condition of TS100 were studied to find the prospective location for MEMS thermoelectric generator. The prototype A was created and successfully tested on the engine TS100 on the base of the simulation modelling. The prototype A proved the functionality of the thermoelectric generator under real condition. The prototype A was able to generate power 34.2 mW. The design of prototype B was based on the experiences obtained during designing and testing of prototype A. There were used three thermoelectric modules in prototype B to ensure the sufficient power for the prospective application.

The prototype B generated power 228.8 mW. The prototype C was designed with an aim to improve the thermal condition by utilizing the plastic screws between the mounting pad and the heat sink. The contact forces were decreased because of the low rigidity of plastic screws in high temperature conditions. That led to the reduction in the heat flow through the thermoelectric modules. Therefore, the metal screws were utilized as was previously successfully tested in the prototype B. The presented dissertation thesis meets the goals defined in the simulation assignment.

Internal resistance of MEMS thermoelectric modules was successfully measured in a wide range of operating conditions (-50+150 °C).

5.2 Recommendation

The ultimate goal of this thesis was a design and development of functional technology demonstrator.Even if this goal wasn't fully satisfied,the major objective of the thesis was satisfied. The measurement and identification part of presented work was time consuming. Many of the measurements had to be carried out multiple times. The major problems with these measurement tasks have included the difficult manipulation with MEMS modules and the technology-related issues with glues, thermal- conductive paste, etc. The biggest issue is the mechanical installation enabling satisfactory thermal isolation of hot and cold sides of a module. This work deals with methods of complex design process and verification of autonomic thermoelectric energy source for aircraft application with using the modern engineering tools and approaches.

A future and development of today's society strongly depends on an ability to utilize clean and renewable energy sources. Energy harvesting (EH) is a new independent branch and current trend in this area, which uses energy freely available in the environment. One of the prospective ways of energy harvesting is based on thermoelectric generator (TEG). The TEG technology is based on the Seebeck effect, which describes direct conversion of temperature difference into the electromotive force (voltage). "*When the junction between dissimilar conductors is heated, electrons are enabled to pass from the material in which the electrons have the lower energy into that in which their energy is higher, giving rise to an electromotive force.*" [1]

New thermoelectric materials and microelectromechanical systems (MEMS) technologies used in manufacturing process of the thermoelectric modules (TEM) significantly reduces

their dimensions and provide sufficient level of the generated power. These are the prospective ways to design the autonomic energy source for wide range of applications. In considering high progress in development of an electronic devices, especially their miniaturization and reduction of energy consumption, the EH technologies becomes ideal solution for their energy supply. With respect to wide range of aircraft operational temperature conditions, the aircraft applications seem to be suitable for thermoelectric technology. The natural temperature gradients ensured due to high operating altitude, heat generated by passengers, temperature on board and nearby engine bay are potential sources of electric energy.

The autonomic energy source based on MEMS TEG technology is a technical object, which needs to be designed with respect to its interdisciplinary character and can be classified as a mechatronic system. Mechatronics is defined as *"The design philosophy that utilizes the synergistic integration of mechanical engineering with electronics and electrical systems with intelligent computer control in the design and manufacture of industrial products, processes and operations."* [2] In accordance with this philosophy, the method of design process is developed using the new engineering tools and approaches. The integration of model based design (MBD) approach, simulation modeling and experimental testing leads to develop the enhance design process and more functional, adaptable and competitive product.

The main global challenges connected with utilization of MEMS TEMs into aerospace industry include the waiting for a utilization of new materials and improvement of their reliability. Nowadays, there is no idea about the reliability of this infant technology.

As the TEG has to be always tailored for such an application, this master's thesis will be further used as a template when developing new thermoelectric generator applications.

5.3 Recommendations for Future Work

In aeronautics, new needs call for the deployment of sensor networks.A lot of applications are related to AHM as illustrated above, but other areas such as flight-tests, aircraft security or logistic, are also demanding for new wireless and battery free communicating sensors. Whatever the application, environmental energy harvesting is then imperative to power new information processing systems.

Flight-tests are likely to be the first field where wireless and energy autonomous sensors will be routinely deployed in the near future because of the

gain induced by reduced design, complexity and installation time, by reason of the reduced number of connectors, on account of easy relocation, of the suppression of cables passing through multiple bulkheads, of the avoidance of rivet removal or hole drilling (an issue with composite materials). It is worth mentioning that in that context, the failure of one system has little consequence, the information lost during one test being accessible again during a future one. It will be an experience that for these temporary deployments, demand for battery free systems is indeed strong.

For permanent applications (such as AHM) autonomous energy generation will be considered only when a high number of sensors, in similar energetic situations, are envisioned. Conversely, if only a small number is needed, a power line is never that far in an aircraft to feed the devices and the complexity added by the extra wiring will be tolerable. In other words, the choice may be between a small number of wired sensors monitoring large areas, and a large number of wireless sensors with a more limited range. On the other hand, the issue of reliability and robustness of energy harvesters is here critical for applications such as AHM. Consequently, the application of WSN to AHM may be regarded as a long-term perspective.

Whatever the context, when solar energy is not possible and when efficient and reliable energy harvesters are required, TEGs will be one of the major competitors, benefiting from a large and for-years established commercial offer, combined with favorable intrinsic characteristics such as the absence of moving parts and maturity of technology.

References

[1] J. A. Paradiso and T. Starner, "Energy Scavenging for Mobile and Wireless Electronics," *IEEE Pervasive Comput.*, vol. 4, no. 1, pp. 18–27, 2005.

[2] J. P. Thomas, M. a. Qidwai, and J. C. Kellogg, "Energy scavenging for small-scale unmanned systems," *J. Power Sources*, vol. 159, no. 2, pp. 1494–1509, Sep. 2006.

[3] S. Priya and D. J. Inman, Eds., *Energy Harvesting Technologies*. New York: Springer Science+Business Media, LLC, 2009.

[4] M. T. Penella-López and M. Gasulla-Forner, *Powering Autonomous Sensors: An Integral Approach with Focus on Solar and RF Energy Harvesting*. Dordrecht Heidelberg London New York: Springer, 2011, p. 147.

[5] T. Becker, M. Kluge, J. Schalk, K. Tiplady, C. Paget, and U. Hilleringmann, "Autonomous Sensor Nodes for Aircraft Structural Health Monitoring," *IEEE Sens. J.*, vol. 9, no. 11, pp. 1589–1595, 2009.

[6] M. Belleville and C. Condemine, Eds., *Energy Autonomous Micro and Nano Systems*. London/Hoboken: ISTE Ltd and John Wiley & Sons, Inc., 2012.

[7] D. Samson, T. Otterpohl, M. Kluge, U. Schmid, and T. Becker, "Aircraft-Specific Thermoelectric Generator Module," *J. Electron. Mater.*, vol. 39, no. 9, pp. 2092–2095, Nov. 2009.

[8] J.-M. Dilhac, R. Monthéard, M. Bafleur, V. Boitier, P. Durand-Estèbe, and P. Tounsi, "Implementation of Thermoelectric Generators in Airliners for Powering Battery-Free Wireless Sensor Networks," *J. Electron. Mater.*, vol. 43, no. 6, pp. 2444–2451, Apr. 2014.

[9] W. Ostachowicz and J. A. Güemes, Eds., *New Trends in Structural Health Monitoring*, CISM Cours. Wien Heidelberg New York Dordrecht London: Springer, 2013, p. 427.

[10] M. R. Pearson, M. J. Eaton, R. Pullin, C. a Featherston, and K. M. Holford, "Energy Harvesting for Aerospace Structural Health Monitoring Systems," *J. Phys. Conf. Ser.*, vol. 382, p. 012025, Aug. 2012.

[11] A. Elefsiniotis, M. E. Kiziroglou, S. W. Wright, T. T. Toh, P. D. Mitcheson, T. Becker, E.

M. Yeatman, and U. Schmid, "Performance evaluation of a thermoelectric energy harvesting device using various phase change materials," *J. Phys. Conf. Ser.*, vol. 476, p. 012020, Dec. 2013.

[12] M. E. Kiziroglou, S. W. Wright, T. T. Toh, T. Becker, P. D. Mitcheson, E. M. Yeatman, D. U. W. Gxw, F. F. Dylrqlf, and Z. Vhqvruv, "HEAT STORAGE POWER SUPPLY FOR WIRELESS AIRCRAFT SENSORS," in *PowerMEMS 2012*, 2012, vol. 1, pp. 7–10.

[13]A. Elefsiniotis, T. Becker, and U. Schmid, "Thermoelectric Energy Harvesting Using Phase Change Materials (PCMs) in High Temperature Environments in Aircraft," *J. Electron. Mater.*, vol. 43, no. 6, pp. 1809–1814, Nov. 2013.

[14]"Autarke flexible Monitoringeinheiten zur Überwachung technischer Systeme (AMETYST)," *EADS GmbH Innovation Works*, 2010. [Online]. Available: http://www.ametyst-projekt.de/. [Accessed: 14-May-2014].

[15] L. Janák, "Application of MEMS Technology in the Field of Thermoelectric Generators," Brno University of Technology, 2012.

[16] D. Samson, M. Kluge, T. Fuss, U. Schmid, and T. Becker, "Flight Test Results of a Thermoelectric Energy Harvester for Aircraft," *J. Electron. Mater.*, vol. 41, no. 6, pp. 1134–1137, Feb. 2012.

[17] K. Thangaraj, A. Elefsiniotis, S. Aslam, T. Becker, U. Schmid, J. Lees, C. a. Featherston, and R. Pullin, "Hybrid energy storage system for wireless sensor node powered by aircraft specific thermoelectric energy harvesting," in *Proc. of SPIE Vol. 8763*, 2013, vol. 8763, p. 876307.

[18]A. Elefsiniotis, D. Samson, T. Becker, and U. Schmid, "Investigation of the Performance of Thermoelectric Energy Harvesters Under Real Flight Conditions," *J. Electron. Mater.*, vol. 42, no. 7, pp. 2301–2305, Jan. 2013.

[19] "Division of Aerospace & Advanced Control, UNIS, a.s." [Online]. Available: www.mechsys.cz. [Accessed: 14-May-2014].

[20] "První brněnská strojírna Velká Bíteš, a.s.," 2014. [Online]. Available: http://www.pbsvb.cz/. [Accessed: 09-May-2014].

[21] "Complex Affordable Aircraft Engine Electronic Control (CAAEEC)," 2014. [Online].

Available:

[22] "ESPOSA - Efficient Systems and Propulsion for Small Aircraft," 2014. [Online]. Available: http://www.esposa-project.eu/. [Accessed:09-May-2014].

[23] Division of Aerospace & Advanced Control UNIS a.s., "Jet Engine Control Unit Datasheet," Brno, 2014.

[24] Z. Ancik, "Thermal phenomena modeling of air electronic unit," Brno University of Technology, 2010.

[25] R. Isermann, "Mechatronic systems—Innovative products with embedded control," *Control Eng. Pract.*, vol. 16, no. 1, pp. 14–29, Jan. 2008.

[26] L. Janak, Z. Ancik, and Z. Hadas, "Simulation Modelling of MEMS Thermoelectric Generators for Mechatronic Applications," in *Mechatronics 2013*, 2014, pp. 265–271.

[27] D. . Rowe, Ed., *Thermoelectrics Handbook: Macro to Nano*. Boca Raton: Taylor & Francis Group, 2006.

[28] J. H. Goldsmith, *Introduction to Thermoelectricity*, Springer S. Heidelberg Dordrecht London New York: Springer, 2010.

[29] V. Leonov, "Simulation of maximum power in the wearable thermoelectric generator with a small thermopile," *Microsyst. Technol.*, vol. 17, no. 4, pp. 495–504, Feb. 2011.

[30] R. McCarty, "Thermoelectric Power Generator Design for Maximum Power: It's All About ZT," *J. Electron. Mater.*, vol. 42, no. 7, pp. 1504–1508, Oct. 2012.

[31] A. Montecucco, J. Siviter, and A. R. Knox, "The effect of temperature mismatch on thermoelectric generators electrically connected in series and parallel," *Appl. Energy*, vol. 123, no. March, pp. 47–54, Jun. 2014.

[32] C. Vadstrup, E. Schaltz, and M. Chen, "Individual Module Maximum Power Point Tracking for Thermoelectric Generator Systems," *J. Electron. Mater.*, vol. 42, no. 7, pp. 2203–2208, Apr. 2013.

[33] E. A. Man, E. Schaltz, and L. Rosendahl, "Thermoelectric Generator Power Converter System Configurations: A Review," in *11th European Conference on Thermoelectrics, Proceedings of Abstracts*, 2013, p. 94.

[34]R. W. Erickson and D. Maksimovic, *Fundamentals of Power Electronics*. New York, Boston, Dordrecht, London, Moscow: Kluwer Academic Publishers, 2004, p. 883.

[35] E. Macii, Ed., *Ultra Low-Power Electronics and Design*. New York, Boston, Dordrecht, London, Moscow: Kluwer Academic Publishers, 2004, p. 273.

[36] O. Lopez-Lapena, M. T. Penella, and M. Gasulla, "A New MPPT Method for Low- Power Solar Energy Harvesting," *IEEE Trans. Ind. Electron.*, vol. 57, no. 9, pp. 3129–3138, Sep. 2010.

[37]C. Chen, W. Hsieh, W. Lai, K. Chen, and C. Wang, "A new PWM/PFM control technique for improving efficiency over wide load range," *2008 15th IEEE Int. Conf. Electron. Circuits Syst.*, pp. 962–965, Aug. 2008.

[38]M. K. Kazimierczuk, *Pulse-Width Modulated DC-DC Power Converters*. Chichester, West Sussex: John Wiley & Sons, Ltd., 2008.

[39]J. Park and S. Kim, "Maximum Power Point Tracking Controller for Thermoelectric Generators with Peak Gain Control of Boost DC–DC Converters," *J. Electron. Mater.*, vol. 41, no. 6, pp. 1242–1246, Jan. 2012.

[40] Linear Technology Corporation, "LTC3108 - Ultralow Voltage Step-Up Converter and Power Manager," 2010.

[41] Linear Technology Corporation, "LTC3109 - Auto-Polarity, Ultralow Voltage Step-Up Converter and Power Manager," 2010.

[42] M. Aureliano, G. De Brito, L. Galotto, L. P. Sampaio, G. De Azevedo, C. A. Canesin, and S. Member, "Evaluation of the Main MPPT Techniques for Photovoltaic Applications," *IEEE Trans. Ind. Electron.*, vol. 60, no. 3, pp. 1156–1167, 2013.

[43] I. Laird, H. Lovatt, N. Savvides, D. Lu, and V. G. Agelidis, "Comparative Study of Maximum Power Point Tracking Algorithms for Thermoelectric Generators," in *Australasian Universities Power Engineering Conference (AUPEC'08)*, 2008, pp. Paper P–217, 1–6.

[44] Micropelt GmbH, "TGP-751 - Thin Film Thermogenerator inside standard package," 2013.

[45]Nextreme Thermal Solutions Inc., "eTEG HV56 Power Generator - Data Sheet," 2011. [46] L. E. Bell, "Addressing the Challenges of Commercializing New Thermoelectric Materials," *J. Electron. Mater.*, vol. 38, no. 7, pp. 1344–1349, Feb. 2009.

[47]M. integrated Products, "Energy-Harvesting Charger and Protector MAX17710 - datasheet,"

2009.

[48] Texas Instruments, "bq25504 - Ultra Low Power Boost Converter with Battery Management for Energy Harvester Applications," 2012.

[49] ST Microelectronics, "SPV1040 - High efficiency solar battery charger with embedded MPPT," 2013.

[50] ST Microelectronics, "SPV1050 - Ultralow power energy harvester and battery charger with embedded MPPT and LDOs," 2013.

[51] Linear Technology Corporation, "LTC3105 - 400mA Step-Up DC/DC Converter with Maximum Power Point Control and 250mV Start-Up," 2010.

[52] AVX, "AVX BestCap Ultra-low ESR High Power Pulse Supercapacitors," 2013. [53] Maxwell Technologies, "Product Guide: BOOSTCAP Ultracapacitors," 2009. [54] Maxwell Technologies, "PC SERIES ULTRACAPACITORS datasheet," 2013. [55] Infinite Power Solutions, "THINERGY MEC202 datasheet," 2012.

[56] Z. Ancik, R. Vlach, L. Janak, P. Kopecek, and Z. Hadas, "Modeling, simulation and experimental testing of the MEMS thermoelectric generators in wide range of operational conditions," vol. 8763, p. 87631M, May 2013.

[57] D. Parthasarathy, P. Enoksson, and R. Johansson, "Prototype energy harvesting wheel speed sensor for anti-lock braking," *2012 IEEE Int. Symp. Robot. Sensors Environ. Proc.*, pp. 115–120, Nov. 2012.

[58] B. Mitchell, "Energy Harvesting Applications and Architectures at Boeing Commercial Airplanes," presented at *NanoPower Forum*, San Jose, CA, 2007.

[59]L. G. dos Santos, "EMBRAER Perspective on SHM Introduction into Commercial Aviation Programs, " in *Proc. 8th International Workshop on Structural Health Monitoring (IWSHM)*, Stanford, CA, 2011, vol.11, pp. 19-26.

[60]Ultra Electronics Aircraft systems: http://www.ultra-electronics.com/aircraft_systems/airframe_fatigue.php

[61] D. Meekhun, V. Boitier, J.M. Dilhac, "Design of a solar harvester system for a wireless sensor network deployed for large aircraft in-flight tests," *Renewable Energy & Power Quality Journal*, Paper no. 856, no. 6, Avril 2012.

[62] R. Montheard, S. Carbonne, M. Bafleur, V. Boitier, J.M. Dilhac, X. Dollat, N. Nolhier, E.

Piot, C. Airiau, "Proof of concept of energy harvesting from aeroacoustic noise," in Proc. *PowerMEMS 2012*, Atlanta, USA, pp.267-270.

[63]D. Meekhun, V. Boitier, J.M. Dilhac, "*Charge and Discharge performance of Secondary Batteries according to Extreme Environment Temperatures*," in Proc. *35th Annual Conference of the IEEE Industrial Electronics Society (IECON 2009)*, Porto, Portugal, Nov. 2009, pp.271-275.

[64]ISO 2533:1975 Standard Atmosphere, ISO/TC20/SC6, 2013-03-20, http://www.iso.org

[65]N. Bailly, J-M. Dilhac, C. Escriba, C. Vanhecke, N. Mauran, M. Bafleur, "Energy Scavenging based on Transient Thermal Gradients: Application to Structural Health Monitoring of Aircrafts," in Proc. *PowerMEMS 2008*, Sendai, Japan, Nov. 2008, pp.205-208.

[66]D. Samson, M. Kluge, T. Becker, U. Schmid, "Energy Harvesting for Autonomous Wireless Sensor Nodes in Aircraft," in *Proc. Eurosensors XXIV*, Linz, Austria, Sept., 2010, pp.1160-1163.

[67]M. E. Kiziroglou, S. W. Wright, T. T. Toh, T. Becker, P. D. Mitcheson and E. M. Yeatman, "Heat storage power supply for wireless aircraft sensors, " in *Proc*. *PowerMEMS 2012*, Atlanta, USA, Dec. 2012, pp.472-475.

[68] H. Durou, G.A. Ardila Rodriguez, A. Ramond, X. Dollat, C. Rossi, D. Estève, "Micromachined bulk PZT piezoelectric vibration harvester to improve effectiveness over low amplitude and low frequency vibrations, " in *Proc*. *PowerMEMS 2010*, Louvain, Belgium, Nov. Dec. 2010, pp.27-30.

[69] H. Durou, "Vers l'autonomie énergétique des réseaux de capteurs embarqués : conception et intégration d'un générateur piézoélectrique et d'un micro dispositif de stockage capacitif en technologie silicium, " *Ph.D. thesis*, Université Paul Sabatier, Toulouse, France, Dec. 2010.

[70] J. Colomer-Farrarons, P. Miribel-Català, A. Saiz-Vela, and J. Samitier, "A Multiharvested Self-Powered System in a Low-Voltage Low-Power Technology," IEEE Trans. Ind. Electron., vol. 58, no. 9, pp. 4250-4263, Sept. 2011.

[71] H. Lhermet, C. Condemine, M. Plissonnier, R. Salot, P. Audebert, and M. Rosset, "Efficient Power Management Circuit: From Thermal Energy Harvesting to Above-IC Microbattery Energy Storage," *IEEE J. of Solid-State Circuits*, vol. 43, no. 1, pp. 246–255, Jan. 2008

[72]E. Beigné, C. Condemine, N. Leblond, P. Vivet, G. Waltisperger, J. Willemin, "Bringing robustness and power efficiency to autonomous energy harvesting microsystems, " *IEEE Design & Test of Computers*, Vol.28, no.5, pp.84-94, Sept. Oct. 2011.

[73] E. Lefeuvre, D. Audigier, C. Richard, and D. Guyomar, "Buck-Boost Converter for Sensorless Power Optimization of Piezoelectric Energy Harvester, " *IEEE Transactions on Power Electronics*, vol. 22, no. 5, pp 2018-2025, Sept. 2007.

[74] Gyorgy D. Szarka, Bernard H. Stark, and Stephen G. Burrow, "Review of Power Conditioning for Kinetic Energy Harvesting Systems, " *IEEE Trans. Power Electron*., vol. 27, no. 2, pp. 803-815, Feb. 2012.

[75] E. Dallago, D. Miatton, G. Venchi, V. Bottarel, G. Frattini, G. Ricotti and M. Schipani, "Comparison of Two Autonomous AC-DC Converters for Piezoelectric Energy Scavenging Systems," *IFIP Advances in Information and Communication Technology*, vol. 313, pp. 61-80, 2010.

[76]Yang Sun, Nguyen Huy Hieu, Chang-Jin Jeong, and Sang-Gug Lee, "An Integrated High-Performance Active Rectifier for Piezoelectric Vibration Energy Harvesting Systems, " *IEEE Trans. Power Electron*., vol. 27, no. 2, pp. 623-627, Feb. 2012.

[77]C. Vanhecke, L. Assouère, M. Bafleur, C. Rossi, J.M. Dilhac, "Convertisseur à faible consommation pour la récupération d'énergie ambiante combinant deux sources pour application aéronautique," in Proc. *8ème Journées d'étude Faible Tension Faible Consommation (FTFC 2009)*, Neuchâtel, Switzerland,
2009.

[78] C. Rossi, P. Aguirre, "Ultra-low Power CMOS Cells for Temperature Sensors", in *Proc. 18th Symposium on Integrated Circuits and Systems Design*, Florianopolis, Brazil, 2005, pp. 202 – 206.

[79] C. Vanhecke, "Current generator, notably for current of the order of nano-amperes, and voltage regulator using such a generator", US Patent n°20120068684 A1, March 2012.

[80] K. Ueno, T. Hirose, T. Asai, Y. Amemiya, "A 300 nW, 15 ppm/ C, 20 ppm/V CMOS Voltage Reference Circuit Consisting of Subthreshold MOSFETs," *IEEE J. of Solid-State Circuits*, vol. 44, no. 7, pp. 2047–2054, Jul. 2009.

Appendix

App. 1 – Measured Values (Nextreme HV56)

	Micropelt TGP-751	Nextreme eTEG HV56
Tavg [°C]	*Ri,TEM* [Ω]	*Ri,TEM* [Ω]
-50	231.0	6.937
-45	234.0	7.045
-40	245.0	7.360
-35	248.0	7.560
-30	257.0	7.923
-25	263.0	8.170
-20	269.0	8.488
-15	275.0	8.650
-10	280.5	8.910
-5	284.9	9.220
0	290.1	9.313
5	299.3	9.457
10	306.6	9.620
15	320.1	9.790
20	330.8	9.922
25	330.2	10.071
30	328.0	10.264
35	332.2	10.407
40	335.8	10.523
45	340.9	10.700
50	349.5	10.831
55	356.2	10.935
60	360.0	11.080
65	366.0	11.122
70	370.4	11.275
75	377.5	11.308
80	384.0	11.350
85	389.6	11.418
90	394.3	11.435
95	396.4	11.540
100	404.6	11.558
105	409.5	11.550

110	409.5	11.584
115	417.8	11.570
120	423.0	11.535
125	426.5	11.442
130	425.5	11.480
135	433.4	11.370
140	438.1	11.300
145	440.7	11.206
150	444.7	11.150

App. 2 – Measured Values (Micropelt TGP-751)

ΔT [°C]	*Uoc*[V]	*Isc* [mA]	*PMPP* [mW]	*Th* [°C]	*Tc* [°C]	*Tavg* [°C]
5	0.350	1.217	0.106	21.0	16.0	18.5
10	0.705	2.449	0.432	28.5	18.5	23.5
15	1.044	3.733	0.974	34.5	19.5	27.0
20	1.397	4.850	1.694	41.5	21.5	31.5
25	1.740	6.057	2.635	47.5	22.5	35.0
30	2.088	7.154	3.734	53.0	23.0	38.0
35	2.419	8.352	5.051	51.0	16.0	33.5
40	2.746	9.456	6.492	57.0	17.0	37.0
45	3.079	10.623	8.177	60.5	15.5	38.0
50	3.405	11.575	9.853	66.5	16.5	41.5
55	3.741	12.552	11.739	74.0	19.0	46.5
60	4.078	13.700	13.967	81.5	21.5	51.5
65	4.400	14.716	16.188	87.0	22.0	54.5
70	4.725	15.904	18.787	89.0	19.0	54.0
75	5.037	16.730	21.067	96.5	21.5	59.0
80	5.360	17.809	23.864	103.0	23.0	63.0
85	5.669	19.062	27.016	107.0	22.0	64.5
90	5.969	20.006	29.854	110.5	20.5	65.5
95	6.277	20.997	32.950	116.0	21.0	68.5
100	6.600	22.050	36.383	122.5	22.5	72.5